

Studies of the Serotonin Type 3A Receptor and the Chemical Preparation of tRNA

Thesis by
Noah Hanville Duffy

In Partial Fulfillment of the Requirements for the
degree of
Doctor of Philosophy



CALIFORNIA INSTITUTE OF TECHNOLOGY

Pasadena, California

2014

(Defended April 30, 2014)

© 2014

Noah H. Duffy

All Rights Reserved

Acknowledgements

Completing my Ph.D. would not have been possible without help from others. First I would like to thank my advisor Dennis Dougherty for all the opportunities he has provided me. I appreciate his endless supply of scientific insights and advice. His public speaking and instruction skills are something I am amazed by, and have been a source of motivation for improvements in my own speaking. Finally, I am grateful for his patience and assistance in securing the next steps after graduate school.

My first project trying to acylate tRNA would not have been a success without the assistance of Scott Virgil, Mona Shahgholi, and Tom Dunn. The chromatography methods Scott helped me develop for the LC/MS greatly accelerated the project. Mona was very helpful with MALDI-MS, and I enjoyed our discussions. Tom Dunn kept all the equipment I needed in working order, and was always willing to lend me whatever tools he had.

The Dougherty group has been helpful throughout my entire Ph.D. I thank Kristin Rule Gleitsman for introducing me to the biology lab. Jai Shanata challenged me with thoughtful questions, and I appreciate his critical analysis of my early writing. I was lucky to share the chemistry lab with Sean Kedrowski and Angela Blum, who both became good friends. Nyssa Puskar was kind enough to collect my first opus data, and for showing me that yes, I do need to learn this technique and collect my own data, which she happily trained me to do. I thank Kay Limapichat for all the great Ernie's lunches. Before leaving for Phoenix, Darren Nakamura was always hosting some sort of entertainment that kept me sane early in my graduate career.

As new people joined the Dougherty group, I made new friends and colleagues who each contributed in their own way. Much of my time overlapped with Ethan Van Arnem, Kristina Daeffler, and Ximena da Silva. I thank Ximena for our discussions of horses. Ethan is a fantastic scientist, and his modifications to opus and tRNA procedures have been appreciated by all. I especially enjoyed our afternoon social hours on the veranda. Kristina Daeffler has been a great friend, and a helpful member of the North Bay. We've been working on graduating, and finishing graduate school has been made better by the shared experience. Tim Miles and I have had overlap in our research—I thank him for all the insightful discussions in all things “serotonin receptor.” I thank Chris Marotta for all his efforts in being the “lab czar,” and introducing me to terrible movies. Clint Regan brought new life to the chemistry lab at a time when I nearly had the place to myself. I thank Erin Lamb for bringing a unique perspective to the lab. I thank Matt Rienzo and Michael Post for being good friends, and making me feel like I will be missed when I graduate. I thank Betty Wong, Matt Davis, Kayla Busby, Paul Walton, Bryce Jarman, Annet Blom, and Catie Blunt for making the end of graduate school more enjoyable.

I thank my Mom (and Tom) and my Dad (and Jill) for their support from afar, and for always coming to LA to visit. I thank my local family Stephanie, Russ, and Rebekah for sharing a place to live. Finally, I'd like to thank my wife Tracy, as I wouldn't have come this far without her—this is as much her Ph.D. as it is mine.

Abstract

This thesis describes studies surrounding a ligand-gated ion channel (LGIC): the serotonin type 3A receptor (5-HT₃AR). Structure-function experiments using unnatural amino acid mutagenesis are described, as well as experiments on the methodology of unnatural amino acid mutagenesis. Chapter 1 introduces LGICs, experimental methods, and an overview of the unnatural amino acid mutagenesis.

In Chapter 2, the binding orientation of the clinically available drugs ondansetron and granisetron within 5-HT₃A is determined through a combination of unnatural amino acid mutagenesis and an inhibition based assay. A cation- π interaction is found for both ondansetron and granisetron with a specific tryptophan residue (Trp183, TrpB) of the mouse 5-HT₃AR, which establishes a binding orientation for these drugs.

In Chapter 3, further studies were performed with ondansetron and granisetron with 5-HT₃A. The primary determinant of binding for these drugs was determined to not include interactions with a specific tyrosine residue (Tyr234, TyrC2). In completing these studies, evidence supporting a cation- π interaction of a synthetic agonist, *meta*-chlorophenylbiguanide, was found with TyrC2.

In Chapter 4, a direct chemical acylation strategy was implemented to prepare full-length suppressor tRNA mediated by lanthanum(III) and amino acid phosphate esters. The derived aminoacyl-tRNA is shown to be translationally competent in *Xenopus* oocytes.

Appendix A.1 gives details of a pharmacological method for determining the equilibrium dissociation constant, K_B , of a competitive antagonist with a receptor, known as Schild analysis. Appendix A.2 describes an examination of the inhibitory activity of

new chemical analogs of the 5-HT₃A antagonist ondansetron. Appendix A.3 reports an organic synthesis of an intermediate for a new unnatural amino acid. Appendix A.4 covers an additional methodological examination for the preparation of amino-acyl tRNA.

Table of Contents

Chapter 1: A Molecular-Scale Approach to Neuroscience

1.1 INTRODUCTION	1
1.2 SUMMARY	9
1.3 REFERENCES	10

Chapter 2: Ondansetron and Granisetron Binding Orientation in the 5-HT₃ Receptor Determined by Unnatural Amino Acid Mutagenesis

2.1 ABSTRACT	11
2.2 INTRODUCTION	12
2.3 RESULTS AND DISCUSSION.....	15
2.3.1 Ondansetron and Granisetron Schild Analysis.....	15
2.3.2 Agonist Behavior at Trp183 and Trp90	17
2.3.3 Ondansetron and Granisetron at Trp183 and Trp90	18
2.4 SUMMARY	24
2.5 METHODS	25
2.5.1 Protein Expression in <i>Xenopus</i> Oocytes	25
2.5.2 Electrophysiology	25
2.5.3 Synthesis.....	27
2.6 ACKNOWLEDGMENTS	30
2.7 REFERENCES	30

Chapter 3: Continuing Studies of 5-HT₃A

3.1 ABSTRACT	32
3.2 INTRODUCTION	33

3.3 RESULTS AND DISCUSSION.....	36
3.3.1 <i>Interactions of Ondansetron and Granisetron with 5-HT_{3A}</i>	36
3.3.2 <i>Examination of Agonists 5-HT and mCPBG at TyrC2</i>	39
3.4 SUMMARY	46
3.5 METHODS	47
3.5.1 <i>Protein Expression in Xenopus Oocytes</i>	47
3.5.2 <i>Electrophysiology</i>	47
3.5.3 <i>Synthesis</i>	48
3.6 REFERENCES	51
Chapter 4: Preparation of Translationally Competent tRNA by Direct Chemical Acylation	
4.1 ABSTRACT	53
4.2 INTRODUCTION, RESULTS, AND DISCUSSION.....	54
4.3 ACKNOWLEDGEMENTS	66
4.4 METHODS	66
4.4.1 <i>Acylation of tRNA</i>	66
4.4.2 <i>Protein Expression in Xenopus Oocytes</i>	67
4.4.3 <i>Electrophysiology</i>	67
4.4.4 <i>Synthesis</i>	68
4.5 REFERENCES	72
Appendix A1: Schild Analysis	
A1.1 INTRODUCTION	75
A1.2 RESULTS AND DISCUSSION.....	78
A1.3 SUMMARY	81

A1.4 METHODS	81
A1.5 REFERENCES.....	82
Appendix A2: The Screening of Ondansetron Analogs	
A2.1 INTRODUCTION	83
A2.2 RESULTS AND DISCUSSION.....	84
A2.3 SUMMARY	87
A2.4 METHODS	87
A2.5 REFERENCES.....	88
Appendix A3: Synthesis of 4,7-Difluoroindole	
A3.1 INTRODUCTION	89
A3.2 RESULTS AND DISCUSSION.....	89
A3.3 SUMMARY	90
A3.4 METHODS	90
<i>A3.3.1 Synthesis</i>	90
A3.5 REFERENCES.....	92
Appendix A4: Preparation of Acylated tRNA Through Adenosine Phosphoro-anhydrides	
A4.1 INTRODUCTION	93
A4.2 RESULTS AND DISCUSSION.....	93
A4.3 SUMMARY	97
A4.4 METHODS	97
<i>A4.4.1 Synthesis</i>	97
<i>A4.4.2 Ligation of tRNA</i>	97
A4.5 REFERENCES.....	98

Chapter 1

A Molecular-Scale Approach to Neuroscience

1.1 INTRODUCTION

Neuroscience is one of the most interdisciplinary fields of science, and for good reason: the brain is the most complex structure on earth.¹ The open question of understanding of the brain is approached at many levels, from the broadly macroscopic view of psychology and medicine, all the way down to the molecular studies of biochemists and chemists. Each approach has its own merits and revelations, but it is the molecular approach that this thesis covers. In order to add context to the following chapters of this thesis, information regarding receptors and the experimental techniques used are covered here.

Communication that occurs in the brain can be viewed as both electrical and chemical (Figure 1.1). A signal, the action potential, is an electrical impulse that propagates down the axon of a neuron. A second neuron slated to receive this signal is not in electrical contact with the sender; the cells are separated at a junction called the synapse. For the neurons to communicate, the electrical signal is converted to a chemical signal. Depolarization of the presynaptic neuron results in the release of small-molecule neurotransmitters into the synaptic cleft, which then passively diffuse to the postsynaptic neuron. These small-molecule neurotransmitters then bind to receptor proteins on the membrane of the postsynaptic neuron. Depending on the nature of the neurotransmitter and the receptor, the electrical signal is regenerated and a new action potential propagates in the postsynaptic neuron.

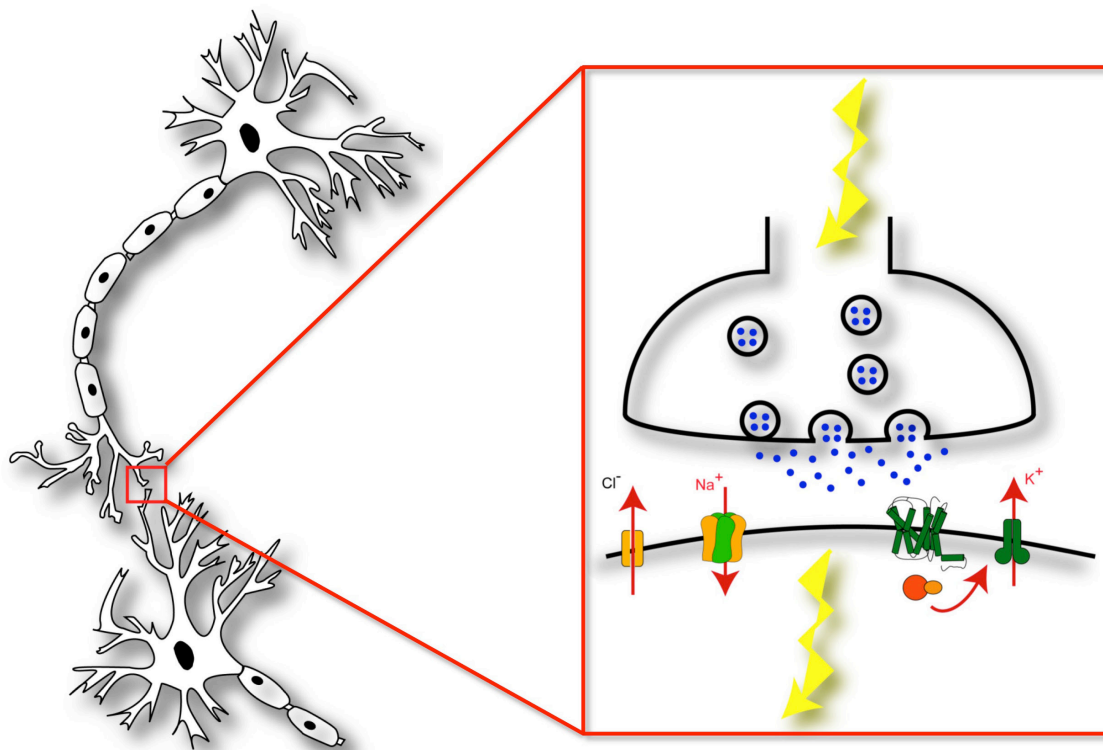


Figure 1.1. A cartoon representing a pair of neurons (left) and a synapse (right). The top neuron represents the presynaptic cell, and the bottom cell represents the postsynaptic cell. Yellow lightning bolts represent an action potential. The action potential in the presynaptic cell triggers the release of small-molecule neurotransmitters (blue dots) into the synaptic cleft. Passive diffusion of the neurotransmitters results in binding to receptors on the postsynaptic cell. The triggering of postsynaptic receptors can cause a new action potential to form in the postsynaptic cell.

The binding of the neurotransmitter to the receptor protein is a molecular event governed by non-covalent interactions. After the binding event, a cascade of conformational changes within the receptor protein occurs, which are also governed by non-covalent interactions. What then, is the nature of these non-covalent interactions? A question such as this is tackled in Chapter 2 regarding ligand-receptor interactions. In the Dougherty group, similar molecular-scale questions have been asked and answered many times over.² Understanding these receptors is more than just scientific curiosity: these receptors are central to human health, and their dysfunction plays roles in diseases such as epilepsy and schizophrenia.^{3,4}

The receptors covered in this thesis are ligand-gated ion channels (LGICs). LGICs allow the passage of ions across a cell membrane in response to the binding of a ligand. The Cys-loop superfamily of LGICs includes the nicotinic acetylcholine receptor (nAChR), serotonin (5-hydroxytryptamine) type 3 receptor (5-HT₃R), γ -aminobutyric acid receptor (GABA), and glycine receptor (GlyR).⁵ The 5-HT₃R is the subject of study in Chapter 2 and Chapter 3. Subtypes of the nAChR make an appearance in Chapter 4.

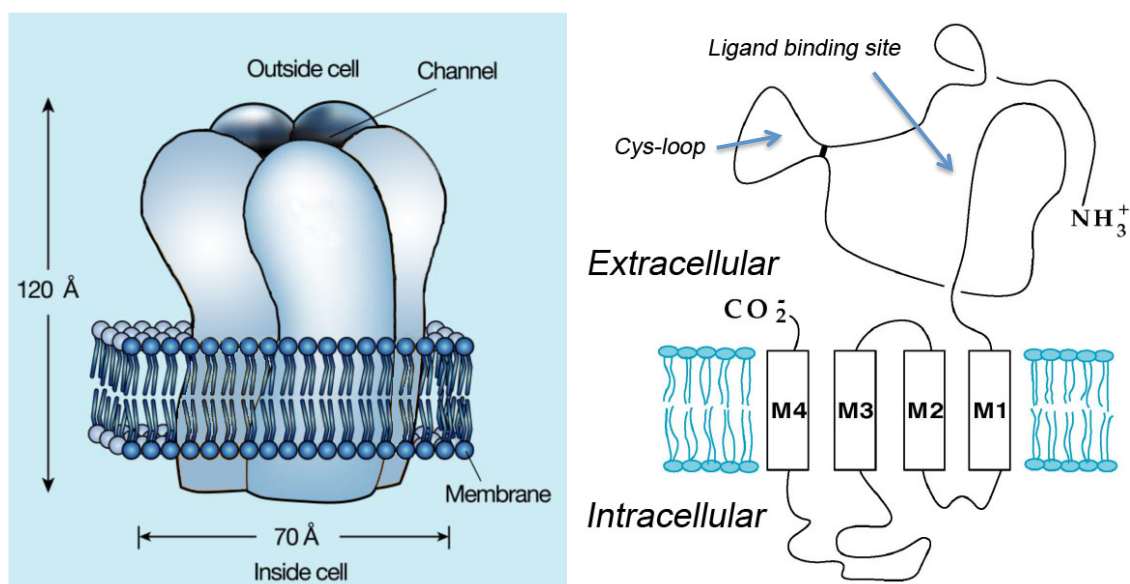


Figure 1.2. A cartoon representing a Cys-loop receptor. Left: General dimensions and a representation of the pentameric nature of Cys-loop receptors. Right: Topology of a Cys-loop receptor, with a general indication of the ligand binding site and a disulfide linkage to form the eponymous “Cys-loop.”

The strategy used for studying these receptors in this thesis is through structure-function experiments: a structural change is made and its effect on function is determined. While such experiments can be performed without prior structural information, design of experiments certainly benefits if some structural information is known. In all cases, Cys-loop receptors form an ion pore by the assembly of five subunits (Figure 1.2). There is a large, extracellular N-terminal domain that is the site of neurotransmitter binding, followed by four membrane-spanning α -helices, and finally an

extracellular C-terminus. Early structural information came from cryo-electron microscopy (cryo-EM) images of receptors from the electric organ of the *Torpedo* ray.⁶ Other insights came from X-ray structures of a soluble protein found in the snail cholinergic synapse, which is homologous to the extracellular domain of Cys-loop receptors.⁷ Finally, an X-ray structure of the glutamate-gated chloride channel from *C. elegans* (GluCl) gave high resolution information to complement the cryo-EM images (Figure 1.3).⁸

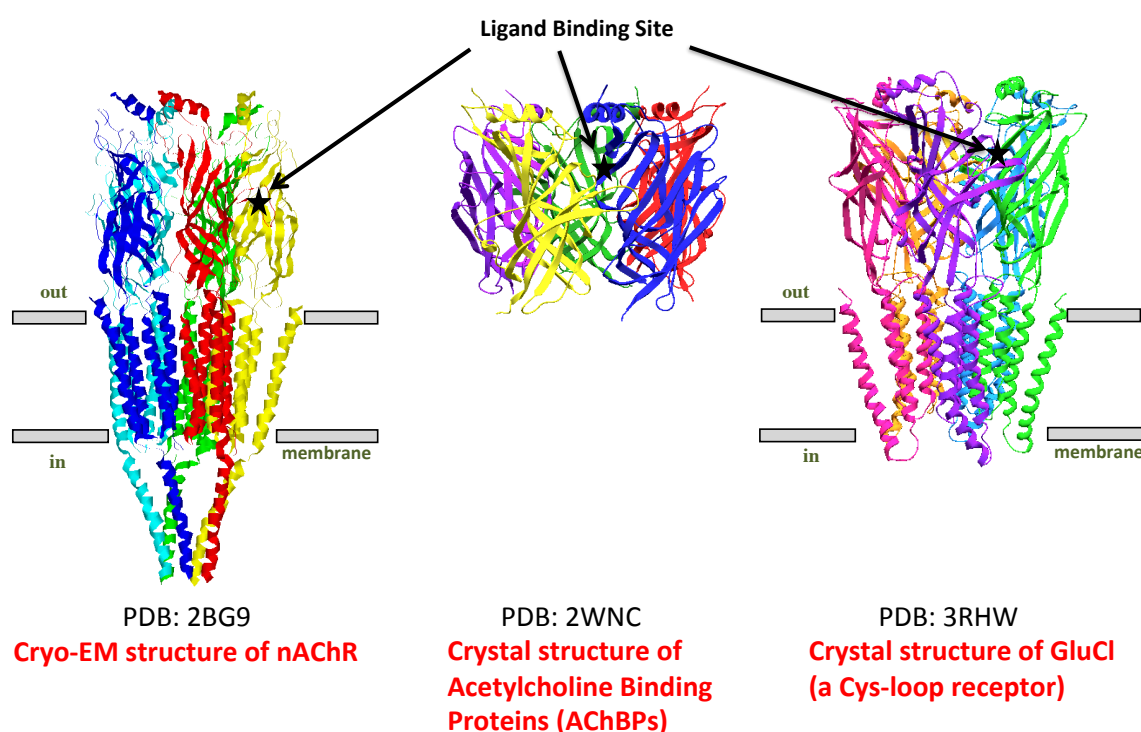


Figure 1.3. Representative structures of Cys-loop receptors. Protein Data Bank codes for each structure shown.

This structural information, while useful, does not provide *functional* insight into the Cys-loop receptors. For that, a functional assay, electrophysiology, is used. The mRNA coding for the appropriate subunits of the LGIC of interest is microinjected into the oocyte of *Xenopus laevis*, which is a large (~ 1 mm) and mostly dormant living cell (Figure 1.4a). After mRNA injection, *Xenopus* oocytes synthesize the LGIC subunit(s),

assemble them into receptors, and transport them to the cell surface. From there, a two-electrode whole-cell voltage clamp experiment, where the potential across the cell membrane is held constant during the experiment, can be performed. In this setup, the membrane potential measured is by one electrode. An activating ligand, called an agonist, is washed over the cell surface, resulting in the opening of a population of receptors. The flow of ions across the cell surface is exactly equivalent to an electric current, and so the second electrode maintains the cell potential by applying an opposing current, which is readily measured. By applying increasing concentrations of agonist to the oocyte, an increase in signal is detected (Figure 1.4b). Plotting these concentration-response data in a semi-log plot and fitting the data to the Hill equation allows one to determine a parameter called the EC_{50} (Figure 1.4c-d). The EC_{50} is the concentration of agonist required to elicit half-maximal current, and is reflective of channel function.

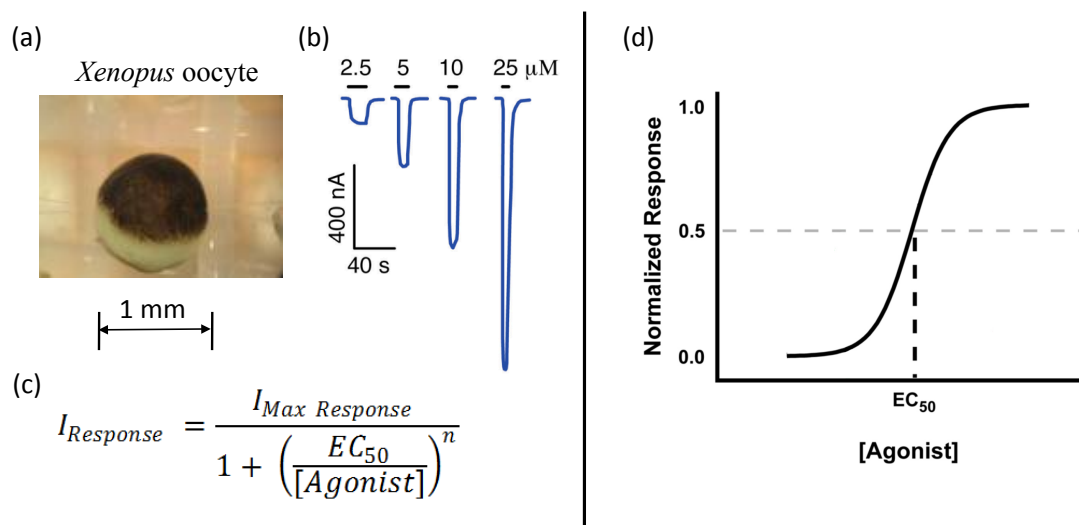


Figure 1.4. Aspects of the functional assay. (a) A *Xenopus* oocyte. (b) Representative increases in measured current in response to increases in the concentration of applied agonist. (c) The Hill equation. (d) A concentration-response curve, and the location of the EC_{50} parameter.

With a functional assay in hand, molecular-scale insight is achieved through structural changes to the receptor. This is done through mutagenesis. Individual amino acids

within the protein are substituted for other amino acids by changing the mRNA code. In its most basic form, this only allows the substitution of an amino acid for one of the 20 naturally occurring amino acids. To obtain truly chemical-scale information, a technique called nonsense suppression is used to install unnatural amino acids, which allows for extremely subtle structural changes.⁹ In this technique, at the site of interest is mutated to a UAG codon (called amber), which is normally interpreted at a “stop” codon. A suppressor tRNA bearing the desired unnatural amino acid, which recognizes the amber codon, is co-injected into the *Xenopus* oocyte (Figure 1.5). In this manner, the unnatural amino acid is installed site-specifically during protein translation. An important feature of the suppressor tRNA is a property called orthogonality: after delivering its amino acid payload, the amino acid synthetases in the *Xenopus* oocyte do not recharge the tRNA with another amino acid. The orthogonality of the tRNAs used in nonsense suppression are not perfect, and so controls using uncharged tRNA should be performed. As the suppressor tRNA does not get recharged, it is a limiting reagent in this process. Chapter 4 explores the methodology for preparing this important component.

Once a structural change is made to a receptor, the functional effect is then measured. A concentration-response plot is constructed for the mutant receptor and the EC_{50} value is determined. If the structural change was detrimental to the function of the receptor (for the agonist used), a rightward shift in the concentration-response curve is seen, with a correspondingly higher EC_{50} value (Figure 1.6a). A larger EC_{50} is referred to as a “loss of function,” while the opposite case (a leftward curve shift and lower EC_{50}) is referred to as a “gain of function.” In this manner, functional changes with respect to activating ligands (agonists) are directly determined. Another class of ligands, antagonists, inhibits

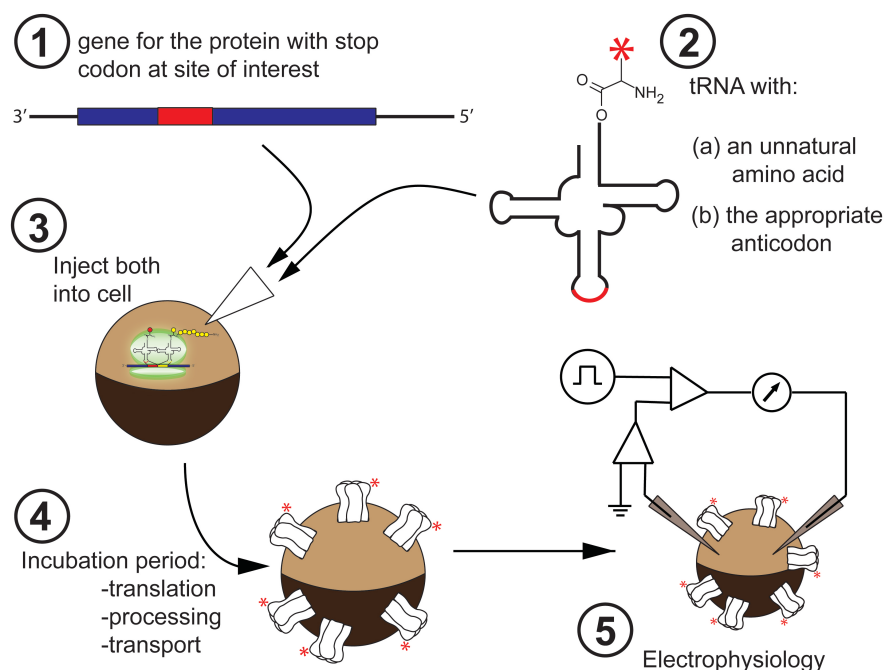


Figure 1.5. Overview of expression of receptors bearing unnatural amino acids in *Xenopus* oocytes. (1) The mRNA for the receptor containing a stop codon at the site of interest and (2) the suppressor tRNA bearing the unnatural amino acid are (3) co-injected into the *Xenopus* oocyte. (4) The translational machinery synthesizes the receptor and inserts the unnatural amino acid into the peptide chain, and after transport to the cell surface, (5) the receptors are probed by electrophysiology.

channel function. Structural changes to the receptor can also affect the ability of an antagonist to inhibit the receptor, but this is not determined through an EC_{50} measurement. As measureable signal is only obtained in the presence of an agonist, an assay involving application of both agonist and antagonist to the receptor is needed. Chapter 2 discusses this measurement and its parameter, the IC_{50} . The IC_{50} is the concentration needed to achieve half-maximal *inhibition* of the signal (Figure 1.6b). In a manner similar to the EC_{50} , the ability of an antagonist to inhibit a receptor with respect to a structural change is determined through increases or decreases in the IC_{50} value.

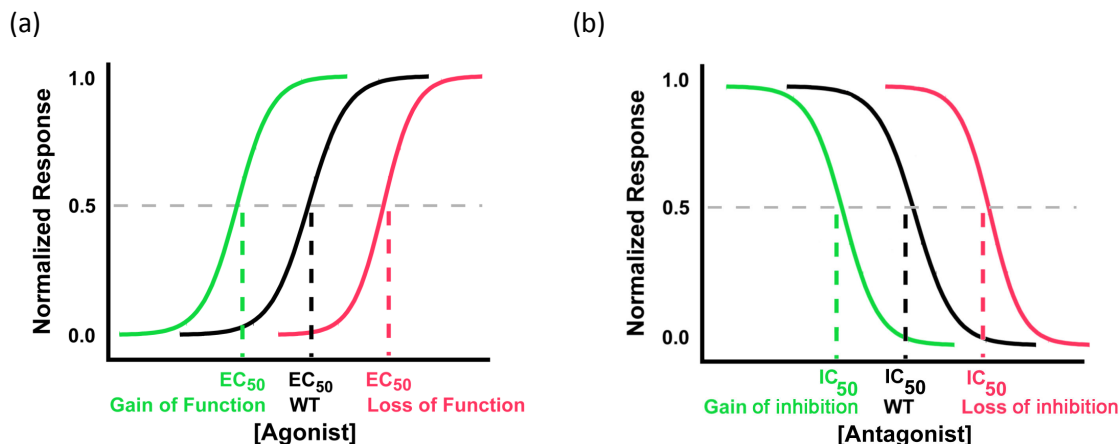


Figure 1.6. Idealized concentration-response curves showing a shift in response as a result of a structural change in the receptor. (a) Shifts activation ability of an agonist. (b) Shifts in inhibition ability of an antagonist.

With the discussion thus far regarding structure-function studies of receptors, the case has not been made as to the need for unnatural amino acid mutagenesis. A particular non-covalent interaction, the cation- π interaction, is well suited for study by unnatural amino acid mutagenesis. A cation- π is a mainly electrostatic interaction between a cation and the π face of an aromatic ring (Figure 1.7a).^{10,11} With conventional mutagenesis, there are only three aromatic amino acids: tryptophan, tyrosine, and phenylalanine. Probing for a cation- π interaction requires more subtle probes than these three amino acids can provide. For example, in mutating a tryptophan to a phenylalanine, there is a change in the cation- π binding ability, but there are also steric perturbations that would complicate the analysis. With unnatural amino acid mutagenesis, a much more subtle change, such as fluorination of the aromatic ring, can be used to probe for this interaction. The steric perturbation of the addition of a fluorine atom to an aromatic ring is minimal, but the electronegative nature of fluorine decreases the cation- π binding ability of the ring system. This effect is additive, and so additional fluorine atoms results in further decreases in ring cation- π binding ability (Figure 1.7b). When the cation- π binding

ability of an aromatic ring is plotted against changes in channel function, information as to the existence of a cation- π interaction can be obtained. This strategy is employed in Chapter 2 and Chapter 3.

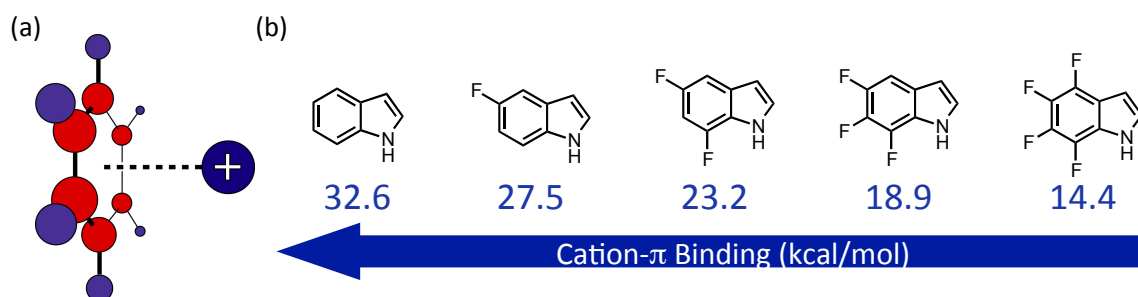


Figure 7. The cation- π interaction. (a) A representation of a Na^+ cation binding to the face of benzene. (b) *Ab initio* calculated cation- π binding energies of indoles and fluorinated indoles.¹²

1.2 SUMMARY

The field of neuroscience benefits from the contributions of a broad range of disciplines. The molecular-scale approach taken in this thesis utilizes a variety of techniques, including organic synthesis, molecular biology, and electrophysiology. Chapter 2 probes the interaction of the antagonists granisetron and ondansetron with the Cys-loop receptor 5-HT₃A. Chapter 3 expands upon the work of Chapter 2 with further examination of antagonist interactions, as well as the synthetic agonist *meta*-chlorophenylbiguanide. Chapter 4 examines a chemical methodology for the preparation of charged suppressor tRNA. There are four appendices which cover: (1) a methodology for measuring competitive antagonist/receptor affinities using pharmacology; (2) an examination of the inhibitory activity of new chemical analogs of the 5-HT₃A antagonist ondansetron; (3) the organic synthesis of an intermediate for a new unnatural amino acid; and (4) an additional methodological examination of the preparation of charged suppressor tRNA.

1.3 REFERENCES

1. Green T, Heinemann SF, & Gusella JF (1998) Molecular neurobiology and genetics: Investigation of neural function and dysfunction. *Neuron* 20(3):427-444.
2. Van Arnam EB & Dougherty DA (2014) Functional Probes of Drug–Receptor Interactions Implicated by Structural Studies: Cys-Loop Receptors Provide a Fertile Testing Ground. *J. Med. Chem.* In press. DOI: 10.1021/jm500023m.
3. Gotti C, Zoli M, & Clementi F (2006) Brain nicotinic acetylcholine receptors: native subtypes and their relevance. *Trends Pharmacol. Sci.* 27(9):482-491.
4. Jensen AA, Frolund B, Lijefors T, & Krogsgaard-Larsen P (2005) Neuronal nicotinic acetylcholine receptors: Structural revelations, target identifications, and therapeutic inspirations. *J. Med. Chem.* 48(15):4705-4745.
5. Corringer PJ, *et al.* (2012) Structure and Pharmacology of Pentameric Receptor Channels: From Bacteria to Brain. *Structure* 20(6):941-956.
6. Unwin N (2005) Refined structure of the nicotinic acetylcholine receptor at 4 angstrom resolution. *J. Mol. Biol.* 346(4):967-989.
7. Hibbs RE, *et al.* (2009) Structural determinants for interaction of partial agonists with acetylcholine binding protein and neuronal alpha 7 nicotinic acetylcholine receptor. *EMBO J.* 28(19):3040-3051.
8. Hibbs RE & Gouaux E (2011) Principles of activation and permeation in an anion-selective Cys-loop receptor. *Nature* 474(7349):54-60.
9. Nowak MW, *et al.* (1998) In vivo incorporation of unnatural amino acids into ion channels in *Xenopus* oocyte expression system. *Methods Enzymol.* 293:504-529.
10. Ma JC & Dougherty DA (1997) The cation- π interaction. *Chem. Rev.* 97(5):1303-1324.
11. Dougherty DA (2013) The Cation- π Interaction. *Accounts Chem. Res.* 46(4):885-893.
12. Zhong WG, *et al.* (1998) From ab initio quantum mechanics to molecular neurobiology: A cation- π binding site in the nicotinic receptor. *Proc. Natl. Acad. Sci. U. S. A.* 95(21):12088-12093.

Chapter 2

Ondansetron and Granisetron Binding Orientation in the 5-HT₃ Receptor Determined by Unnatural Amino Acid Mutagenesis.

Noah H. Duffy[†], Henry A. Lester[‡], Dennis A. Dougherty[†]

[†]Division of Chemistry and Chemical Engineering and [‡]Division of Biology, California Institute of Technology, Pasadena, California 91125

2.1 ABSTRACT

The serotonin type 3 receptor (5-HT₃R) is a ligand-gated ion channel that mediates fast synaptic transmission in the central and peripheral nervous systems. The 5-HT₃R is a therapeutic target, and the clinically available drugs ondansetron and granisetron inhibit receptor activity. Their inhibitory action is through competitive binding to the native ligand binding site, although the binding orientation of the drugs at the receptor has been a matter of debate. Here we heterologously express mouse 5-HT_{3A} receptors in *Xenopus* oocytes, and use unnatural amino acid mutagenesis to establish a cation- π interaction for both ondansetron and granisetron to tryptophan 183 in the ligand binding pocket. This cation- π interaction establishes a binding orientation for both ondansetron and granisetron within the binding pocket.

2.2 INTRODUCTION

The serotonin type 3 receptor (5-HT₃R)^{1,2} is a ligand-gated ion channel in the Cys-loop (pentameric) family of receptors, which also includes GABA_A, glycine, and nicotinic acetylcholine (nACh) receptors.³ The 5-HT₃ receptor is a cation selective channel found in the central and peripheral nervous systems. Conduction occurs through a central pore, formed by the pseudo-symmetric assembly of five subunits (Figure 2.1). There are five known 5-HT₃R subunits (A – E),⁴ with the best characterized receptors being the homomeric 5-HT₃A receptor (5-HT₃AR) and the heteromeric 5-HT₃AB receptors.⁵

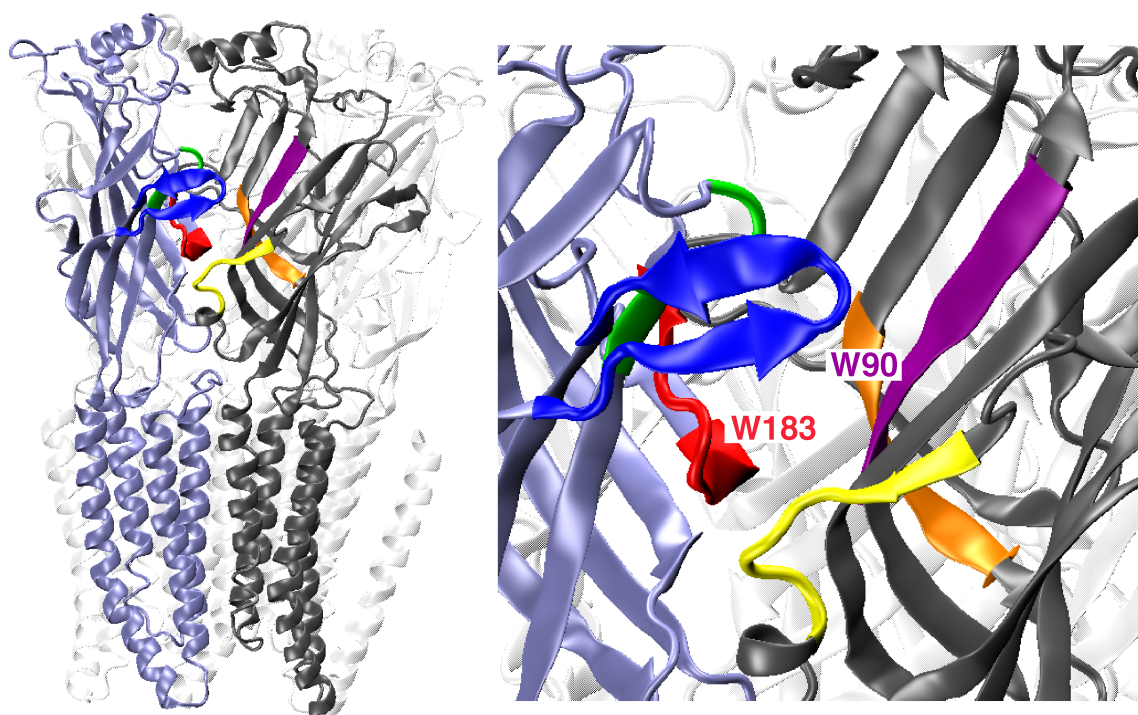


Figure 2.1. Basic layout of a Cys-loop (pentameric) receptor. The structure is that of the GluCl α subunit⁶ (pdb 3RIF). Left: The full receptor, with two subunits highlighted; one (blue) contributes principal agonist binding site residues, found on loops A (red), B (green), and C (blue). The complementary subunit (black) contributes loops D (purple), E (orange), and F (yellow). The α -helical region corresponds to the transmembrane domain; the region above it is extracellular. Right: Detail of agonist binding site, noting approximate locations of key residues considered here.

The 5-HT₃ receptor has been validated as a therapeutic target—antagonists are currently used to control chemotherapy-induced nausea, as well as to treat irritable bowel

syndrome.^{7,8} Beyond current clinical uses, there is evidence that compounds targeting the 5-HT₃ receptor could be useful for the treatment of a variety of disorders including schizophrenia and substance abuse, as well as management of pain associated with, for example, fibromyalgia. Prototype antagonists of the 5-HT₃ receptor are ondansetron (Zofran®) and granisetron (Kytril®) (Figure 2.2a).

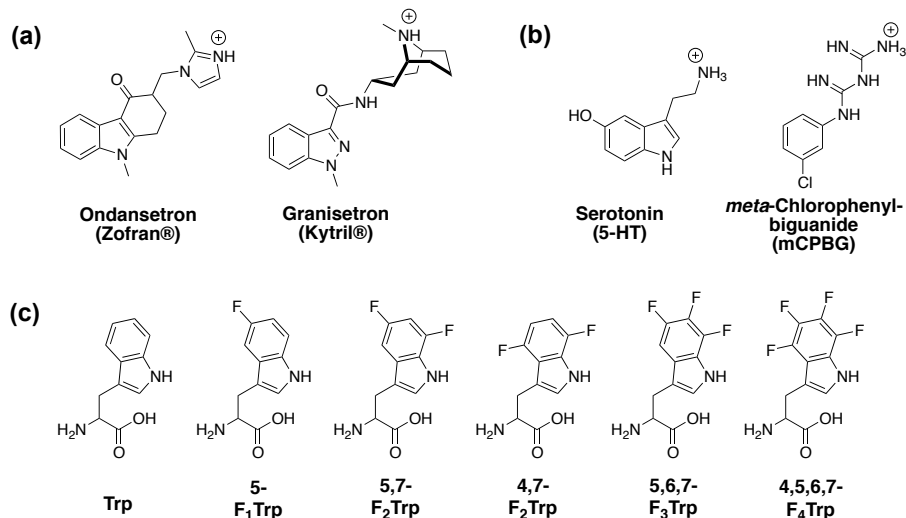


Figure 2.2. Chemical structures of drugs and amino acids used in this study. (a) 5-HT₃A receptor antagonists. (b) 5-HT₃A receptor agonists. (c) Tryptophan analogs.

There is no high-resolution structure of the 5-HT₃ receptor. There is, however, structural information from a number of sources, including cryoelectron microscopy images of the nACh receptor,⁹ high resolution structures of the homologous acetylcholine binding protein,¹⁰ and the recently published x-ray structure of the glutamate-gated chloride channel from *C. elegans*, GluCl.⁶ These data, along with homology modeling and biochemical studies, have provided a putative binding site for 5-HT₃ antagonists that coincides with the binding site of the native agonist, serotonin (5-HT, Figure 2.2b). This binding site is formed by a series of β -strands and connecting loops (labeled A-F), with loops A-C contributed by the “principal” subunit and β -strands D-F contributed by the

“complementary” subunit (Figure 2.1). Docking studies using homology models have found multiple energetically favorable poses of the antagonist granisetron within this binding site, and the orientation of the drug and the identities of the interacting residues are not constant across poses.¹¹⁻¹⁴ For example, Thompson *et. al.* reported two classes of poses of granisetron.¹³ In one class, the cationic ammonium was oriented between Trp183 (loop B) and Tyr234 (loop C), while the aromatic indazole was oriented between Trp90 (β -strand D) and Phe226 (loop C). In the second class of poses, this orientation was reversed, with the cationic ammonium towards Trp90 and Phe226. Experimentally, both Trp183 and Trp90 have been established to be important for granisetron binding. In other experimental work, Yan and White found that Trp90 is important for both ondansetron and granisetron binding, and they interpreted their results as providing evidence that the cationic ammonium of granisetron was oriented towards Trp90.¹⁴

The accepted pharmacophore model for 5-HT₃R includes an amine group on the ligand. Past studies in our laboratory have established the primary amine of 5-HT to make a cation- π interaction with a conserved tryptophan residue on loop B (Trp183).¹⁵ Mutation of Trp183 (as well as Trp90, Glu129 (loop A), and Tyr234) to alanine abolishes binding of [³H]granisetron.¹³ Taken together, these results identify Trp183 as a prime candidate for more detailed studies. Moreover, the docking studies of Thompson *et. al.* provide us with testable guidelines as to other possible interactions; specifically, with Trp90.¹³ In the present work, we set out to better understand the binding of the high affinity antagonistic drugs ondansetron and granisetron to the 5-HT₃AR. The cationic center of granisetron is a tertiary ammonium ion in a granatane moiety ($pK_a = 9.6$), but ondansetron has a structurally distinct *N*-alkylimidazolium moiety ($pK_a = 7.4$).¹⁶ We

sought to determine if this structural difference leads to different binding orientations for the two drugs.

2.3 RESULTS AND DISCUSSION

2.3.1 Ondansetron and Granisetron Schild Analysis. In examining the interaction of a competitive antagonist with a receptor, equilibrium dissociation constants, K_b , provide the most direct indicator of binding interactions.¹⁷ Previous reports have indicated that granisetron and ondansetron act competitively with 5-HT at the 5-HT₃AR.^{2,18} Both antagonists bind reversibly, in that after a several minute washout of either ondansetron or granisetron, agonist responses recover completely. Previous studies have established dissociation rate constants of 0.58 min⁻¹ for ondansetron, and 0.13 min⁻¹ for granisetron,¹⁹ consistent with our observations. It has also been shown that granisetron and ondansetron directly compete with each other for the same binding site.¹⁹ We attempted to determine K_b for ondansetron and granisetron using Schild (dose-ratio) analysis;¹⁷ this requires measurements of dose-response relationships (Figure 2.3). Schild analysis of ondansetron applied to preparations of rat vagus nerves gave parallel shifts, indicative of a competitive interaction, but efforts to perform similar studies with granisetron were not successful.²⁰ As shown in Figure 2.3, during our standard 15 second agonist application (see Methods), the inhibition by ondansetron and granisetron was insurmountable by 5-HT—full receptor activity could not be restored even with high concentrations of 5-HT. We attribute the insurmountable inhibition to the slow off rates. The granisetron data are better behaved than the ondansetron data, but in either case we face a requirement of agonist applications several minutes in duration. However, the 5-HT₃AR desensitizes on this time scale before full equilibrium is achieved. Thus, for the high-affinity 5-HT₃AR

antagonists ondansetron and granisetron, determination of true K_b by functional measurements is not possible.

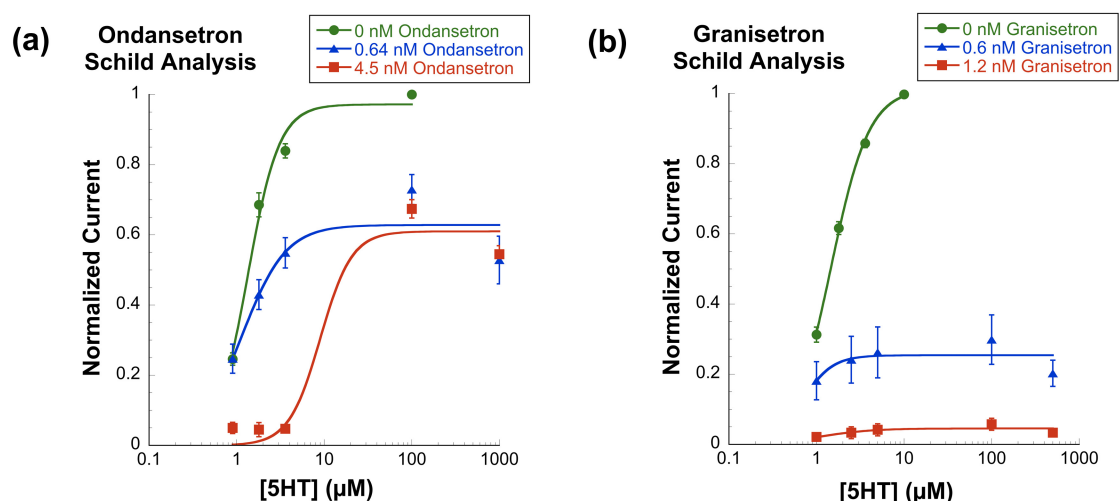


Figure 2.3. Dose-response curves of wild-type 5-HT₃A receptor. Responses to 5-HT with increasing concentrations of (a) ondansetron, and (b) granisetron. Data fit to the Hill equation. Fit parameters (a) Mean maximal current: 8 ± 4 μ A. [ondansetron] = 0 nM, EC_{50} : 1.3 ± 0.2 μ M, n_H : 2.4 ± 0.6 ; [ondansetron] = 0.64 nM, I_{max} : 63%, EC_{50} : 1.1 ± 0.4 μ M, n_H : 2 ± 1 ; [ondansetron] = 4.5 nM, I_{max} = 61%, EC_{50} : 9 ± 29 μ M, n_H : 2 ± 8 . (b) Mean maximal current: 9 ± 4 μ A. [granisetron] = 0 nM, EC_{50} : 1.5 ± 0.1 μ M, n_H : 2.0 ± 0.1 ; [granisetron] = 0.6 nM, I_{max} : 25%, EC_{50} : 0.7 ± 0.7 μ M, n_H : 2 ± 7 ; [granisetron] = 1.2 nM, I_{max} : 4%, EC_{50} : 1 ± 1 μ M, n_H : 1 ± 2 .

Thus, the concentration required for 50% receptor inhibition (IC_{50}) was the only viable functional measurement, and so modified procedures were developed to render IC_{50} values a good direct measure of antagonist binding. The IC_{50} measurement is taken in the context of multiple equilibria, including both agonist and antagonist binding/dissociation, conformational changes in the protein, and the “gating” equilibria between the open the closed states of the receptor. We sought to reduce the contribution from changes in *agonist* potency, while retaining an index of *antagonist* potency. When evaluating competitive antagonists, it is useful to consider more than one agonist, so that one can be sure that IC_{50} determinations are not distorted by agonist-receptor interactions. To

determine IC₅₀ values for ondansetron and granisetron, we studied both 5-HT and an additional agonist, *meta*-chlorophenylbiguanide (mCPBG, Figure 2.2b).²¹

2.3.2 Agonist behavior at Trp183 and Trp90. The effective concentrations for 50% receptor activation (EC₅₀) were determined for both the native agonist 5-HT, as well as the potent partial agonist mCPBG. The EC₅₀ values were also determined for a series of fluorinated tryptophan derivatives (Figure 2.2c) introduced by nonsense suppression at Trp183 (Table 2.1). The EC₅₀ values confirm the previously reported¹⁵ cation- π interaction for 5-HT at Trp183. Interestingly, we have recently found that mCPBG does not respond to fluorination at Trp183 in the same manner as 5-HT,²² and the data of Table 2.1 produced for this work confirm that result. Detailed experiments and discussion concerning the activation of 5-HT₃ receptors by mCPBG will be presented in a separate publication.²² For the present purposes, the key point is that mCPBG responds to fluorination at Trp183 differently than 5-HT.

Table 2.1. EC₅₀ data for wild type and mutant 5-HT₃AR in response to 5-HT or mCPBG.

Agonist	Mutation	<i>N</i> ^a	EC ₅₀ (μ M) ^b	Fold Shift ^c	Hill ^d
5-HT	Wild Type	25	1.6 \pm 0.1	-	2.1 \pm 0.2
	W183F ₁ W (5)	18	3.4 \pm 0.2	2.2	2.0 \pm 0.2
	W183F ₂ W (5,7)	11	18 \pm 1	11	2.9 \pm 0.2
	W183F ₂ W (4,7)	19	36 \pm 2	23	2.2 \pm 0.3
	W183F ₃ W (5,6,7)	10	250 \pm 10	160	5 \pm 1
	W90F ₃ W (5,6,7)	20	0.23 \pm 0.01	1 / 6.8	2.0 \pm 0.2
	W90F ₄ W (4,5,6,7)	29	0.64 \pm 0.03	1 / 2.4	2.3 \pm 0.2
mCPBG	Wild Type	9	0.50 \pm 0.02	-	2.2 \pm 0.1
	W183F ₁ W (5)	14	5.8 \pm 0.4	12	1.6 \pm 0.1
	W183F ₂ W (5,7)	9	2.6 \pm 0.1	5.3	1.8 \pm 0.1
	W183F ₂ W (4,7)	19	0.34 \pm 0.03	1 / 1.5	1.4 \pm 0.1
	W183F ₃ W (5,6,7)	13	6.6 \pm 0.2	13	2.6 \pm 0.2
	W183F ₄ W (4,5,6,7)	14	8.4 \pm 0.6	17	1.5 \pm 0.1
	W90F ₃ W (5,6,7)	15	0.092 \pm 0.004	1 / 5.4	3.2 \pm 0.5
	W90F ₄ W (4,5,6,7)	7	0.20 \pm 0.02	1 / 2.5	2.1 \pm 0.3

^aNumber of oocytes averaged in EC₅₀ determination. ^bThe effective concentration for half-maximal receptor activation. ^cEC₅₀(mutant)/EC₅₀(wild type). ^dThe Hill coefficient, *n*_H, as determined from fitting the Hill equation.

When the fluorinated tryptophans F₃Trp and F₄Trp were installed at Trp90, both 5-HT and mCPBG show a *gain* of function. These data are consistent with no cation- π interaction for 5-HT or mCPBG with Trp90.

2.3.3 Ondansetron and Granisetron at Trp183 and Trp90. An important aspect of the complex nature of measuring IC₅₀ in receptors is the concentration of agonist used for receptor activation. For a competitive interaction, a measured IC₅₀ value will depend on the agonist concentration.¹⁷ In order to make meaningful comparisons of IC₅₀ values across mutant receptors, the concentration of agonist used was kept at a constant value of twice EC₅₀. The choice of a constant ratio of twice EC₅₀ was made to ensure sufficient signal, even in cases of low receptor expression. We also emphasize that the series of mutations being introduced represents a much more subtle variation in structure than is possible with conventional mutagenesis. This provides further confidence that no dramatic changes in receptor-antagonist interactions are occurring in the study. We also exploited the difference in the binding modes of 5-HT and mCPBG to control for possible artificial trends in IC₅₀ measurements.

Dose-response/inhibition relations were determined for ondansetron and granisetron, using both 5-HT and mCPBG as agonists, with representative voltage-clamp traces shown in Figure 2.4. These measurements were performed on the wild type 5-HT₃AR, as well as for a series of fluorinated tryptophan derivatives at Trp183. Agonist concentrations were 2 x EC₅₀ for each agonist at each receptor, and data were fit to the Hill equation (Figure 2.4). The resultant IC₅₀ values are presented in Table 2.2. Inhibition data for F₄Trp could not be gathered using 5-HT as the agonist, because of channel block by high concentrations of 5-HT.

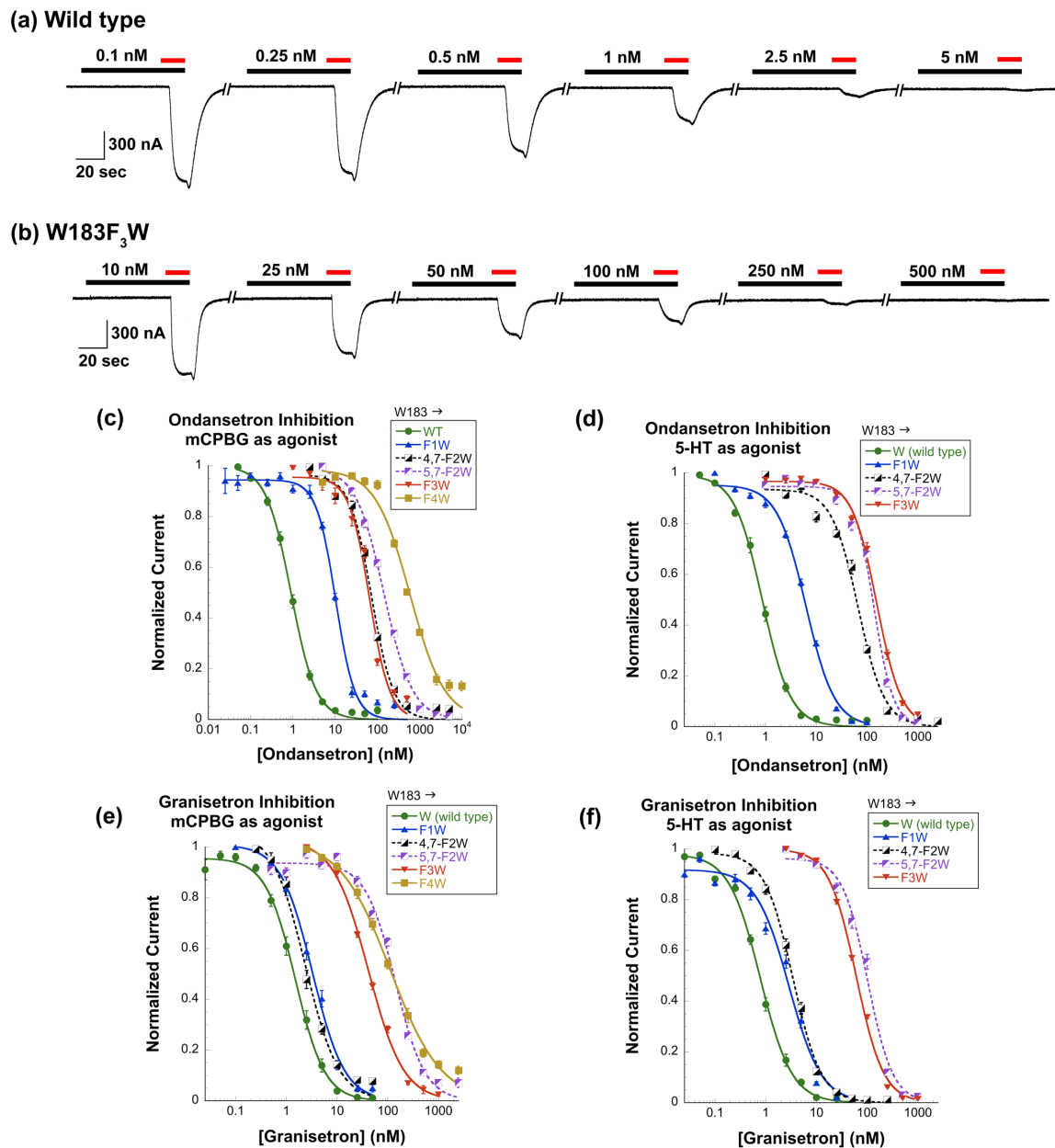


Figure 2.4. Representative voltage-clamp traces and dose-inhibition curves for antagonists for wild type and Trp183 mutant 5-HT₃A receptors. Representative traces for inhibition of (a) wild-type and (b) W183F₃W receptors by increasing doses of granisetron. Time of application and concentration noted by black bars. Channels opened by addition of mCPBG (red bars) at (a) 1 μ M and (b) 13 μ M. Hashes indicate wash times. Ondansetron inhibition curves shown for receptors activated by (c) mCPBG, and (d) 5-HT. Granisetron inhibition curves shown for receptors activated by (e) mCPBG, and (f) 5-HT. Data fit to the Hill equation; fit parameters (IC₅₀ and n_H) are in Table 2.2.

Table 2.2. IC₅₀ data for wild type and mutant 5-HT₃AR for granisetron and ondansetron in response to 5-HT or mCPBG.

Antagonist	Agonist ^a	Mutation	N ^b	IC ₅₀ (nM) ^c	Fold Shift ^d	Hill ^e
Granisetron	5-HT	Wild Type	27	0.78 ± 0.04	-	-1.4 ± 0.1
		W183F ₁ W (5)	17	2.9 ± 0.3	3.7	-1.4 ± 0.2
		W183F ₂ W (5,7)	14	100 ± 10	130	-1.7 ± 0.2
		W183F ₂ W (4,7)	11	3.4 ± 0.2	4.4	-1.6 ± 0.1
		W183F ₃ W (5,6,7)	9	61 ± 2	78	-1.6 ± 0.1
		W90F ₃ W (5,6,7)	11	0.20 ± 0.03	1 / 3.9	-1.1 ± 0.1
		W90F ₄ W (4,5,6,7)	12	0.64 ± 0.03	1 / 1.2	-1.8 ± 0.1
	mCPBG	Wild Type	27	1.5 ± 0.1	-	-1.5 ± 0.1
		W183F ₁ W (5)	8	3.3 ± 0.2	2.2	-1.4 ± 0.1
		W183F ₂ W (5,7)	16	140 ± 10	93	-1.5 ± 0.1
		W183F ₂ W (4,7)	13	2.4 ± 0.3	1.6	-1.3 ± 0.2
		W183F ₃ W (5,6,7)	9	41 ± 2	27	-1.2 ± 0.1
		W183F ₄ W (4,5,6,7)	14	110 ± 10	74	-0.9 ± 0.1
		W90F ₃ W (5,6,7)	7	0.20 ± 0.02	1 / 7.6	-1.2 ± 0.1
Ondansetron	5-HT	Wild Type	21	0.87 ± 0.04	-	-1.6 ± 0.1
		W183F ₁ W (5)	16	6.2 ± 0.4	7.1	-1.5 ± 0.1
		W183F ₂ W (5,7)	11	140 ± 10	160	-2.2 ± 0.2
		W183F ₂ W (4,7)	9	67 ± 6	77	-1.7 ± 0.2
		W183F ₃ W (5,6,7)	9	160 ± 10	180	-1.8 ± 0.1
		W90F ₃ W (5,6,7)	13	0.40 ± 0.03	1 / 2.2	-1.3 ± 0.1
		W90F ₄ W (4,5,6,7)	11	1.3 ± 0.1	1.4	-1.7 ± 0.1
	mCPBG	Wild Type	23	0.91 ± 0.04	-	-1.5 ± 0.1
		W183F ₁ W (5)	15	10 ± 1	11	-1.9 ± 0.2
		W183F ₂ W (5,7)	13	140 ± 10	160	-1.3 ± 0.1
		W183F ₂ W (4,7)	13	73 ± 6	80	-1.7 ± 0.2
		W183F ₃ W (5,6,7)	8	89 ± 5	99	-1.1 ± 0.1
		W183F ₄ W (4,5,6,7)	15	590 ± 80	650	-1.1 ± 0.1
		W90F ₃ W (5,6,7)	11	0.37 ± 0.03	1 / 2.4	-1.5 ± 0.2
		W90F ₄ W (4,5,6,7)	9	1.5 ± 0.1	1.6	-1.3 ± 0.1

^aAgonist used in the presence of antagonist for channel activation. ^bNumber of oocytes averaged in IC₅₀ determination. ^cThe effective concentration for half-maximal receptor inhibition. ^dIC₅₀(mutant)/IC₅₀(wild type). ^eThe Hill coefficient, n_H , as determined from fitting the Hill equation.

The effect of fluorine substitution in modulating a cation- π interaction has been well established.^{15,23-25} For both ondansetron and granisetron, incremental substitutions of fluorine to Trp183 increased IC₅₀. As in previous studies of fluorination trends, IC₅₀ fold-shift values were plotted against cation- π binding ability of fluorinated indoles, producing the “fluorination plots” shown in Figure 2.5. Ondansetron inhibition linearly correlates with the energy of cation- π binding, regardless of whether 5-HT or mCPBG was used as an agonist. Granisetron also displayed a strong correlation with respect to degree of fluorination, regardless of agonist identity.

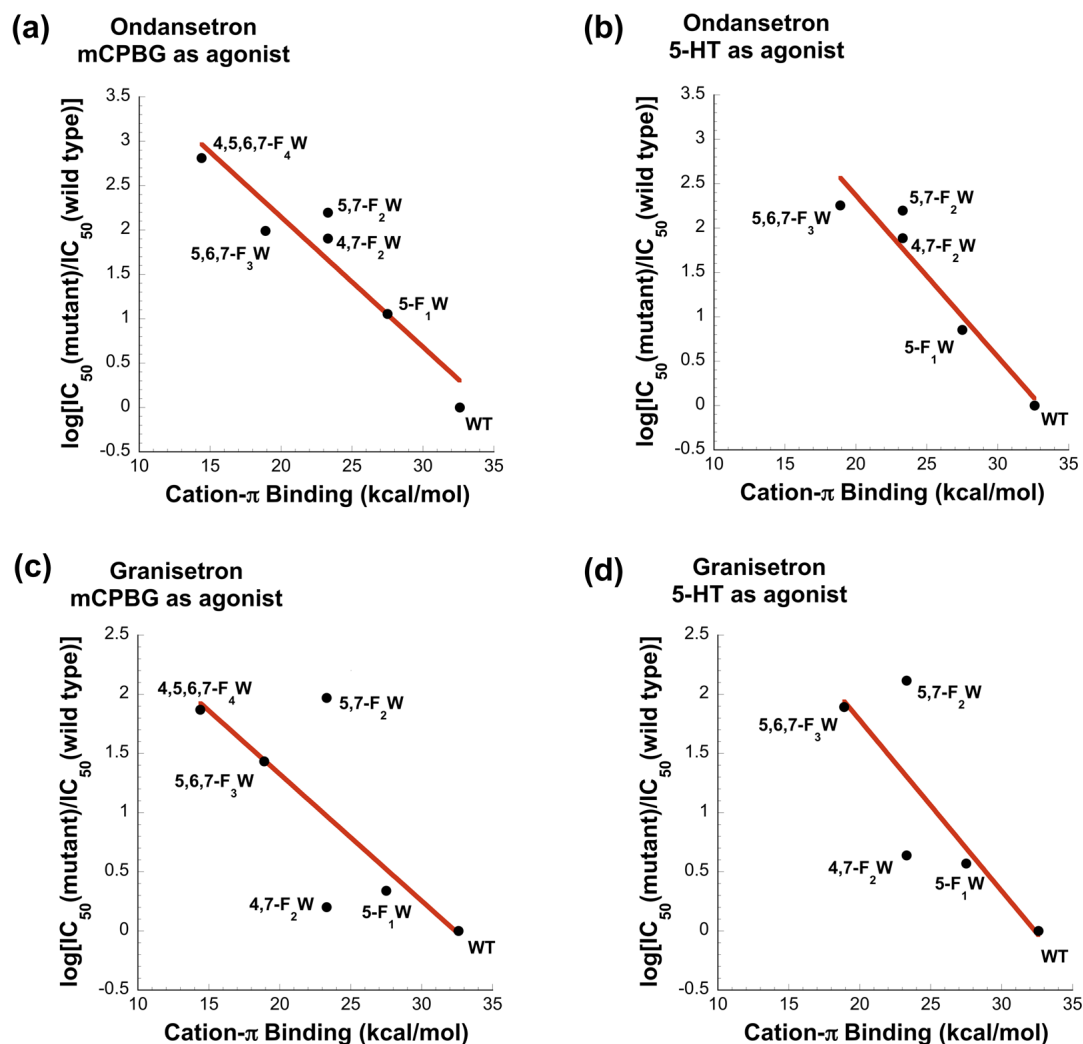


Figure 2.5. Fluorination plots. Calculated cation- π binding ability versus $\log[IC_{50}/IC_{50}(wt)]$ for a series of fluorinated tryptophan derivatives at Trp183. Ondansetron fluorination plots for receptors activated by (a) mCPBG, and (b) 5-HT. Granisetron fluorination plots for receptors activated by (c) mCPBG, and (d) 5-HT. Red lines are linear fits ($y = mx + b$) inclusive of all points. Fit parameters (a) $m: -0.15 \pm 0.03$, $b: 5.1 \pm 0.6$, $R: 0.94$; (b) $m: -0.18 \pm 0.03$, $b: 6.0 \pm 0.8$, $R: 0.96$; (c) $m: -0.11 \pm 0.04$, $b: 3 \pm 1$, $R: 0.77$; (d) $m: -0.14 \pm 0.06$, $b: 5 \pm 2$, $R: 0.82$.

We interpret these results as establishing a cation- π interaction between each drug and Trp183. The results of Figure 2.5 highlight the value of having two distinct agonists to evaluate an antagonist. With 5-HT as the agonist, we see linear fluorination plots for the antagonists. The agonist alone, 5-HT, shows a similar plot in a study of its EC_{50} . We corrected for this by always using a 5-HT dose of $2 \times EC_{50}$ for the particular fluorination

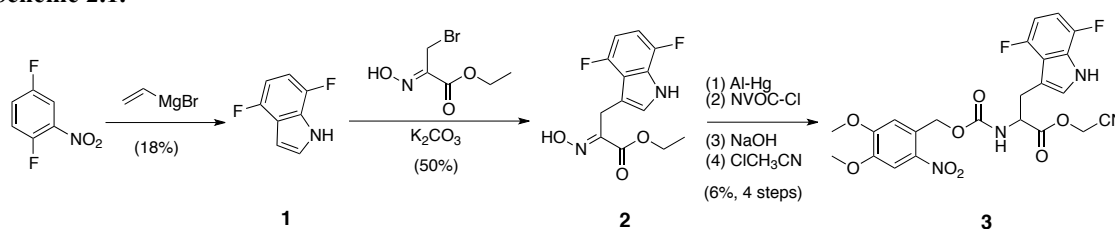
mutant. Nevertheless, there could be concern about deconvoluting the effect of fluorination on the agonist vs. the antagonist. With mCPBG as the agonist, there is no such concern, as it does not respond to fluorination at Trp183 in a manner consistent with a cation- π interaction. Thus, the fluorination trends seen in Figure 2.5 can confidently be assigned as reflecting the response of the antagonist to the mutation. We also note that the fluorination effect remains regardless of the structural identity of the cation. Ondansetron, with a *N*-alkylimidazolium moiety, and granisetron, with a tertiary ammonium, show similar trends at the same residue, which is evidence that their binding orientations are similar.

While the general trends in our data are clear, the detailed behaviors of the F₂Trp unnatural amino acids present interesting details. In the fluorination plots, 5,7-F₂Trp, a residue that we have used extensively, deviates from the line set by the other derivatives, especially for granisetron. The effect is evident, but much less pronounced, in studies of ondansetron. We considered the possibility that an additional unique, perhaps steric, feature of 5,7-F₂Trp was influencing the analysis.

As such, we prepared 4,7-F₂Trp (Scheme 2.1), which should have the same cation- π binding ability, but different steric requirements. Synthesis began by direct formation of 4,7-difluoroindole (**1**) in a Bartoli reaction between the appropriate nitrodifluorobenzene and vinyl magnesium bromide.^{26,27} In a sequence similar to Gilchrist *et. al.*²⁸ the difluoroindole (**1**) was then reacted with ethyl-3-bromo-2-hydroxyiminopropanoate to yield the oxime (**2**), which was then reduced using aluminum/mercury amalgam. The amine of the resulting amino acid ester was protected with the photocleavable 2-nitroveratryloxycarbonyl (NVOC), and the ester hydrolyzed with sodium hydroxide.

Conversion to the cyanomethyl ester (**3**) gave material suitable for acylation of the dinucleotide dCA, and for preparation of tRNA necessary for incorporation into the 5-HT₃R (methods described previously).²⁹ The unnatural amino acid prepared by this route is, of course, racemic, but only the natural L configuration will be incorporated; the ribosome of the *Xenopus* oocyte in effect performs a kinetic resolution.

Scheme 2.1.



From an electrostatic point of view, 5,7-F₂Trp and 4,7-F₂Trp are, to first order, indistinguishable, and so they should be equivalent in a cation- π interaction. This is born out in the EC₅₀ data for serotonin (Table 2.1), where the two F₂Trp residues differ only by a factor of two, while the full fluorination series spans more than a factor of 150. In contrast, the EC₅₀ values for mCPBG differ by 8-fold for the two F₂Trps. Recall that mCPBG does not make a cation- π interaction to the Trp. This again suggests that specific steric interactions at Trp183 may be involved.

In the granisetron IC₅₀ plots, 4,7-F₂Trp gives a quite different response than 5,7-F₂Trp. We have suggested the possibility of a special steric effect with 5,7-F₂Trp, but 5,6,7-F₃Trp and 4,5,6,7-F₄Trp both have fluorine atoms at the positions in 5,7-F₂Trp, yet follow the trend indicative of electrostatics as the major determinant to binding. As such, we cannot provide a simple rationalization of the behaviors of the two difluoro-Trp residues. Nevertheless, the consistent linear trend of Trp, F₁Trp, F₃Trp, and F₄Trp

(Figure 2.5) provides compelling evidence for a cation- π interaction to Trp183 for both granisetron and ondansetron.

Both ondansetron and granisetron either increase their potencies or retain their potencies when Trp90 is mutated to F₃Trp or F₄Trp, respectively. This holds for both 5-HT and mCPBG used as the agonist, which indicates no cation- π interaction at that site. A loss of potency would be expected if a cation- π interaction were present. We noted above that Yan and White concluded that Trp90 is important for binding of ondansetron and granisetron.¹⁴ Based on the observation that granisetron and ondansetron responded differently to a W90F mutation, the authors concluded that the bicyclic amine of granisetron interacts with Trp90. Our results position this moiety in contact with Trp183, and we conclude that the importance of Trp90 is for reasons other than a cation- π interaction.

The present results provide evidence that the cationic centers of ondansetron and granisetron are oriented towards Trp183, and not towards Trp90. Establishing a cation- π interaction with ondansetron and granisetron at Trp183 determines a binding orientation for these antagonists. Docking studies of granisetron performed in other laboratories have generated a series of poses, some of which are consistent with the cation pointed towards Trp183. Our data provide evidence that these poses are the most viable, while those with the cation pointed away from Trp183 are not likely to be relevant.

2.4 SUMMARY

We have identified a cation- π interaction with the antagonists ondansetron and granisetron to Trp183 in the 5-HT₃AR. This interaction is consistent with the binding mode of 5-HT, but not mCPBG. The use of agonists with alternate binding modes

validates our data as direct measurements of ondansetron and granisetron. Thus, the common antagonists follow the basic pharmacophore established by 5-HT, and not the structurally dissimilar agonist mCPBG.

2.5 METHODS

Procedures for incorporating unnatural amino acids, expressing receptors in *Xenopus* oocytes, and characterization by electrophysiology followed established protocols.²⁹

2.5.1 Protein Expression in *Xenopus* Oocytes. The mouse 5-HT₃A receptor in the pGEMHE vector was linearized with the restriction enzyme *Sbf*I (New England Biolabs). mRNA was prepared by *in vitro* transcription using the mMessage Machine T7 kit (Ambion). Unnatural mutations were introduced by the standard Stratagene QuickChange protocol using a TAG mutation at W183 and W90. Stage V-VI *Xenopus laevis* oocytes were injected with mRNA. Each cell was injected with 50 nL containing only mRNA (5 ng) for wild type 5-HT₃AR or a mixture of mRNA (5-32 ng, typically ~12 ng) and tRNA (18-30 ng, typically ~18 ng) for unnatural amino acids. Uncharged full length tRNA was injected as a negative control.

2.5.2 Electrophysiology. Electrophysiological experiments were performed 24-48 hours after injection using the OpusXpress 6000A instrument (Axon Instruments) in two-electrode voltage clamp mode at a holding potential of -60 mV. The running buffer was Ca²⁺-free ND96 solution (96 mM NaCl, 2 mM KCl, 1 mM MgCl₂ and 5 mM HEPES, pH 7.5). Serotonin hydrochloride (5-HT) was purchased from Alfa Aesar. 1-(3-Chlorophenyl)biguanide (mCPBG) was purchased from Sigma-Aldrich. Granisetron hydrochloride and ondansetron hydrochloride were purchased from Tocris Bioscience.

For EC₅₀ determinations, oocytes were superfused with running buffer at 1 mL/min for 30 s before application of 5-HT or mCPBG for 15 s followed by a 116 s wash with the running buffer. Data were sampled at 125 Hz and filtered at 50 Hz. Dose-response data were obtained for ≥ 9 concentrations of 5-HT or mCPBG on ≥ 9 cells. All EC₅₀ and Hill coefficient values were obtained by fitting dose-response relations to the Hill equation ($I_{\text{norm}} = 1 / [1 + (EC_{50}/[\text{agonist}])^n]$), and are reported as means \pm standard error of the fit.

For IC₅₀ determinations, oocyte response to either 5-HT or mCPBG at 2 x EC₅₀ for each receptor was measured before application of antagonists by application of the agonist for 15 s, followed by 116 s of wash with the running buffer. Granisetron or ondansetron doses were then pre-applied and the oocyte allowed to incubate for 60 s, followed by application of a mixture of the antagonist dose with 5-HT or mCPBG at 2-fold EC₅₀. The oocytes were then washed with the running buffer for 116 s. Every four antagonist doses, the oocytes were washed for 10 min, and oocyte response reconfirmed using either 5-HT or mCPBG at 2-fold EC₅₀. Oocytes that did not give consistent responses to 5-HT or mCPBG alone throughout the experiment were discarded. Dose-response data were obtained for ≥ 8 concentrations of granisetron or ondansetron on ≥ 8 cells. All EC₅₀ and Hill coefficient values were obtained by fitting Dose-response relations to the Hill equation ($I_{\text{norm}} = 1 / [1 + (EC_{50}/[\text{antagonist}])^n]$), and are reported as means \pm standard error of the fit.

For Schild analysis, the protocol for EC₅₀ determinations was repeated with the following changes: during the course of the experiment (after each minimal EC₅₀ curve was determined) running buffer containing granisetron or ondansetron was used for the

subsequent EC₅₀ determinations. Agonist applications in the subsequent EC₅₀ determinations contained the same concentration of antagonist as the running buffer.

2.5.3 Synthesis. *4,7-Difluoroindole (1)*– A solution of 3.5 mL (32.3 mmol) of 1,4-difluoro-2-nitrobenzene in 30 mL of dry THF was cooled in an acetone/dry ice bath to -78 °C under argon. A 1 M solution of vinylmagnesium bromide in THF (100 mL, 100 mmol, 3 eq.) was added via cannula over 20 min. The reaction was stirred for 1 h at -78 °C. Reaction quenched by the addition of 20 mL of saturated aq. NH₄Cl. Upon warming to room temperature, 20 mL of water was added, which formed a thick emulsion. The reaction was filtered through a layer of sand and washed copiously with ethyl acetate. The organic layer was separated and dried over Na₂SO₄. The solvent was removed under reduced pressure to yield a brown oil containing multiple compounds. Purification by silica gel chromatography using a gradient of 3% to 10% ethyl acetate in hexanes yielded a slightly volatile amber oil. 871 mg (18%). Silica TLC (4% EtOAc in hexanes) R_f = 0.26, stains red/pink using *p*-anisaldehyde. ¹H NMR (300 MHz, CDCl₃): δ 8.47 (br, 1H), 7.18 (t, *J* = 2.8 Hz, 1H), 6.78 (ddd, *J* = 10.3, 8.6, 3.5 Hz, 1H), 6.71 – 6.60 (m, 2H). ¹⁹F NMR (282 MHz, CDCl₃): δ -124.1 – -129.8 (m), -139.4 – -142.3 (m). ¹³C NMR (126 MHz, CDCl₃): δ 152.2 (dd, *J* = 239, 2.4 Hz), 145.8 (dd, *J* = 238.6, 3.0 Hz), 126.0 (dd, *J* = 15.9, 11.5 Hz), 124.7, 119.9 (dd, *J* = 24.9, 5.7 Hz), 106.4 (dd, *J* = 18.9, 8.2 Hz), 103.9 (dd, *J* = 18.9, 8.2 Hz), 99.8. HRMS EI(+) *m/z* for C₈H₅NF₂ found 153.0395, calculated 153.0390 (M+•).

Ethyl 3-(4,7-difluoro-1H-indol-3-yl)-2-(hydroxyimino)propanoate (2)– A solution of 424 mg (2.8 mmol, 2 eq.) of 4,7-difluoroindole in 10 mL CH₂Cl₂ was added to 290 mg (1.4 mmol, 1 eq.) of ethyl 3-bromo-2-(hydroxyimino)propanoate and 205 mg (1.9 mmol,

1.4 eq.) of Na_2CO_3 . The mixture was stirred overnight under argon at room temperature. The reaction was diluted with 50 mL of CH_2Cl_2 and 50 mL of ethyl acetate, and washed with 50 mL of water, then 50 mL of brine. The organic phase was separated and dried over Na_2SO_4 . Purification was performed by silica chromatography, gradient of 25% to 40% EtOAc in hexanes, to yield a white solid. 195 mg (50%). ^1H NMR (300 MHz, CD_3CN): δ 9.93 (s, 1H), 9.64 (br, 1H), 7.01 (m, 1H), 6.81 (ddd, $J = 10.5, 8.5, 3.5$ Hz, 1H), 6.67 (ddd, $J = 10.7, 8.5, 3.2$ Hz, 1H), 4.21 (q, $J = 7.2$ Hz, 2H), 4.12 (d, $J = 1.1$ Hz, 2H), 1.23 (t, $J = 7.1$ Hz, 3H). ^{19}F NMR (282 MHz, CD_3CN): δ -130.99 – -131.20 (m), -141.02 – -141.19 (m). ^{13}C NMR (126 MHz, CDCl_3): δ 164.80, 153.77 (dd, $J = 240.4, 2.3$ Hz), 152.58, 146.84 (dd, $J = 238.1, 2.9$ Hz), 127.18 (dd, $J = 16.4, 12.1$ Hz), 125.12, 119.55 (dd, $J = 22.1, 5.7$ Hz), 110.05 (dd, $J = 3.7, 1.6$ Hz), 106.94 (dd, $J = 19.7, 9.1$ Hz), 104.42 (dd, $J = 22.9, 7.5$ Hz), 62.28, 21.96 (d, $J = 3.1$ Hz), 14.33. HRMS FAB(+) m/z for $\text{C}_{13}\text{H}_{13}\text{O}_3\text{N}_2\text{F}_2$ found 283.0888, calculated 283.0894 (M+H).

N-(2-nitroveratryloxycarbonyl)-4,7-difluorotryptophan cyanomethyl ester (**3**)— In a beaker 1.5 g of 8-20 mesh aluminum was stirred under 15 mL of 2 M NaOH for 5 min. After decanting, the aluminum was rinsed with water and 15 mL of a 2% HgCl_2 solution was added and stirred slowly. The solution was decanted after formation of the Hg-Al (~10 minutes) and added to 195 mg (0.69 mmol) of **2** in 20 mL of 9:1 dioxane:water. The reaction was stirred slowly at room temperature overnight (~24 h). The reaction was filtered through fluted paper, then applied to a silica plug, eluting with EtOAc followed by 4% MeOH in EtOAc. After concentration under reduced pressure, the resulting oil was used directly. The oil was dissolved in 20 mL of 1:1 THF:water and 151 mg of Na_2CO_3 (1.42 mmol), and 248 mg of 4,5-dimethoxy-2-nitrobenzyl chloroformate (0.9

mmol) was added. The reaction was stirred at room temperature for 3 h, followed by dilution with 20 mL CH₂Cl₂ and 20 mL 1 N HCl. The organic phase was separated, washed with brine, and dried over Na₂SO₄. Initial purification by silica chromatography 20% to 40% EtOAc in hexanes did not separate the product from nitroveratryl side products. This mixture was dissolved in 3 mL dioxane and 3 mL 2N NaOH and stirred for 15 min. The reaction was quenched with 6 mL 1 N HCl and diluted with 20 mL EtOAc. The organic phase was separated, and the aqueous phase washed with 20 mL CH₂Cl₂. The combined organic phases were dried over Na₂SO₄, concentrated under reduced pressure, and filtered through a silica plug, eluting with EtOAc followed by 0.5 % acetic acid in EtOAc. This residue (~35 mg, 0.07 mmol) was dissolved in 1 mL DMSO, and added to a reaction flask containing 0.5 mL of chloroacetonitrile (7.9 mmol) and 0.5 mL of triethylamine (3.6 mmol). The reaction was allowed to stir at room temperature for 5 h. The reaction was poured onto a dry column of silica and eluted with EtOAc to recover 23 mg of a yellow solid (6%, 4 steps). ¹H NMR (300 MHz, DMSO-d₆): δ 11.71 (s, 1H), 8.21 (d, *J* = 7.7 Hz, 1H), 7.68 (s, 1H), 7.23 (d, *J* = 2.0 Hz, 1H), 7.09 (s, 1H), 6.92 – 6.80 (m, 1H), 6.74 – 6.62 (m, 1H), 5.39 – 5.21 (m, 2H), 4.99 (s, 2H), 4.48 – 4.35 (m, 1H), 3.85 (s, 3H), 3.83 (s, 3H), 3.32 – 2.99 (m, 2H). ¹⁹F NMR (282 MHz, DMSO-d₆): δ -130.18 (dd, *J* = 22.4, 9.9 Hz), -138.53 (ddd, *J* = 22.6, 10.6, 3.1 Hz). ¹³C NMR (126 MHz, DMSO-d₆): δ 171.56, 156.03, 153.83, 152.62 (d, *J* = 239.6 Hz), 148.15, 146.10 (dd, *J* = 238.5, 2.2 Hz), 139.55, 128.09, 126.70 (dd, *J* = 16.1, 12.2 Hz), 126.36, 118.82 – 118.30 (m), 116.08, 110.61, 109.18, 108.59, 106.23 (dd, *J* = 18.8, 8.7 Hz), 103.90 – 103.23 (m), 63.15, 56.55, 55.30, 49.97, 27.84. HRMS FAB(+) *m/z* for C₂₃H₂₀O₈N₄F₂ found 518.1271, calculated 518.1249 (M+•).

2.6 ACKNOWLEDGMENTS

We thank S. Lummis for helpful discussions and input. This work was supported by the NIH (NS 34407 and DA19375).

2.7 REFERENCES

1. Nichols DE & Nichols CD (2008) Serotonin receptors. *Chem. Rev.* 108(5):1614-1641.
2. Thompson AJ & Lummis SCR (2006) 5-HT₃ receptors. *Curr. Pharm. Design* 12(28):3615-3630.
3. Thompson AJ, Lester HA, & Lummis SCR (2010) The structural basis of function in Cys-loop receptors. *Q. Rev. Biophys.* 43(4):449-499.
4. Niesler B, *et al.* (2007) Characterization of the novel human serotonin receptor subunits 5-HT_{3C}, 5-HT_{3D}, and 5-HT_{3E}. *Molecular Pharmacology* 72(1):8-17.
5. Jensen AA, Davies PA, Brauner-Osborne H, & Krzywkowski K (2008) 3B but which 3B? And that's just one of the questions: the heterogeneity of human 5-HT(3) receptors. *Trends Pharmacol. Sci.* 29(9):437-444.
6. Hibbs RE & Gouaux E (2011) Principles of activation and permeation in an anion-selective Cys-loop receptor. *Nature* 474(7349):54-U80.
7. Machu TK (2011) Therapeutics of 5-HT₃ receptor antagonists: Current uses and future directions. *Pharmacol. Ther.* 130(3):338-347.
8. Thompson AJ & Lummis SC (2007) The 5-HT₃ receptor as a therapeutic target. *Expert Opin. Ther. Targets* 11(4):527-540.
9. Unwin N (2005) Refined structure of the nicotinic acetylcholine receptor at 4 angstrom resolution. *J. Mol. Biol.* 346(4):967-989.
10. Hibbs RE, *et al.* (2009) Structural determinants for interaction of partial agonists with acetylcholine binding protein and neuronal alpha 7 nicotinic acetylcholine receptor. *EMBO J.* 28(19):3040-3051.
11. Joshi PR, *et al.* (2006) Interactions of Granisetron with an agonist-free 5-HT_{3A} receptor model. *Biochemistry* 45(4):1099-1105.
12. Maksay G, Bikadi Z, & Simonyi M (2003) Binding interactions of antagonists with 5-hydroxytryptamine(3A) receptor models. *J. Recept. Signal Transduct.* 23(2-3):255-270.
13. Thompson AJ, *et al.* (2005) Locating an antagonist in the 5-HT₃ receptor binding site using modeling and radioligand binding. *J. Biol. Chem.* 280(21):20476-20482.
14. Yan D & White MM (2005) Spatial orientation of the antagonist granisetron in the ligand-binding site of the 5-HT₃ receptor. *Mol. Pharmacol.* 68(2):365-371.
15. Beene DL, *et al.* (2002) Cation-pi interactions in ligand recognition by serotonergic (5-HT_{3A}) and nicotinic acetylcholine receptors: The anomalous binding properties of nicotine. *Biochemistry* 41(32):10262-10269.

16. Delorenzi FG, Bridal TR, & Spinelli W (1994) Block of the Delayed Rectifier Current (I-K) by the 5-HT₃ Antagonists Ondansetron and Granisetron in Feline Ventricular Myocytes. *Br. J. Pharmacol.* 113(2):527-535.
17. Wyllie DJA & Chen PE (2007) Taking the time to study competitive antagonism. *Br. J. Pharmacol.* 150(5):541-551.
18. Barnes NM, Hales TG, Lummis SCR, & Peters JA (2009) The 5-HT₃ receptor - the relationship between structure and function. *Neuropharmacology* 56(1):273-284.
19. Rojas C, *et al.* (2008) Palonosetron exhibits unique molecular interactions with the 5-HT₃ receptor. *Anesth. Analg.* 107(2):469-478.
20. Ito H, *et al.* (1995) Comparative Study of the Affinities of the 5-HT₃ Receptor Antagonists, YM060 YM114 (KAE-393), Granisetron and Ondansetron in Rat Vagus Nerve and Cerebral Cortex. *Neuropharmacology* 34(6):631-637.
21. Kilpatrick GJ, Butler A, Burridge J, & Oxford AW (1990) 1-(m-Chlorophenyl)-Biguanide, a Potent High-Affinity 5-HT₃ Receptor Agonist. *Eur. J. Pharmacol.* 182(1):193-197.
22. Miles TF, Bower KS, Lester HA, & Dougherty DA (2012) A Coupled Array of Noncovalent Interactions Impacts the Function of the 5-HT₃A Serotonin Receptor in an Agonist-Specific Way. *ACS Chem. Neurosci.* 3(10):753-760.
23. Xiu XA, Puskar NL, Shanata JAP, Lester HA, & Dougherty DA (2009) Nicotine binding to brain receptors requires a strong cation- π interaction. *Nature* 458(7237):534-U510.
24. Dougherty DA (2008) Physical organic chemistry on the brain. *J Org Chem* 73(10):3667-3673.
25. Dougherty DA (2008) Cys-loop neuroreceptors: structure to the rescue? *Chem Rev* 108(5):1642-1653.
26. Choi-Sledeski Y-M, *et al.* (2011) Preparation of aminomethylphenylpiperidiny-indolylmethanone derivatives for use as tryptase inhibitors. Patent WO 2011022449.
27. Ricci A & Fochi M (2003) Reactions between organomagnesium reagents and nitroarenes: Past, present, and future. *Angew. Chem.-Int. Edit.* 42(13):1444-1446.
28. Gilchrist TL, Lingham DA, & Roberts TG (1979) Ethyl 3-Bromo-2-hydroxyiminopropanoate, a Reagent for the Preparation of Ethyl Esters of Alpha-Amino Acids. *J. Chem. Soc.-Chem. Commun.* (23):1089-1090.
29. Nowak MW, *et al.* (1998) In vivo incorporation of unnatural amino acids into ion channels in *Xenopus* oocyte expression system. *Methods Enzymol.* 293:504-529.

Chapter 3

Continuing Studies of 5-HT₃A

3.1 ABSTRACT

The serotonin type 3 receptor (5-HT₃R) is a ligand-gated ion channel that mediates fast synaptic transmission in the central and peripheral nervous systems. The 5-HT₃R is a therapeutic target, and the clinically available drugs ondansetron and granisetron inhibit receptor activity. Their inhibitory action is through competitive binding to the native ligand binding site, and Chapter 2 established a binding orientation. In this chapter, mouse 5-HT₃A receptors are heterologously expressed in *Xenopus* oocytes using unnatural amino acid mutagenesis to probe for other interactions in the ligand binding pocket. No substantive interactions for inhibition were found for granisetron and ondansetron. During the course of these studies, an interesting interaction between the partial agonist *meta*-chlorophenylbiguanide and 5-HT₃A was discovered.

3.2 INTRODUCTION

The work in Chapter 2 established a cation- π interaction for the antiemetic drugs granisetron and ondansetron (Figure 3.1) with tryptophan 183 (W183, TrpB) of the serotonin type 3A (5-HT₃A) receptor. Although this work established a binding orientation of granisetron and ondansetron, it only established one direct interaction to the 5-HT₃AR. The soluble acetylcholine binding protein (AChBP) found in the snail cholinergic synapse is homologous to the extracellular ligand-binding domain of 5-HT₃A.¹ A high resolution x-ray structure of AChBP from *Aplysia californica* in complex with the ligand tropisetron (Figure 3.2) shows a cation- π interaction at both TrpB and Tyrosine C2 (TyrC2, Y234 in 5-HT₃A).² A more recent structure of AChBP with granisetron also shows a cation- π with TrpB and TyrC2.³ With the binding orientation of ondansetron and granisetron established, we sought to determine additional interaction(s) to 5-HT₃A, including a possible cation- π interaction at TyrC2.

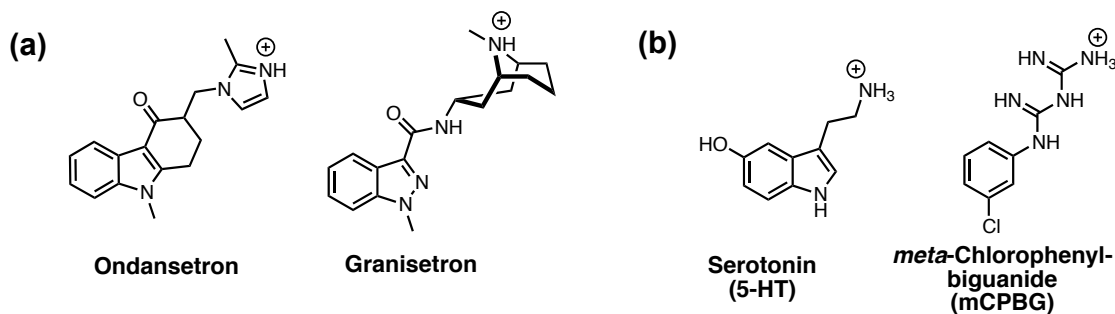


Figure 3.1. Chemical structures of drugs used in this study. (a) 5-HT₃AR antagonists. (b) 5-HT₃AR agonists.

In probing a cation- π interaction at a tyrosine residue, one must consider that direct fluorination results in decreasing pK_a of the side chain hydroxyl group; the pK_a of tyrosine is 10.0 while the pK_a of tetrafluorotyrosine is 5.3.⁴ While it is possible for receptor function to be unaffected by this shift in pK_a (e.g. Nowak *et al.*⁵), determining

functional changes resulting from a cation- π interaction versus hydroxyl ionization is not straightforward. To circumvent this complication, one strategy is to mutate the tyrosine to a phenylalanine, which is then successively fluorinated. Although this strategy simplifies cation- π analysis, there may be functional consequences resulting from removal of a hydrogen bond acceptor/donor.

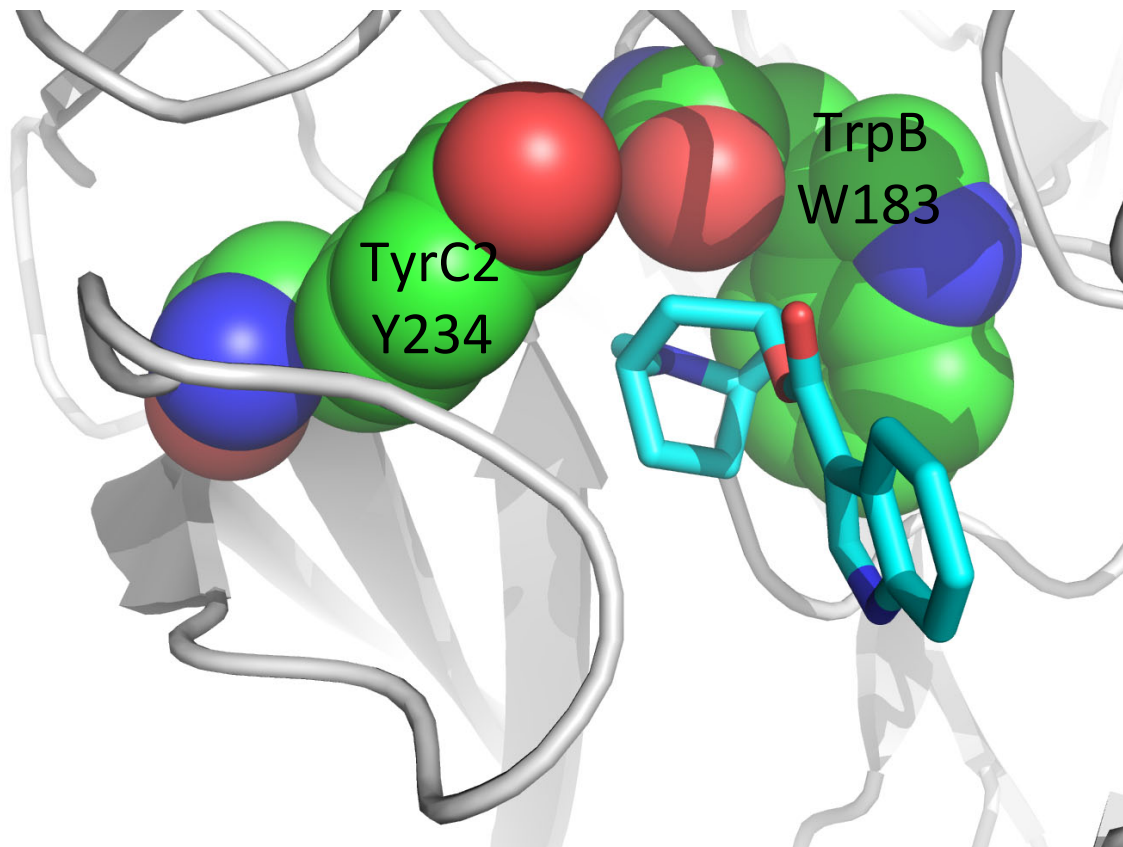


Figure 3.2. Crystal structure of tropisetron binding to *Aplysia californica* AChBP (PDB 2WNC). Detail of tropisetron cation- π interactions with TyrC2 and TrpB (Y234 and W183 in 5-HT₃A numbering) and TrpB backbone carbonyl shown.

In 5-HT₃A, TyrC2 has been previously studied with the agonist serotonin (5-HT, Figure 3.1).⁶ The concentration of agonist required to achieve 50% of the maximum signal (EC₅₀) could not be measured for the full complement of fluorinated phenylalanine mutations; only the EC₅₀ 4-F-Phe could be determined. Measurement of a possible

cation- π for ondansetron and granisetron with only two data points (Phe and 4-FPhe) would not be very compelling, and so a twofold strategy was employed. First, the partial agonist *meta*-chlorophenylbiguanide (mCPBG, Figure 3.1) has been shown to make different interactions with 5-HT₃A than 5-HT,⁷ and so EC₅₀ measurements of fluorinated phenylalanines using mCPBG were attempted. Second, other mutations beyond fluorinated phenylalanines were made to probe for a cation- π interaction (Figure 3.3). These efforts resulted in interesting insights into the binding of mCPBG directly, which were explored independently from antagonist binding.

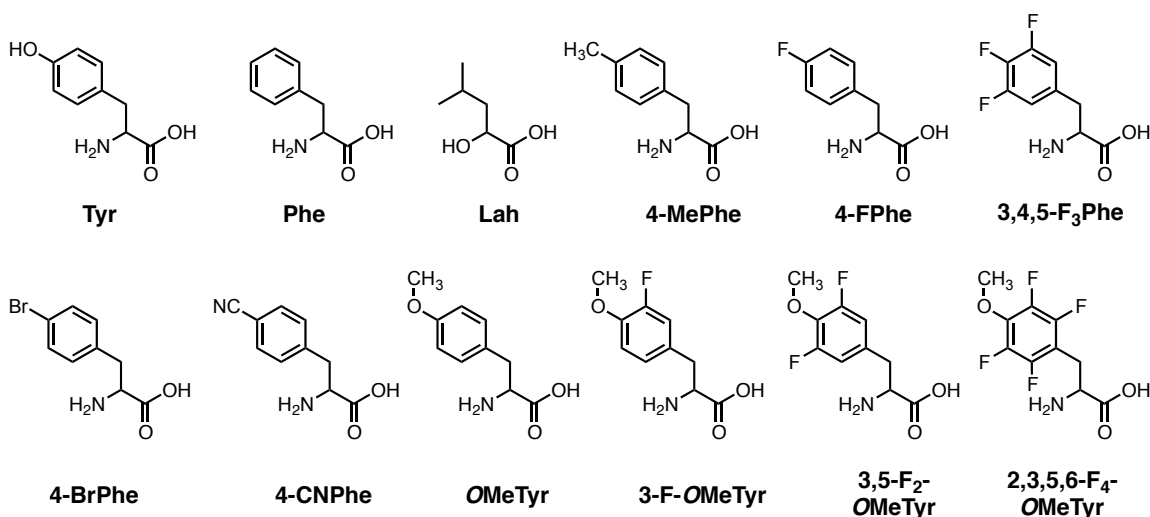


Figure 3.3. Chemical structures of the natural and unnatural amino acids used in this study.

In addition to the putative cation- π interaction at TyrC2, both 5-HT₃A antagonist-containing AChBP crystal structures show a hydrogen bond between the ligand and the backbone carbonyl of TrpB.^{2,3} The functional importance of this interaction was also examined. The strategy employed for this measurement was conversion of the backbone amide to a backbone ester. This amide to ester mutation was made by nonsense suppression of the N+1 residue using an α -hydroxy acid in place of an α -amino acid.⁸

As in Chapter 2, the functional data collected for the antagonists is the concentration required to inhibit 50% of the signal (IC_{50}) generated from application of 2-fold the EC_{50} of an agonist. When possible, an IC_{50} is separately measured for a particular mutant receptor using 5-HT and mCPBG to control for possible effects of the agonist behavior.⁹

3.3 RESULTS AND DISCUSSION

3.3.1 Interactions of Ondansetron and Granisetron with 5-HT_{3A}. At TyrC2, mutation to 3,5-F₂Phe and 3,4,5-F₃Phe results in no detectable signal from 5-HT as the agonist. Fortunately, fluorine is not the only electron-withdrawing group at our disposal. Installation of a cyano group onto a benzene ring reduces the calculated cation- π binding ability of the ring to a gas phase sodium ion (Na^+) to 15.7 kcal/mol from 27.1 kcal/mol, which is less deactivating towards binding than F₃-benzene (12.4 kcal/mol), but more deactivating than F₂-benzene (16.8 kcal/mol).¹⁰ A cyano group, however, is larger than a fluorine, so steric effects may be observed in a receptor experiment. The sterically similar bromo group, which is less deactivating (21.6 kcal/mol) than cyano, can be used to test for a possible steric perturbation.

When 5-HT is the agonist, the IC_{50} for granisetron at TyrC2 with 4-BrPhe is essentially wild type, with only a 1.4-fold loss of inhibition (Table 3.1). For ondansetron, the IC_{50} for 4-BrPhe is also wild type. In order to take into account possible steric effects, 4-BrPhe rather than the wild type receptor is used as the reference point when examining the change in cation- π binding ability. Mutation of TyrC2 to 4-CN-Phe slightly reduces the inhibition of granisetron and ondansetron by 2.2-fold and 1.8-fold, respectively, from 4-BrPhe (Table 3.2). From these data alone, we would not consider electrostatics at TyrC2 to play a significant role in the function of granisetron and ondansetron. For

example, acetylcholine makes a cation- π interaction with TrpB (W149) of the muscle nicotinic acetylcholine receptor (nAChR), and the loss of function in going from 5-BrTrp to 5-CNTrp is 57-fold.¹¹

Table 3.1. IC₅₀ data for wild type and mutant 5-HT₃AR for granisetron and ondansetron in response to 5-HT or mCPBG.

Antagonist	Agonist	Mutation	N ^a	IC ₅₀ (nM) ^b	Fold Shift ^c	Hill ^d
Granisetron	5HT	Wild Type	27	0.78 ± 0.04	-	-1.40 ± 0.08
		Y234 4-BrPhe	13	1.06 ± 0.06	1.4	-1.5 ± 0.1
		Y234 4-CNPhe	13	2.3 ± 0.2	2.9	-1.5 ± 0.1
		L184 Lah	12	2.52 ± 0.08	3.2	-2.0 ± 0.1
	mCPBG	Wild Type	27	1.51 ± 0.07	-	-1.49 ± 0.09
		Y234 4-BrPhe	14	0.24 ± 0.04	1 / 6.3	-1.1 ± 0.2
		Y234 4-CNPhe	5	2.6 ± 0.1	1.7	-1.40 ± 0.08
Ondansetron	5HT	Wild Type	21	0.87 ± 0.04	-	-1.56 ± 0.09
		Y234 4-BrPhe	10	0.90 ± 0.06	1.0	-1.18 ± 0.08
		Y234 4-CNPhe	14	1.58 ± 0.08	1.8	-1.47 ± 0.08
		L184 Lah	8	3.8 ± 0.2	4.4	-1.8 ± 0.2
	mCPBG	Wild Type	23	0.91 ± 0.04	-	-1.47 ± 0.08
		Y234 4-BrPhe	12	0.22 ± 0.04	1 / 4.1	-1.1 ± 0.2
		Y234 4-CNPhe	7	1.78 ± 0.08	2.0	-1.30 ± 0.06

^aNumber of oocytes averaged in IC₅₀ determination. ^bThe effective concentration for half-maximal receptor inhibition. ^cIC₅₀(mutant)/IC₅₀(wild type). ^dThe Hill coefficient, n_H , as determined from fitting the Hill equation.

The inhibition of granisetron and ondansetron at TyrC2 was then examined using mCPBG as the agonist (Table 3.1). Both antagonists were better at inhibiting the 4-BrPhe mutant receptor than the wild type receptor by 6.3-fold for granisetron and 4.1-fold for ondansetron. Converting 4-BrPhe into 4-CNPhe reduced the ability of granisetron and ondansetron to inhibit the receptor by 11-fold and 8.1-fold, respectively (Table 3.2). Considering these data independently from the IC₅₀ data using 5-HT, there is a slight electrostatic dependence of the inhibitory ability of the antagonists to TyrC2. This electrostatic dependence is not as strong as one would expect if TyrC2 were the primary determinant of binding, and can be contrasted to the strong electrostatic dependence of inhibition measured for TrpB in Chapter 2.

Table 3.2. Fold shift of antagonist IC₅₀ referenced to 4-BrPhe.

Antagonist	Agonist	Mutation	IC ₅₀ (nM) ^a	Fold Shift ^b
Granisetron	5HT	Y234 4-BrPhe ^c	1.06 ± 0.06	-
		Y234 4-CNPhe	2.3 ± 0.2	2.2
	mCPBG	Y234 4-BrPhe ^c	0.24 ± 0.04	-
		Y234 4-CNPhe	2.6 ± 0.1	11
Ondansetron	5HT	Y234 4-BrPhe ^c	0.90 ± 0.06	-
		Y234 4-CNPhe	1.58 ± 0.08	1.8
	mCPBG	Y234 4-BrPhe ^c	0.22 ± 0.04	-
		Y234 4-CNPhe	1.78 ± 0.08	8.1

^aIC₅₀ data from Table 3.1. ^b IC₅₀(mutant)/IC₅₀(reference). ^cReference IC₅₀ value used in place of wild type.

Examining the TyrC2 results of granisetron and ondansetron when using the agonists 5-HT and mCPBG independently, one might come to different conclusions—namely, a lack of electrostatic dependence versus a weak electrostatic dependence. This reiterates the discussion in Chapter 2 regarding the importance of having two distinct agonists to evaluate an antagonist. In examining the electrostatic dependence of inhibition at TrpB, the analysis benefited from the *trend* of many mutations. In the case of TyrC2, we are limited to comparing a single mutation pair. To better understand the discrepancy of the 5-HT and mCPBG results, it is worth discussing the magnitude of the discrepancy. The fold-shift discrepancy (FSD) will be defined as the ratio of the mutation pair fold-shift for one agonist to the mutation pair fold-shift to the second agonist, e.g.

$$FSD = \frac{IC_{50}(\text{mutant, agonist 1}) / IC_{50}(\text{reference, agonist 1})}{IC_{50}(\text{mutant, agonist 2}) / IC_{50}(\text{reference, agonist 2})}$$

Starting with granisetron, the TyrC2 IC₅₀ fold shift of 4-CNPhe/4-BrPhe goes from 2.2-fold using 5-HT to 11-fold using mCPBG, resulting in a FSD of 5-fold comparing mCPBG over 5-HT. For ondansetron, the IC₅₀ for 4-CNPhe/4-BrPhe is 1.8-fold using 5-HT to 8.1-fold using mCPBG, giving a FSD of 4.5-fold. These FSD values are close to

the FSD values measured in Chapter 2. For example, for granisetron at TrpD (W90), the FSD for 4,5,6,7-F₄Trp/Trp is 3.3 comparing mCPBG over 5-HT. For the IC₅₀ values measured thus far, this variability in the data is common. These data indicate that interpretations of small shifts in IC₅₀ should be made with caution; even an 11-fold 4-CNPhe/4-BrPhe ratio for TyrC2 may be insufficient to claim an electrostatic effect.

The backbone carbonyl of TrpB (W183) was then examined by mutation of L184 to the corresponding α -hydroxy acid of leucine (Lah, Table 3.1). The mutation L184Lah is known to completely abolish agonist activity for mCPBG,⁷ so the IC₅₀ values for granisetron and ondansetron could only be made using 5-HT as the agonist. The L184Lah fold-shifts for granisetron and ondansetron are 3.2-fold and 4.4-fold, respectively. These shifts are fairly small compared to previous measurements, e.g. in the nAChR subtype (α 4)₃(β 2)₂ the fold-shift for the drug cytosine is 27-fold.¹² This relatively small fold-shift shows a hydrogen bond to the backbone carbonyl of TrpB is not a strong functional determinant for inhibition of 5-HT₃A.

3.3.2 Examination of agonists 5-HT and mCPBG at TyrC2. Considering the results of our studies of granisetron and ondansetron with TyrC2, fluorinated phenylalanine mutations were reexamined using 5-HT. As shown in Table 3.3, removal of the 4-hydroxy substituent by mutation of Tyr to Phe resulted in a 7-fold loss of function. The loss of function in replacement of the 4-hydroxy with a 4-methyl was too small to be considered significant, indicating that the hydrogen-bonding features of an alcohol are not important for channel function with 5-HT. This point is recapitulated by the wild type behavior of 4-BrPhe. As seen in previous studies,⁶ mutation to 4-FPhe gave a measureable EC₅₀, but 3,5-F₂Phe did not respond to 5-HT. It was reasoned that the lack

of a 4-position substituent, along with the change in ring electronic structure, was the cause of non-responsive receptors.⁶

Table 3.3. EC₅₀ data for wild type and mutant 5-HT₃AR in response to 5-HT or mCPBG.

Agonist	Mutation	N ^a	EC ₅₀ (μM) ^b	Fold Shift ^c	Hill ^d
5HT	Wild Type	25	1.57 ± 0.05	-	2.1 ± 0.16
	Y234 Phe	11	10.9 ± 0.6	6.9	2.0 ± 0.2
	Y234 4-MePhe	16	2.7 ± 0.1	1.7	1.9 ± 0.1
	Y234 4-F1Phe	10	6.3 ± 0.2	4.0	2.1 ± 0.1
	Y234 3,5-F2Phe	16	NR ^e	-	-
	Y234 3,4,5-F3Phe	8	NR ^e	-	-
	Y234 4-BrPhe	14	1.48 ± 0.04	1 / 1.1	1.9 ± 0.1
	Y234 4-CNPh	15	20.8 ± 0.8	13	2.4 ± 0.2
	Y234 OMeTyr	8	2.6 ± 0.1	1.7	1.8 ± 0.1
	Y234 3-F-OMeTyr	6	10.7 ± 0.6	6.8	1.9 ± 0.2
	Y234 3,5-F2-OMeTyr	28	NR ^e	-	-
	Y234 2,3,5,6-F4-OMeTyr	8	NR ^e	-	-
	L184 Lah	15	14.7 ± 0.4	9.4	2.11 ± 0.09
mCPBG	Wild Type	9	0.50 ± 0.02	-	2.2 ± 0.1
	Y234 Phe	13	8.8 ± 0.4	18	1.62 ± 0.09
	Y234 4-MePhe	13	0.87 ± 0.04	1.7	1.40 ± 0.07
	Y234 4-F1Phe	15	1.6 ± 0.1	3.2	2.1 ± 0.3
	Y234 3,5-F2Phe	16	NR ^e	-	-
	Y234 3,4,5-F3Phe	7	16 ± 1	32	2.0 ± 0.2
	Y234 4-BrPhe	9	0.049 ± 0.002	1 / 10	3.5 ± 0.7
	Y234 4-CNPh	14	0.63 ± 0.02	1.3	1.9 ± 0.1
	Y234 OMeTyr	19	0.06 ± 0.002	1 / 8.3	4.1 ± 0.5
	Y234 3-F-OMeTyr	7	0.10 ± 0.01	1 / 5	3.0 ± 0.5
	Y234 3,5-F2-OMeTyr	10	4.8 ± 0.3	9.6	2.1 ± 0.3
	Y234 2,3,5,6-F4-OMeTyr	8	NR ^e	-	-

^aNumber of oocytes averaged in EC₅₀ determination. ^bThe effective concentration for half-maximal receptor activation. ^cEC₅₀(mutant)/EC₅₀(wild type). ^dThe Hill coefficient, n_H , as determined from fitting the Hill equation. ^eNo measurable response

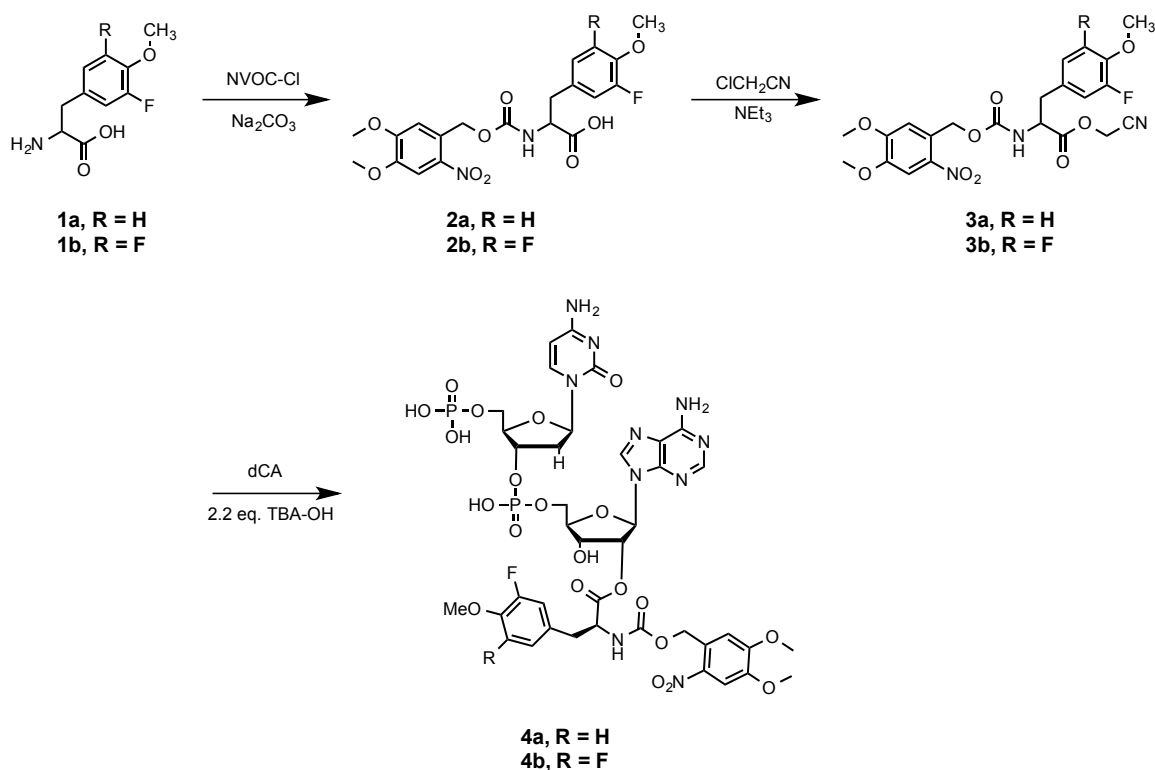
TyrC2 was then examined using mCPBG as the agonist (Table 3.3). Like 5-HT, removal of the 4-hydroxy by mutation to Phe resulted in a loss in channel function, although to a larger extent (18-fold). Replacement of the 4-hydroxy substituent with a 4-methyl gives nearly wild type behavior for mCPBG, which indicates the need of a 4-position substituent. As with 5-HT, mutation to 3,5-F₂Phe (which lacks a 4-position substituent) gave no response to mCPBG. Interestingly, 3,4,5-F₃Phe gave a measureable

EC₅₀ of 16 μ M, while remaining unresponsive to 5-HT. It has been previously shown that mCPBG does not make a cation- π interaction at TrpB.⁷ Such an interaction may exist at TyrC2, but determination with competing steric effects adds an additional challenge.

Mutation of TyrC2 to 4-BrPhe results in a 10-fold *gain* of function for mCPBG. Wild type function is measured for 4-CNPhe, but when referenced to 4-BrPhe the 4-CN substituent causes a 13-fold increase in EC₅₀. In addition to the importance of sterics of the 4-position, the polarity of the substituent also plays a role. These data provided the motivation to attempt a series of unnatural amino acids that were previously untested in the Dougherty group—namely successive fluorination of tyrosine residues in which the 4-hydroxyl has been methylated.

The amino acids 3-F-OMeTyr and 3,5-F₂-OMeTyr were purchased and used without purification. The amino group was protected by 6-nitroveratryl chloroformate, followed by formation of the cyanomethyl ester (Scheme 3.1). Coupling to deoxycytidine-adenosine (dCA) and then ligation by enzymatic T4 ligase as previously described¹³ gave suitable tRNA for unnatural amino acid mutagenesis. The amino acid 2,3,5,6-F₄-OMeTyr was kindly provided by Matthew Rienzo.

Scheme 3.1.



Evidence for a cation- π interaction in a receptor is often obtained by a ‘fluorination plot’ in which the *ab initio* quantum mechanical binding energy of Na^+ to the π face of the ring system is plotted against the log of the functional change in EC_{50} .¹¹ In preparation for construction of such a plot, the Na^+ binding energies of the fluorinated tyrosines were calculated at the 6-311G** level using Spartan 08.¹⁴ Electrostatic potential surfaces were calculated and contoured to -25 to +25 kcal/mol (Figure 3.4).¹⁵ The cation- π binding energies of the *O*-methylated Tyr amino acids start at 27.3 kcal/mol for *OMeTyr*, and remain weakly attractive to Na^+ in the fully fluorinated 2,3,5,6-F₄-*OMeTyr* at 12.6 kcal/mol (similar to 3,4,5-F₃Phe at 12.4 kcal/mol).

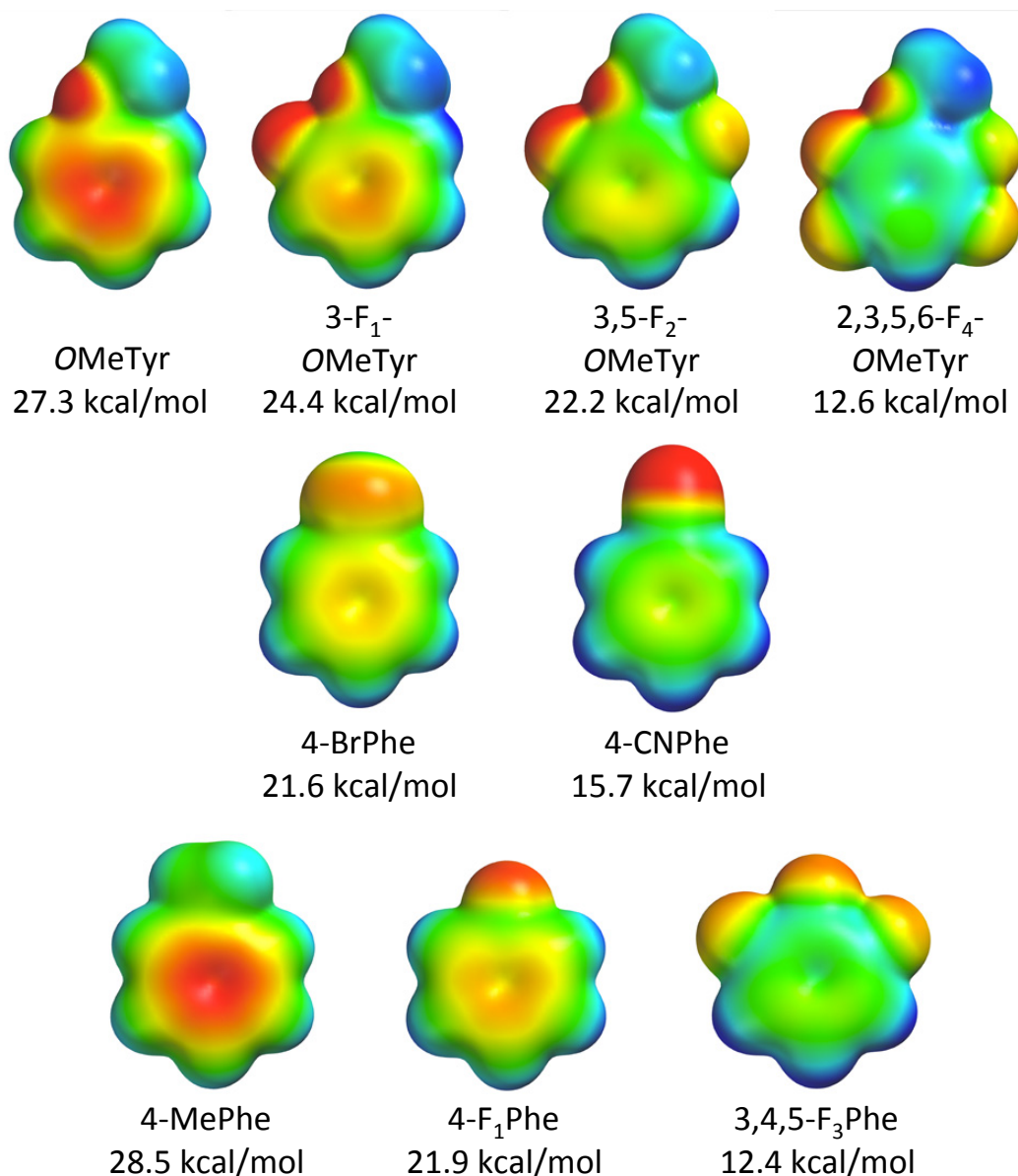


Figure 3.4. *Ab initio* 6-311G** electrostatic potential surfaces of side chains corresponding to unnatural amino acids. Calculated binding energies of a gas phase Na⁺ are shown for each ring system. Red signifies a value greater than or equal to the maximum in negative potential (-25 kcal/mol), and blue signifies a value greater than or equal to the maximum in positive potential (+25 kcal/mol).

Mutation of TyrC2 to OMeTyr results in a 8.3-fold *gain* of function for mCPBG, which reinforces the notion that both polarity and size is important at the 4-position. Using OMeTyr as the reference point, a single fluorine (3-F-OMeTyr) results in a small 1.7-fold loss of function, and two fluorines (3,5-F₂-OMeTyr) results in a large 63-fold

loss of function. In addition to the loss of function (EC_{50}), the expression levels of 3,5-F₂-OMeTyr at TyrC2 are very low; extended oocyte incubation times (48 hours vs. 24 hours) and doubling mRNA/tRNA injections gives receptors that average ~100 nA of response (vs. multiple μ A for other unnatural amino acid mutations). This low level of measureable signal precludes the use of 3,5-F₂-OMeTyr for determination of antagonist binding. No signal was detected for mCPBG or 5-HT when 2,3,5,6-F₄-OMeTyr was installed at TyrC2.

The steric and polar requirements for substituents at the 4-position of TyrC2 complicate the analysis of a possible cation- π interaction. Two fluorination plots were constructed using different reference amino acids, but each mutation contains a substituent in the 4-position. The first plot (Figure 3.5a) was constructed referencing 4-MePhe, and contains the hydrophobic residues 4-FPhe and 3,4,5-F₃Phe (Table 3.4). The second plot (Figure 3.5b) was constructed using OMeTyr as the reference, and contains the mutations with polar groups in the 4-position (3-F-OMeTyr; 3,5,-F₂-OMeTyr; 4-CNPhe; 4-BrPhe; Table 3.4).

Table 3.4. Fold Shift of EC_{50} data referenced to 4-MePhe or OMeTyr.

Agonist	Mutation	EC_{50} (μ M) ^a	Fold Shift ^b
mCPBG	Y234 4-Me-Phe ^c	0.87 \pm 0.04	-
	Y234 4-F1-Phe	1.6 \pm 0.1	1.8
	Y234 3,4,5-F3-Phe	16 \pm 1	18
mCPBG	Y234 OMeTyr ^d	0.06 \pm 0.002	-
	Y234 3-F-OMeTyr	0.10 \pm 0.01	1.7
	Y234 3,5-F2-OMeTyr	4.8 \pm 0.3	80
	Y234 4-Br-Phe	0.049 \pm 0.002	0.82
	Y234 4-CN-Phe	0.63 \pm 0.02	11

^a EC_{50} data from Table 3.3. ^b $EC_{50}(\text{mutant})/EC_{50}(\text{reference})$. ^cReference EC_{50} value used in place of wild type for hydrophobic substituents in the 4-position. ^dReference EC_{50} value used in place of wild type for polar substituents in the 4-position.

The “hydrophobic” fluorination plot in Figure 3.5a is indicative of a cation- π interaction for mCPBG at TyrC2, albeit with a small number of measurements. The “polar” fluorination plot in Figure 3.5b follows a similar trend with 3-F-OMeTyr and 4-CNPhe, but both 4-BrPhe and 3,5-F₂-OMeTyr are considerably outside the trend. The slope of the fit for a fluorination plot has been interpreted to correlate with the strength of a cation- π interaction.¹⁶ The equivalent slopes of both fluorination plots suggests the measurement of the same interaction: the biguanide cation of mCPBG with TyrC2. The same slope in both fluorination plots also justifies the construction of the third fluorination plot in Figure 3.5c. In this plot, the same reference amino acids for polar and hydrophobic groups in the 4-position are used; however, the fit includes all points from both fluorination plots in Figure 3.5a and Figure 3.5b. This combined fluorination plot gives evidence that a cation- π interaction plays a functional role for mCPBG with TyrC2, and the scatter in measurements are from imperfect control of substituent effects in the 4-position.

The cation- π interaction for mCPBG at TyrC2 is atypical; for cation selective Cys-loop channels agonists tend to make a cation- π with a Trp rather than a Tyr.¹⁷ The native agonist 5-HT follows this trend by making a cation- π with TrpB. This again shows that mCPBG and 5-HT uniquely respond to structural changes within the 5-HT₃A binding site.

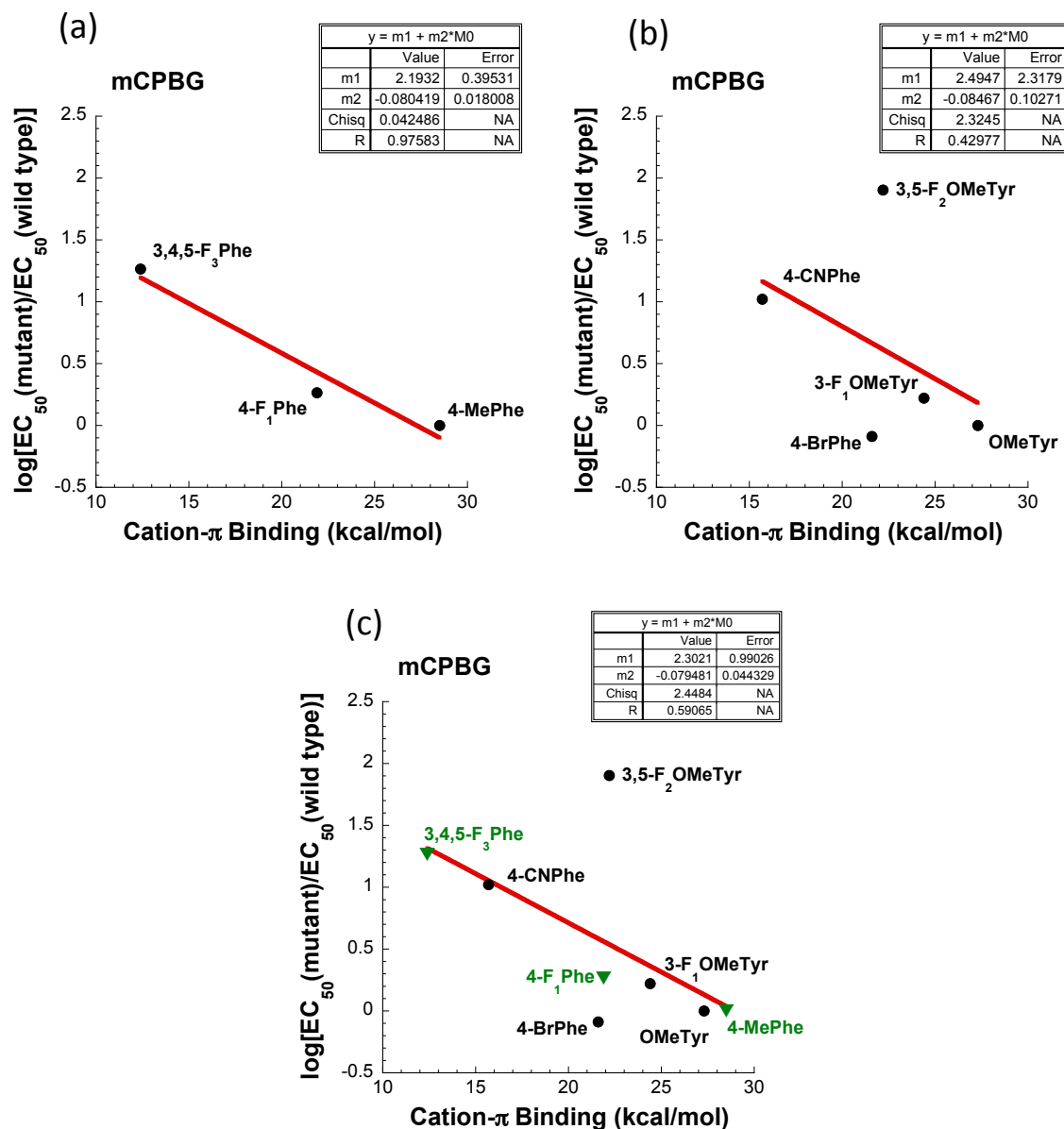


Figure 3.5. “Fluorination plots” of 5-HT₃AR mutagenesis. The horizontal axis is the calculated cation- π binding energy (kcal/mol) values from Figure 3.4. The vertical axis is the log of fold shift values from Table 3.4. Linear fits of the data shown; inset is the fit parameters. (a) Fit of hydrophobic 4-position residues referenced to 4-MePhe. (b) Fit of polar 4-position residues referenced to OMeTyr. (c) Fit containing all points from (a) and (b) while maintaining respective reference residues.

3.4 SUMMARY

Slight changes in inhibition were found when probing TyrC2 and the backbone carbonyl of TrpB for the antagonists granisetron and ondansetron. These small changes

in IC₅₀ indicate these sites are not primary determinants of inhibition for 5-HT_{3A}. In probing for antagonist interactions, an interesting binding mode for the partial agonist mCPBG was discovered: a cation- π interaction between mCPBG and TyrC2, which is distinct from the native agonist 5-HT. This interaction illustrates the differing requirements of 5-HT and mCPBG for activation of 5-HT_{3A}.

3.5 METHODS

Procedures for incorporating unnatural amino acids, expressing receptors in *Xenopus* oocytes, and characterization by electrophysiology followed established protocols.¹³

3.5.1 Protein Expression in *Xenopus* Oocytes. The mouse 5-HT_{3A} receptor in the pGEMHE vector was linearized with the restriction enzyme *Sbf* I (New England Biolabs). mRNA was prepared by *in vitro* transcription using the mMessage Machine T7 kit (Ambion). Unnatural mutations were introduced by the standard Stratagene QuickChange protocol using a TAG mutation at W183 and W90. Stage V-VI *Xenopus laevis* oocytes were injected with mRNA. Each cell was injected with 50 nL containing only mRNA (5 ng) for wild type 5-HT_{3A}AR or a mixture of mRNA (5-32 ng, typically ~12 ng) and tRNA (18-30 ng, typically ~18 ng) for unnatural amino acids. Uncharged full length tRNA was injected as a negative control.

3.5.2 Electrophysiology. Electrophysiological experiments were performed 24-48 hours after injection using the OpusXpress 6000A instrument (Axon Instruments) in two-electrode voltage clamp mode at a holding potential of -60 mV. The running buffer was Ca²⁺-free ND96 solution (96 mM NaCl, 2 mM KCl, 1 mM MgCl₂ and 5 mM HEPES, pH 7.5). Serotonin hydrochloride (5-HT) was purchased from Alfa Aesar. 1-(3-

Chlorophenyl)biguanide (mCPBG) was purchased from Sigma-Aldrich. Granisetron hydrochloride and ondansetron hydrochloride were purchased from Tocris Bioscience.

For EC₅₀ determinations, oocytes were superfused with running buffer at 1 mL/min for 30 s before application of 5-HT or mCPBG for 15 s followed by a 116 s wash with the running buffer. Data were sampled at 125 Hz and filtered at 50 Hz. Dose-response data were obtained for ≥ 9 concentrations of 5-HT or mCPBG on ≥ 6 cells. All EC₅₀ and Hill coefficient values were obtained by fitting dose-response relations to the Hill equation ($I_{\text{norm}} = 1 / [1 + (EC_{50}/[\text{agonist}])^n]$), and are reported as means \pm standard error of the fit.

For IC₅₀ determinations, oocyte response to either 5-HT or mCPBG at 2 x EC₅₀ for each receptor was measured before application of antagonists by application of the agonist for 15 s, followed by 116 s of wash with the running buffer. Granisetron or ondansetron doses were then pre-applied and the oocyte allowed to incubate for 60 s, followed by application of a mixture of the antagonist dose with 5-HT or mCPBG at 2-fold EC₅₀. The oocytes were then washed with the running buffer for 116 s. Every 4 antagonist doses, the oocytes were washed for 10 min, and oocyte response reconfirmed using either 5-HT or mCPBG at 2-fold EC₅₀. Oocytes that did not give consistent responses to 5-HT or mCPBG alone throughout the experiment were discarded. Dose-response data were obtained for ≥ 8 concentrations of granisetron or ondansetron on ≥ 5 cells. All EC₅₀ and Hill coefficient values were obtained by fitting Dose-response relations to the Hill equation ($I_{\text{norm}} = 1 / [1 + (EC_{50}/[\text{antagonist}])^n]$), and are reported as means \pm standard error of the fit.

3.5.3 Synthesis. *NVOC-3-F-4-OMe-DL-phenylalanine (2a)*. In a round bottom flask, 3-F-4-OMe-DL-phenylalanine (100.7 mg, 0.472 mmol) was dissolved in 20 mL of 1:1

THF:water, and 101.8 mg of Na_2CO_3 (0.960 mmol), and 171.3 mg of 4,5-dimethoxy-2-nitrobenzyl chloroformate (0.621 mmol) were added. The reaction was stirred at room temperature for 4.5 h. The reaction was concentrated to ~10 mL under reduced pressure, followed by dilution with 10 mL H_2O . The reaction was extracted 2 x 10 mL of CH_2Cl_2 and the organic phases discarded. The aqueous phase was acidified to ~pH 2 with 1 N HCl and extracted 2 x 10 mL of CH_2Cl_2 . The organic phase was separated, washed with brine, and dried over Na_2SO_4 . During slow concentration under reduced pressure, crystallization was induced to recover 66 mg (31%) of the desired product. Additional material present in mother liquor could be recovered if desired. ^1H NMR (300 MHz, CDCl_3): δ 7.67 (s, 1H), 7.00 – 6.81 (m, 5H), 5.49 (s, 2H), 4.64 (dt, J = 8.3, 5.9 Hz, 1H), 3.92 (s, 3H), 3.90 (s, 3H), 3.84 (s, 3H), 3.15 (dd, J = 14.3, 5.4 Hz, 1H), 3.02 (dd, J = 14.3, 6.6 Hz, 1H). ^{19}F NMR (282 MHz, CDCl_3) δ -134.72 (m). ESI-MS(+) m/z for $\text{C}_{20}\text{H}_{21}\text{FN}_2\text{NaO}_9$ found 471.1, calculated 475.1 ($\text{M}+\text{Na}^+$).

NVOC-3,5-F₂-4-OMe-DL-phenylalanine (2b). In a round bottom flask, 3,5-F₂-4-OMe-DL-phenylalanine (102.7 mg, 0.444 mmol) was dissolved in 20 mL of 1:1 THF:water, and 94.5 mg of Na_2CO_3 (0.892 mmol), and 159.7 mg of 4,5-dimethoxy-2-nitrobenzyl chloroformate (0.579 mmol) were added. The reaction was stirred at room temperature for 15.5 h. The reaction was concentrated under reduced pressure, followed by dilution with 15 mL H_2O . The reaction was extracted 3 x 10 mL of CH_2Cl_2 and the organic phases discarded. The aqueous phase was acidified to ~pH 2 with 1 N HCl and extracted 1 x 10 mL of CH_2Cl_2 . The emulsion was broken by addition of EtOAc. The organic phase was separated, washed with brine, and dried over Na_2SO_4 . The solution was concentrated under reduced pressure, and the residue recrystallized from CH_2Cl_2 to give

the desired product (113 mg, 54%). Additional material present in mother liquor could be recovered if desired. Material carried on to the next step without characterization.

NVOC-3-F-4-OMe-DL-phenylalanine cyanomethyl ester (3a). Compound **2a** (66mg, 0.146 mmol) was dissolved in 1 mL (15.8 mmol) of chloroacetonitrile and 100 μ L (0.721 mmol) of triethylamine was added. The reaction was allowed to stir at room temperature for 28 h. After evaporating to dryness under high vacuum, the crude material was purified by silica gel chromatography eluting with 1:1 EtOAc/hexanes to yield 71.8 mg (100%) of the desired product. ^1H NMR (300 MHz, CDCl_3) δ 7.71 (s, 1H), 6.94 (s, 1H), 6.93 – 6.83 (m, 3H), 5.57 (d, J = 15.0 Hz, 1H), 5.48 (d, J = 14.7 Hz, 1H), 5.26 (d, J = 8.3 Hz, 1H), 4.84 (d, J = 15.7 Hz, 1H), 4.70 (d, J = 15.7 Hz, 1H), 4.72 – 4.65 (m, 1H), 3.97 (s, 3H), 3.95 (s, 3H), 3.87 (s, 3H), 3.18 – 3.01 (m, 2H). ^{19}F NMR (282 MHz, CDCl_3) δ -134.19 (m)..

NVOC-3,5-F₂-4-OMe-DL-phenylalanine cyanomethyl ester (3b). Compound **2b** (113 mg, 0.240 mmol) was dissolved in 1 mL (15.8 mmol) of chloroacetonitrile and 150 μ L (1.08 mmol) of triethylamine was added. The reaction was allowed to stir at room temperature for 16.5 h. After evaporating to dryness under high vacuum, the crude material was purified by silica gel chromatography eluting with 1:1 EtOAc/hexanes to yield 115 mg (94%) of the desired product. ^1H NMR (300 MHz, $\text{DMSO}-d_6$) δ 8.16 (d, J = 8.1 Hz, 1H), 7.67 (s, 1H), 7.27 – 6.88 (m, 3H), 5.32 (s, 2H), 5.02 (s, 2H), 4.71 – 4.30 (m, 1H), 3.86 (br, 6H), 3.33 (s, 3H), 3.05 (dd, J = 13.8, 5.4 Hz, 1H), 2.98 – 2.78 (m, 1H). ^{19}F NMR (282 MHz, $\text{DMSO}-d_6$) δ -129.32 , -129.34. ESI-MS(+) m/z for $\text{C}_{22}\text{H}_{21}\text{F}_2\text{N}_3\text{NaO}_9$ found 532.2, calculated 532.1 ($\text{M}+\text{Na}^+$).

dCA- NVOC-3-F-4-OMe-DL-phenylalanine (4a). Compound **3a** (9.3 mg, 0.019 mmol) was dissolved in 0.5 mL of dry DMF and added to premixed dCA (5.9 mg, 0.009 mmol) and tetrabutylammonium hydroxide (4.2 mg, 0.021 mmol). The reaction was stirred under argon at room temperature for 18 h. It was diluted with 1:1 MeCN:water and purified by reverse phase HPLC running a gradient of 95% to 0% aq. NH₄OAc pH 4.5 in MeCN to obtain 2.4 mg (24%) of the desired product. HRMS ES(+) *m/z* for C₃₉H₄₅FN₁₀O₂₁P₂ found 1071.2289, calculated 1071.2293 (M+H).

dCA- NVOC-3,5-F₂-4-OMe-DL-phenylalanine (4b). Compound **3b** (10 mg, 0.019 mmol) was dissolved in 0.5 mL of dry DMF and added to premixed dCA (5.9 mg, 0.009 mmol) and tetrabutylammonium hydroxide (4.2 mg, 0.021 mmol). The reaction was stirred under argon at room temperature for 18 h. It was diluted with 1:1 MeCN:water and purified by reverse phase HPLC running a gradient of 95% to 0% aq. NH₄OAc pH 4.5 in MeCN to obtain 2.2 mg (22%) of the desired product. HRMS ES(+) *m/z* for C₃₉H₄₄F₂N₁₀O₂₁P₂ found 1089.2201, calculated 1089.2199 (M+H).

3.6 REFERENCES

1. Brejc K, *et al.* (2001) Crystal structure of an ACh-binding protein reveals the ligand-binding domain of nicotinic receptors. *Nature* 411(6835):269-276.
2. Hibbs RE, *et al.* (2009) Structural determinants for interaction of partial agonists with acetylcholine binding protein and neuronal alpha 7 nicotinic acetylcholine receptor. *EMBO J.* 28(19):3040-3051.
3. Kesters D, *et al.* (2013) Structural basis of ligand recognition in 5-HT₃ receptors. *EMBO Rep.* 14(1):49-56.
4. Thorson JS, Chapman E, Murphy EC, Schultz PG, & Judice JK (1995) Linear Free Energy Analysis of Hydrogen Bonding in Proteins. *J. Am. Chem. Soc.* 117(3):1157-1158.
5. Nowak MW, *et al.* (1995) Nicotinic Receptor Binding Site Probed with Unnatural Amino Acid Incorporation in Intact Cells. *Science* 268(5209):439-442.
6. Beene DL, Price KL, Lester HA, Dougherty DA, & Lummis SCR (2004) Tyrosine residues that control binding and Gating in the 5-hydroxytryptamine(3)

- receptor revealed by unnatural amino acid mutagenesis. *J. Neurosci.* 24(41):9097-9104.
7. Miles TF, Bower KS, Lester HA, & Dougherty DA (2012) A Coupled Array of Noncovalent Interactions Impacts the Function of the 5-HT(3)A Serotonin Receptor in an Agonist-Specific Way. *ACS Chem. Neurosci.* 3(10):753-760.
 8. England PM, Zhang YN, Dougherty DA, & Lester HA (1999) Backbone mutations in transmembrane domains of a ligand-gated ion channel: Implications for the mechanism of gating. *Cell* 96(1):89-98.
 9. Wyllie DJA & Chen PE (2007) Taking the time to study competitive antagonism. *Br. J. Pharmacol.* 150(5):541-551.
 10. Mecozzi S, West AP, & Dougherty DA (1996) Cation-pi interactions in simple aromatics: Electrostatics provide a predictive tool. *J. Am. Chem. Soc.* 118(9):2307-2308.
 11. Zhong WG, *et al.* (1998) From ab initio quantum mechanics to molecular neurobiology: A cation-pi binding site in the nicotinic receptor. *Proc. Natl. Acad. Sci. U. S. A.* 95(21):12088-12093.
 12. Tavares XDS, *et al.* (2012) Variations in Binding Among Several Agonists at Two Stoichiometries of the Neuronal, alpha 4 beta 2 Nicotinic Receptor. *J. Am. Chem. Soc.* 134(28):11474-11480.
 13. Nowak MW, *et al.* (1998) In vivo incorporation of unnatural amino acids into ion channels in *Xenopus* oocyte expression system. *Methods Enzymol.* 293:504-529.
 14. SPARTAN, Wavefunction, Inc., Irvine, CA.
 15. Mecozzi S, West AP, & Dougherty DA (1996) Cation-pi interactions in aromatics of biological and medicinal interest: Electrostatic potential surfaces as a useful qualitative guide. *Proc. Natl. Acad. Sci. U. S. A.* 93(20):10566-10571.
 16. Beene DL, *et al.* (2002) Cation-pi interactions in ligand recognition by serotonergic (5-HT3A) and nicotinic acetylcholine receptors: The anomalous binding properties of nicotine. *Biochemistry* 41(32):10262-10269.
 17. Van Arnem EB & Dougherty DA (2014) Functional Probes of Drug–Receptor Interactions Implicated by Structural Studies: Cys-Loop Receptors Provide a Fertile Testing Ground. *J. Med. Chem.* In press. DOI: 10.1021/jm500023m.

Chapter 4

Preparation of Translationally Competent tRNA by Direct Chemical Acylation

Noah H. Duffy and Dennis A. Dougherty

Division of Chemistry and Chemical Engineering, California Institute of Technology, Pasadena, California 91125

4.1 ABSTRACT

Nonsense codon suppression for unnatural amino acid incorporation requires the preparation of a suppressor aminoacyl-tRNA. Chemical acylation strategies are general, but inefficient and arduous. A recent report (*J. Am. Chem. Soc.* **2007**, *129*, 15848) showed acylation of RNA mediated by lanthanum(III) using amino acid phosphate esters. The successful implementation of this methodology to full-length suppressor tRNA is described, and it is shown that the derived aminoacyl-tRNA is translationally competent in *Xenopus* oocytes.

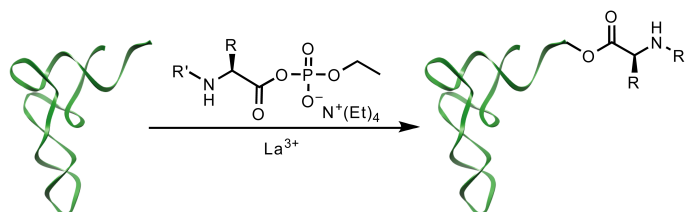
4.2 INTRODUCTION, RESULTS, AND DISCUSSION

Structure-function studies using unnatural amino acid mutagenesis provide precision beyond that which can be obtained with the 20 natural amino acids.¹⁻³ This is usually achieved through nonsense suppression, in which the site of interest is mutated to a stop codon, and an aminoacyl-tRNA bearing the appropriate anticodon delivers the unnatural amino acid during translation. The aminoacyl-tRNA is critical to this methodology, and several approaches to generating it have been developed.^{2,4,5} Native aminoacyl-tRNAs are generated via reactions of ATP-activated amino acids with the cognate tRNA, mediated by the corresponding aminoacyl-tRNA synthetase (aaRS).⁶ In some cases, the natural system can be hijacked to charge an unnatural amino acid onto a tRNA, if the difference between the unnatural and cognate amino acids is not large. Methods for generating orthogonal aaRS/tRNA pairs that accept unnatural amino acids have been shown to be a viable source of aminoacyl-tRNA.⁷ Alternatively, amino acids may be appended to tRNA using chemical synthesis. All strategies have particular advantages and disadvantages, and the chemical acylation approach is the focus of the present work.

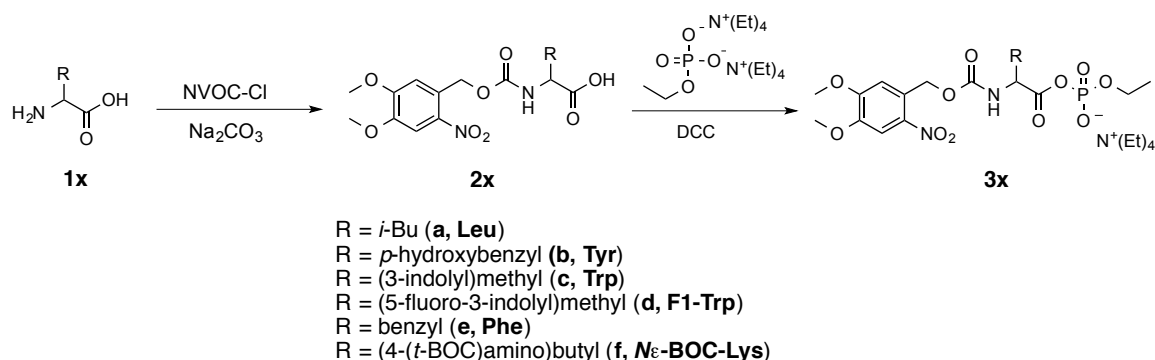
The standard chemical aminoacylation strategy begins with chemically synthesized dinucleotide pdCpA (dCA), which is then acylated with the desired amino acid.^{4,8} The derived aminoacyl-dCA is then enzymatically appended to tRNA via T4 ligase. This method provides maximal flexibility, as virtually any amino acid can be used. When combined with an appropriate expression system, the chemically synthesized aminoacyl-tRNA does not get recharged by an endogenous aaRS (an intentional aspect of the experimental design), and so the aminoacyl-tRNA is a stoichiometric reagent. Since the synthesis of the aminoacyl-tRNA is arduous, the quantity of protein that can be produced

using the chemical aminoacylation strategy is limited. For the most part, the methodology has been exploited to study ion channels and neuroreceptors, where the extraordinary sensitivity of electrophysiology overcomes the quantity limitation.¹

Scheme 4.1. La^{3+} mediated acylation of the 3' end of tRNA.



Tzvetkova and Kluger reported selective acylation of the 3' end of RNAs through the use of La^{3+} salts and amino acids activated as ethyl phosphate esters (Scheme 4.1).⁹ We will refer to this biomimetic strategy as the La^{3+} /EP approach. If direct aminoacylation of full length tRNA can produce translationally competent tRNAs, the synthesis of dCA, one of the most laborious aspects of the chemical aminoacylation strategy, would become unnecessary. As such, we have evaluated the La^{3+} /EP strategy, focusing on two questions: (1) can we optimize the direct acylation of full length, suppressor tRNAs; and (2) are the resulting aminoacyl-tRNAs translationally competent in protein synthesis? In particular, our application of nonsense suppression to studies of neuroreceptors and ion channels requires expression in a vertebrate cell, the *Xenopus laevis* oocyte.⁴ This adds additional challenges to the methodology, compared to *in vitro* protein synthesis strategies.

Scheme 4.2. Synthesis of amino acid ethyl phosphates

To address these questions, we prepared a variety of amino acids as derivatives **3a–3f** (Scheme 4.2), in which the carboxylate is activated as an ethyl phosphate, and the amino group is protected with NVOC. This protecting group has been previously established to be compatible with the *Xenopus* oocyte expression system – it is removed photochemically before use in translation.⁴ The amino acid ethyl phosphates (aaEP) were prepared by protection of the amino group, followed by coupling of bis(tetraethylammonium) ethyl phosphate to the carboxylate using DCC¹⁰ (Scheme 4.2). As a consequence of our selected protecting groups, the NVOC-amino acids were insoluble in CH₂Cl₂, but readily soluble in THF. Addition of THF as a co-solvent to CH₂Cl₂ was required to alleviate solubility issues, and a system only using THF was not viable because of DCC solubility issues. Water solubility of the resulting aaEP is an important factor in purification of the aaEP as well as later reactivity. Protection of the phenolic OH on tyrosine was not necessary under these reaction conditions for preparation of TyrEP (**3b**). Tetraethylammonium salts of aaEPs **3a–3f** were obtained by extraction into water, followed by lyophilization. The resulting foamy materials were used directly without further purification.

Before attempting La^{3+} mediated acylation to tRNA, a preliminary screen of acylation of uridine (**4**) was performed (Scheme 4.3). Initial conditions were based on literature precedent,⁹ using PheEP (**3e**). Reactions were quantified by integration of HPLC or LC/MS traces using a UV detector. Acylation of uridine to form 2'/3' esters (**5e**) was inefficient (Table 4.1). Variations in reaction time or temperature (Table 4.1, entry 1–5), or the buffer (Table 4.1, entry 9–14) did not significantly improve the yield of 2'/3' esters. Addition of La^{3+} to the reaction caused significant precipitation of a solid material, and therefore a co-solvent was introduced to alleviate solubility issues (Table 4.1, entry 15–23). Observing the increases in yield by addition of a co-solvent lead to further reaction optimization. In anticipation of optimization experiments using tRNA as the substrate, further reactions were run with LysEP (**3f**) as the amino acid (see below).

Scheme 4.3. Acylation of uridine using amino acid ethyl phosphates.

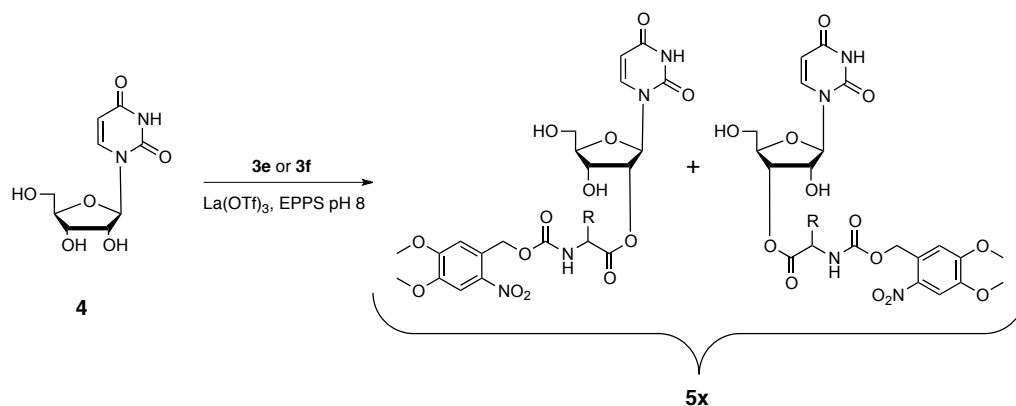


Table 4.1. Reaction screen for acylation of uridine (**4**) using PheEP (**3e**).

PheEP							
Entry	Equivalents aaEP / La ³⁺	Co-solvent%	Co-solvent	Reaction Time	Reaction Temp.	Yield	Notes
1	1	-	-	20 min	25 °C	8%	-
2	1	-	-	190 min	25 °C	12%	-
3	1	-	-	450 min	25 °C	11%	-
4	1	-	-	450 min	42 °C	9%	-
5	1	-	-	30 min	25 °C	5%	Change order of addition
6	10 EP / 1 La	-	-	465 min	25 °C	5%	-
7	1 EP / 0.66 La	-	-	240 min	25 °C	3%	-
8	10	-	-	300 min	25 °C	11%	-
9	1	-	-	120 min	25 °C	4%	1 eq. EPPS buffer pH 8
10	1	-	-	110 min	25 °C	5%	1 eq. EPPS buffer pH 7.5
11	1	-	-	25 min	25 °C	6%	1 eq. EPPS buffer pH 8
12	1	-	-	170 min	25 °C	7%	1 eq. MOPS buffer pH 7.5
13	1	-	-	50 min	25 °C	11%	7.5 eq. TRIS buffer pH 8
14	1	-	-	130 min	25 °C	0%	No buffer
15	1	50%	DMSO	100 min	25 °C	22%	-
16	1	25%	DMSO	60 min	25 °C	21%	-
17	1	25%	DMSO	40 min	25 °C	26%	-
18	1	25%	MeCN	30 min	25 °C	20%	-
19	10	25%	DMSO	200 min	25 °C	27%	-
20	1 EP / 0.66 La	25%	DMSO	200 min	25 °C	15%	-
21	10 EP / 0.66 La	25%	DMSO	200 min	25 °C	4%	-
22	10 EP / 1 La	25%	DMSO	200 min	25 °C	6%	-
23	1	10%	DMSO	35 min	25 °C	16%	-

Applying La³⁺ mediated acylation conditions to uridine with LysEP (**3f**) gave 2’/3’ esters (**5f**) in low overall conversion (Table 4.2, entry 46–47). Initial inclusion of DMSO as a co-solvent decreased yield (Table 4.2, entry 40–45), however increasing equivalents of LysEP and La³⁺ while concurrently increasing the %DMSO (v/v) in the reaction lead to increased yields (Table 4.2, entry 1–39, Figure 4.1). Acetonitrile also improved 2’/3’ ester yield, but not to the same extent as DMSO. At high %DMSO (v/v) conditions, some acylation of the reaction buffer was detected (by LC/MS); however, under no conditions were multiple acylations of uridine detected. It was reasoned that generation of these additional side products would not pose a problem when acylating tRNA, as they would be removed during tRNA purification.

Table 4.2. Reaction screen for acylation of uridine (4) using LysEP (3f).

LysEP							
Entry	Equivalents aaEP / La ³⁺	Co-solvent%	Co-solvent	Reaction Time	Reaction Temp.	Yield	Notes
24	67	50%	DMSO	90 min	45 °C	57%	-
25	67	20%	DMSO	90 min	45 °C	25%	-
26	20	60%	DMSO	90 min	25 °C	49%	-
27	20	45%	DMSO	90 min	25 °C	42%	-
28	10	60%	DMSO	90 min	25 °C	35%	-
29	10	60%	DMSO	90 min	45 °C	37%	-
30	10	45%	DMSO	90 min	25 °C	32%	-
31	10	45%	DMSO	90 min	45 °C	36%	-
32	10	20%	DMSO	90 min	25 °C	17%	-
33	10	20%	DMSO	90 min	45 °C	16%	-
34	5	60%	DMSO	90 min	25 °C	19%	-
35	5	60%	DMSO	90 min	45 °C	17%	-
36	5	45%	DMSO	90 min	25 °C	21%	-
37	5	45%	DMSO	90 min	45 °C	19%	-
38	5	20%	DMSO	90 min	25 °C	13%	-
39	5	20%	DMSO	90 min	45 °C	11%	-
40	1	60%	DMSO	90 min	25 °C	7%	-
41	1	60%	DMSO	90 min	45 °C	3%	-
42	1	45%	DMSO	90 min	25 °C	6%	-
43	1	45%	DMSO	90 min	45 °C	4%	-
44	1	20%	DMSO	90 min	25 °C	5%	-
45	1	20%	DMSO	90 min	45 °C	3%	-
46	1	- -		60 min	25 °C	11%	Sonicate reaction
47	1	- -		300 min	25 °C	12%	-
48	20	60%	MeCN	90 min	25 °C	21%	-
49	1	60%	MeCN	90 min	25 °C	5%	-
50	1	45%	MeCN	90 min	25 °C	4%	-
51	1	20%	MeCN	90 min	25 °C	3%	-

Further increases to beyond ~66 equivalents of LysEP and La³⁺ were impractical for detection of 2'/3' esters by HPLC and LC/MS, because at this ratio the analytical aliquots reached the limit of total material capable of being injected onto the respective instrument columns. Further dilution of the reaction aliquot reduced the observable signal of 2'/3' esters beyond detection.

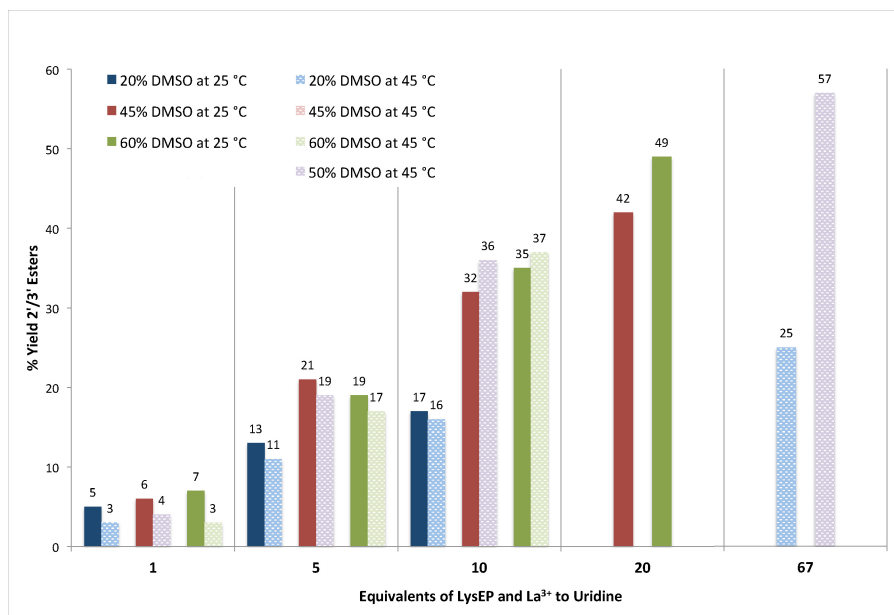


Figure 4.1. Yield of the acylation of uridine to form 2'/3' esters of Lys (**5f**) as a function of equivalents, %DMSO (v/v), and reaction temperature.

In their report, Tzvetkova and Kluger detected acylation of RNA by careful selection of the amino acid — specifically, a fluorinated amino acid (¹⁹F-NMR detection) or a dansylated amino acid (fluorescence detection). Our aaEPs were not selected with these detection methods in mind, and therefore we needed a more general method of detecting acylation. Previously our laboratory developed a MALDI-TOF mass spectrometry method for detecting enzymatic ligation of a dCA-amino acid to a tRNA transcript lacking the 3'-terminal pCpA.¹¹ Runoff transcription of tRNA gave a mixture of tRNA lengths (N+1, N+2, etc.) from addition of non-templated nucleotides at the 3' end.¹² LysEP (**3f**) was used for reaction screening with tRNA, as the mass of NVOC-BOC-Lys acylated tRNA does not coincide with the mass of N+ species (Figure 4.2). We anticipated that with this shift in the MALDI signal, acylated tRNA could be detected even if conversion was incomplete. A report by Kao *et al.*¹³ was adapted to tRNA by Ethan Van Arnem in the Dougherty lab to generate tRNA with greatly reduced N+

activity from modified DNA oligos (Figure 4.2). Without the interfering signals from N⁺ activity, tRNA generated following this preparation was used exclusively for further acylation reaction screens.

Following the trends established in the uridine acylations, acylations were then applied to a full length tRNA (Figure 4.2). Very large excesses of aaEPs and La³⁺ with respect to the tRNA (>1000 equivalents) were required to detect any acylation in the MALDI mass spectra. Key to the successful application of MALDI was treatment of the reaction mixture with the well-known lanthanide chelator diethylenetriamine pentaacetic acid (DTPA).^{14,15} While the standard tRNA precipitation protocols removed most of the excess La³⁺, enough remained (~500 μ M, as measured by ICP-MS), presumably strongly associated with the tRNA, to disrupt the MALDI. DTPA application followed by size exclusion chromatography resulted in clean samples (\leq 100 nM La³⁺). A typical microinjection volume of 50 nL exposed oocytes to a negligible \leq 5 fmol of La³⁺. It seems likely that an injection of large amounts of La³⁺ into the *Xenopus* oocyte would be detrimental to receptor synthesis and/or function, further justifying the DTPA treatment.

Even though a large excess of aaEP was used, products arising from multiple acylations were not detected in the MALDI mass spectra; only unacylated and monoacylated tRNA was seen (Figure 4.2). Our previous work has shown that the aminoacyl-tRNA ionizes differently than the free tRNA, and therefore exact quantitation of acylation via MALDI is not possible. Therefore, reference mixtures with known ratios of tRNA:aminoacyl-tRNA were prepared and evaluated by MALDI (Figure 4.3). Mass spectra of reaction products then allowed us to estimate conversion of tRNA to aminoacyl-tRNA to be 5-25%.

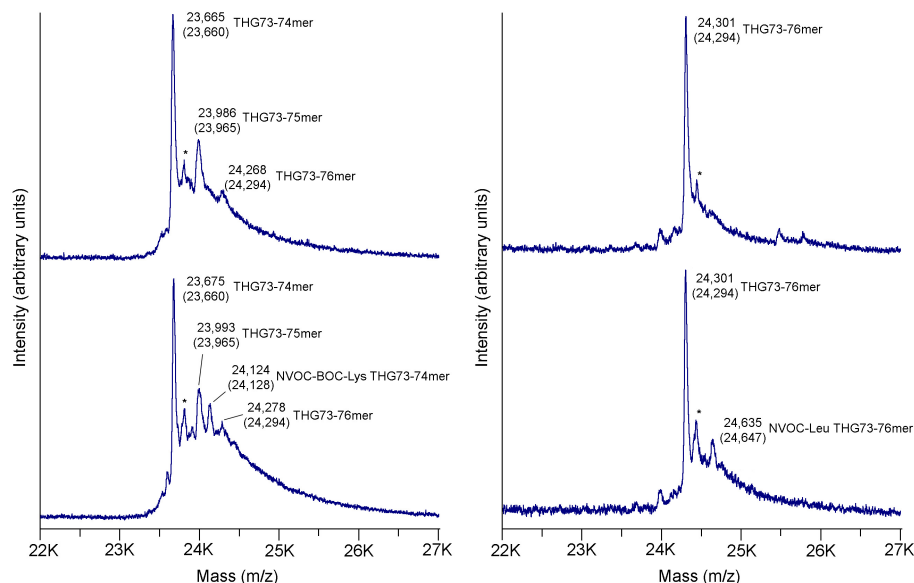


Figure 4.2. MALDI mass spectra of THG73 74mer or 76mer tRNA prepared by runoff transcription from native DNA (top left) or modified oligos (top right) followed by exposure to La^{3+} mediated acylations conditions using LysEP (**3f**, bottom left) or LeuEP (**3a**, bottom right). Observed masses shown, theoretical masses in parentheses. A new peak indicative of monoacylation appears, along with unacylated tRNA. (*) Additional peak at 24,438 m/z present from transcription of tRNA, which remains unaffected by the acylation conditions.

The monoacylation detected in the MALDI mass spectra was consistent with, but does not prove, the notion that only the 3' end of the tRNA was acylated. As further evidence, as well as to determine if these La^{3+} /EP derived tRNAs could be used in unnatural amino acid mutagenesis, we sought a functional test. Nonsense suppression has been extensively employed to probe the nicotinic acetylcholine receptor (nAChR) expressed in *Xenopus* oocytes, involving hundreds of experiments with scores of unnatural amino acids.^{1,16} The nAChR is a membrane-bound, ligand gated ion channel that can be functionally interrogated by whole cell electrophysiology. Briefly, aminoacyl-tRNA and mRNA coding for the nAChR and containing a strategically positioned stop codon are microinjected into *Xenopus* oocytes. Following an incubation time of 24-48 hours, expressed nAChRs are probed by application of acetylcholine (ACh) and measuring the resulting current. Channel function is typically expressed as EC_{50} , the concentration of

ACh required to achieve the half-maximal response. As a negative control, injection of unacylated suppressor tRNA produces no measurable current as a result of the introduction of the stop codon for nonsense suppression.

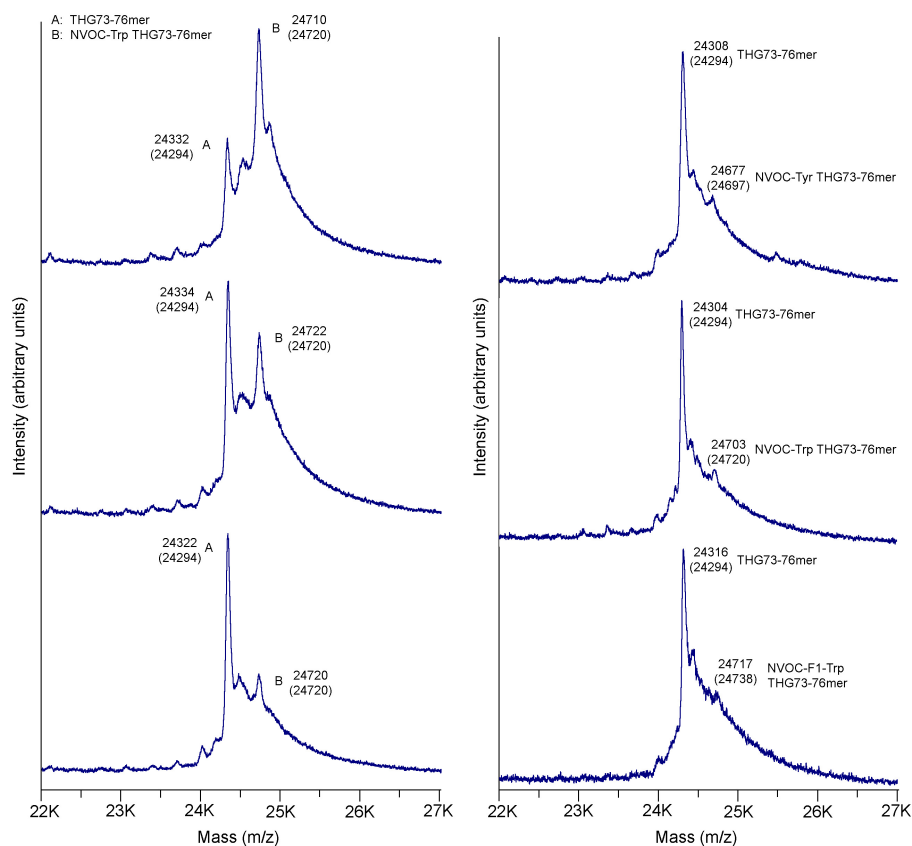


Figure 4.3. MALDI mass spectra of THG73-76mer tRNA mixed with THG73-dCA-NVOC-Trp, in 1:3 (top left), 1:1 (middle left), and 3:1 (bottom left). Acylated tRNA signal consistently smaller than expected. MALDI mass spectra of THG73-76mer after exposure to La³⁺ mediated acylation conditions of TyrEP (**3b**, top right), TrpEP (**3c**, middle right), or F1-TrpEP (**3d**, bottom right) used for nonsense suppression experiments. Observed masses shown, theoretical masses in parentheses.

Initial studies focused on so-called wild type recovery experiments, in which the amino acid appended to the suppressor tRNA is the amino acid conventionally found at the site where the stop codon was inserted. This experiment should produce wild type receptor, with behaviors indistinguishable from conventionally expressed receptor. As shown in Table 4.3, using three different amino acids (Leu, Tyr, and Trp), two different tRNAs (THG73¹⁷ and TQOpS^{18,19}), and two variants of the nAChR (the neuronal

($\alpha 4$)₂($\beta 2$)₃ and the muscle-type ($\alpha 1$)₂ $\beta 1\delta\gamma$), wild type receptors were prepared. This provides strong evidence that the La³⁺/EP methodology produces translationally competent aminoacyl-tRNAs. To confirm compatibility with unnatural amino acids, 5-fluorotryptophan (F1-Trp) was incorporated at the cation- π binding site of the muscle-type receptor (Trp149 of the α subunit).²⁰ The 4-fold shift in EC₅₀ produced in previous studies was recapitulated (Figure 4.4). These results clearly establish that the aminoacyl-tRNA derived from the La³⁺/EP method produced ion channels whose functional responses match those of channels produced by the dCA method.

Table 4.3. Data for suppression experiments using La³⁺/EP or dCA methods.

	Leu		Tyr	
receptor	$\alpha 4_2\beta 2_3$		$\alpha 1_2\beta 1_2\delta\gamma$	
mutation(s)	$\alpha L9^*A:\beta 119TGA$		$\alpha 1Y190TAG$	
tRNA	TQOpS ^a		THG73	
acylation method	La ³⁺ /EP	dCA	La ³⁺ /EP	dCA
oocytes (N)	19	18	26	16
EC ₅₀ (μM)	0.55 \pm 0.02	0.47 \pm 0.01	52 \pm 2	44 \pm 2
mean I _{max} (μA)	2 \pm 2	4 \pm 2	1 \pm 1	9 \pm 8
mean I _{max} /ng _{tRNA} ($\mu A/ng$) ^a	0.5 \pm 0.3	0.8 \pm 0.5	0.6 \pm 0.4	1.0 \pm 0.5

	Trp		F1-Trp	
receptor	$\alpha 1_2\beta 1_2\delta\gamma$		$\alpha 1_2\beta 1_2\delta\gamma$	
mutation(s)	$\alpha 1W149TAG$		$\alpha 1W149TAG$	
tRNA	THG73		THG73	
acylation method	La ³⁺ /EP	dCA	La ³⁺ /EP	dCA
oocytes (N)	52	15	36	27
EC ₅₀ (μM)	55 \pm 2	47 \pm 1	230 \pm 18	200 \pm 9
mean I _{max} (μA)	8 \pm 8	15 \pm 11	3 \pm 3	11 \pm 5
mean I _{max} /ng _{tRNA} ($\mu A/ng$) ^a	2 \pm 2	3 \pm 2	2 \pm 2	0.6 \pm 0.4

^aI_{max} values normalized to ng of acylated tRNA injected into oocytes. Acylated tRNA estimated as fraction of total tRNA injected based on percent conversion measured by MALDI-MS. The La³⁺/EP method yielded 5-25% of total tRNA acylated; the dCA method yielded 100% of total tRNA acylated.

A notable difference between the dCA and La³⁺/EP experiments relates to protein yield. The whole cell maximal currents measured for dCA-derived aminoacyl-tRNAs were generally higher than those from La³⁺/EP-derived tRNAs (Table 4.3). We suspected that this reflects the decreased quantity of aminoacyl-tRNA being injected with the La³⁺/EP method because of the incomplete acylation. Indeed, when we correct for the amount of *acylated* tRNA injected, the yields of receptor from La³⁺/EP-derived tRNAs

are comparable to dCA-derived (Table 4.3). It is worth reiterating that control experiments show that THG73 and TQOpS' are not appreciably acylated by an endogenous aaRS, and injection of unacylated tRNA yields no meaningful signal. Injection of a mixture of acylated and unacylated tRNA from the La^{3+} /EP method therefore simply produces an effective dilution of acylated tRNA.

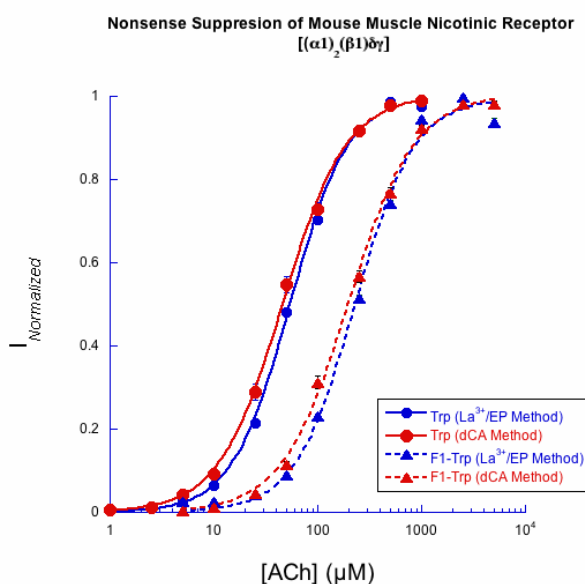


Figure 4.4. Dose-response curves of mouse muscle nAChR, $[\alpha 1(\text{W149TAG})]_2\beta 1\delta\gamma$ when injected with suppressor tRNA. Source of tRNA indicated.

In summary, we have shown that direct acylation of tRNA is a viable alternative to the more labor-intensive dCA methodology. Although acylation yields are not high, in appropriately chosen systems the unacylated tRNA does not interfere with ion channel characterization. The low acylation yield gives rise to a comparable reduction in protein expression, suggesting the approach will only be viable for systems that express well in the *Xenopus* oocyte or other cell of choice. Importantly, ion channels derived from aminoacyl-tRNA prepared by the La^{3+} /EP method are functionally indistinguishable from channels derived from the dCA method, establishing the viability of the approach for

whole-cell expression of proteins. Further work will seek to improve protein yield by improving acylation efficiency, or alternatively by separation and concentration of the aminoacyl-tRNA.

4.3 ACKNOWLEDGMENTS.

We thank Dr. Scott Virgil (Caltech) for assistance with LC/MS, Dr. Russell Jacobs (Caltech) for suggesting DTPA, and Dr. Ronald Kluger (University of Toronto) and students for helpful suggestions. This work was supported by the NIH (NS 34407).

4.4 METHODS

4.4.1 Acylation of tRNA. Acylation reaction conditions as follows: 10-30 μ g tRNA (~4-12 μ M), 80 mM HEPES pH 7.5, 15-80 mM amino acid ethyl phosphate, and 15-80 mM La(OTf)₃ (1 equivalent to aaEP) in a final volume of 100 μ L. Addition of La³⁺ started the reaction and generated insoluble complexes. The reaction was stirred vigorously at room temperature for 30 min. The reaction was quenched by addition of 50 μ L of 300 mM diethylenetriamine pentaacetic acid (DTPA) and 1.25 M NH₄OAc pH 7.5 (final concentrations 100 mM DTPA and 417 mM NH₄OAc). Excess amino acid was extracted with 1 volume of 25:24:1 phenol:chloroform:isoamyl alcohol, pH 5.2. The organic layer was then extracted with 0.5 volume of DTPA/NH₄OAc quench solution. The combined aqueous solutions were then washed with 1 volume of 24:1 chloroform:isoamyl alcohol. tRNA was then precipitated by addition of 3 volumes of ethanol and stored at -20 °C overnight. tRNA was pelleted by centrifugation and dissolved in 1 mM NaOAc pH 4.5, followed by removal of co-precipitated DTPA-La³⁺ using a CHROMA SPIN DEPC-water gel filtration column (Clontech, Mountain View, CA). The resulting tRNA solution was used directly for MALDI-MS analysis or protein expression.

4.4.2 Protein Expression in *Xenopus* Oocytes. Mouse muscle $\alpha 1$, $\beta 1$, δ , and γ ; and rat neuronal $\alpha 4$ and $\beta 2$ nAChR cDNA in the pAMV vector was linearized with the restriction enzyme Not I. mRNA was prepared by *in vitro* transcription using the mMessage Machine T7 kit (Ambion, Austin, TX). Unnatural mutations were introduced by the standard Stratagene QuickChange protocol using a TAG or TGA mutation at the site of interest. The $\alpha 4$ subunit contained a known mutation in the M2 transmembrane helix (L9'A). Stage V-VI *Xenopus laevis* oocytes were injected with mRNA in a 10:2:1:1 ratio for $\alpha 1_2\beta 1_2\delta\gamma$ or 1:20 for $\alpha 4_2\beta 2_3$. Stoichiometry of $\alpha 4\beta 2$ was confirmed by monitoring I-V relationships of acetylcholine-induced currents, as described previously.²⁰ Each cell was injected with 50 nL of a mixture of mRNA (10-19 ng, typically ~13 ng): tRNA (3-42 ng, typically ~27 ng). Uncharged full length tRNA was injected as a negative control.

4.4.3 Electrophysiology. Electrophysiology experiments were performed 24-48 hours after injection using the OpusXpress 6000A instrument (Axon Instruments, Union City, CA) in two-electrode voltage clamp mode at a holding potential of -60 mV. The running buffer was Ca^{2+} -free ND96 solution (96 mM NaCl, 2 mM KCl, 1 mM MgCl_2 and 5 mM HEPES, pH 7.5). Oocytes were superfused with running buffer at 1 mL/min for 30 s before application of acetylcholine for 15 s, followed by a 116 s wash with the running buffer. Data were sampled at 125 Hz and filtered at 50 Hz. Acetylcholine chloride was purchased from Sigma-Aldrich/RBI (St. Louis, MO). Does-response data were obtained for ≥ 10 acetylcholine concentrations on ≥ 15 cells. All EC_{50} and Hill coefficient values were obtained by fitting does-response relations to the Hill equation ($I_{\text{norm}} = 1 / [1 + (\text{EC}_{50}/[\text{ACh}])^n]$), and are reported as means \pm standard error of the fit. A detailed error

analysis of nonsense suppression experiments reveals data are reproducible to $\pm 50\%$ in EC_{50} .²¹

4.4.4 Synthesis. *Tetraethylammonium NVOC-leucine ethyl phosphate (3a)*. A round bottom flask was charged with α -NVOC-leucine (170 mg, 0.46 mmol) and *N,N'*-dicyclohexylcarbodiimide (94 mg, 0.46 mmol) in 10 mL of dry CH_2Cl_2 . The reaction was allowed to stir for 10 min at room temperature. A separately prepared solution of bis(tetraethylammonium) ethyl phosphate (175 mg, 0.46 mmol) in 10 mL dry CH_2Cl_2 was added via syringe. The reaction was allowed to stir for 4 h at room temperature. The reaction mixture was concentrated and resuspended in 5 mL of CH_2Cl_2 . Upon filtration, the organic solution was extracted three times with 5 mL of water. Saturated NaCl solution was added dropwise to aid in emulsion breaking. The combined aqueous extracts were washed with 5 mL $CHCl_3$ followed by lyophilization. The resulting solid was extracted with CH_2Cl_2 and filtered. Concentration of the CH_2Cl_2 solution gave 182 mg (66 %) of a yellow foam. Analytical sample obtained by reverse phase HPLC. 1H NMR (300 MHz, DMSO- d_6) δ 7.76 (d, J = 8.9 Hz, 1H), 7.68 (s, 1H), 7.17 (s, 1H), 5.34 (s, 2H), 4.03 – 3.91 (m, 1H), 3.90 (s, 3H), 3.84 (s, 3H), 3.70 (dt, J = 14.3, 7.2 Hz, 2H), 3.17 (q, J = 7.3 Hz, 8H), 1.72 – 1.58 (m, 1H), 1.54 – 1.45 (m, 2H), 1.18 – 1.08 (m, 12H), 1.03 (t, J = 7.1 Hz, 3H), 0.85 (dd, J = 12.9, 6.5 Hz, 6H). ^{13}C NMR (126 MHz, $CDCl_3$) δ 169.69, 169.62, 155.57, 154.01, 147.91, 139.09, 128.76, 109.53, 107.99, 63.35, 61.81, 61.76, 56.80, 56.43, 53.62, 53.58, 52.59, 41.35, 24.82, 23.08, 21.61, 16.64, 16.58, 7.78. HRMS ES (–) m/z for $C_{18}H_{26}N_2O_{11}P$, found 477.1259, calculated 477.1274.

Tetraethylammonium N-NVOC-tyrosine ethyl phosphate (3b). A round bottom flask was charged with α -NVOC-tyrosine (150 mg, 0.36 mmol) and *N,N'*-dicyclohexylcarbodiimide (147 mg, 0.71 mmol) in 1.5 mL of dry THF and 1 mL of dry CH_2Cl_2 . The reaction was allowed to stir for 4 min at room temperature. A separately prepared solution of bis(tetraethylammonium) ethyl phosphate (91 mg, 0.24 mmol) in 4 mL dry CH_2Cl_2 was added via syringe. The reaction was allowed to stir for 19 h at room temperature. The reaction mixture was filtered, and extracted three times with 5 mL of water. Saturated NaCl solution was added dropwise to aid in emulsion breaking. The combined aqueous extracts were lyophilized. The resulting solid was extracted with acetonitrile and filtered. Concentration of the acetonitrile solution gave a yellow oil, 92 mg (63 %). Analytical sample obtained by reverse phase HPLC. ^1H NMR (300 MHz, CD_3CN) δ 8.93 (br, 1H), 7.69 (s, 1H), 7.07 (d, J = 8.6 Hz, 3H), 6.78 (d, J = 8.5 Hz, 2H), 6.13 (d, J = 8.5 Hz, 1H), 5.39 (s, 2H), 4.44 – 4.32 (m, 1H), 4.05 – 3.79 (m, J = 12.5, 5.1 Hz, 8H), 3.18 (q, J = 7.3 Hz, 8H), 3.14 – 3.05 (m, 1H), 2.99 – 2.84 (m, 1H), 1.28 – 1.15 (m, 15H). ^{13}C NMR (126 MHz, CD_3CN) δ 168.88, 168.80, 157.53, 155.99, 154.27, 147.96, 139.02, 130.28, 128.93, 127.23, 117.50, 115.60, 109.63, 108.09, 62.96, 61.45, 61.40, 57.13, 56.62, 56.00, 52.24, 52.22, 52.19, 35.89, 16.18, 16.12, 6.93. ^{31}P NMR (121 MHz, CD_3CN) δ -8.52. HRMS ES (–) m/z for $\text{C}_{21}\text{H}_{24}\text{N}_2\text{O}_{12}\text{P}$, found 527.1062, calculated 527.1067.

Tetraethylammonium NVOC-tryptophan ethyl phosphate (3c). A round bottom flask was charged with α -NVOC-tryptophan (107 mg, 0.24 mmol) and *N,N'*-dicyclohexylcarbodiimide (50 mg, 0.24 mmol) in 6 mL of dry THF. The reaction was allowed to stir for 10 min. A separately prepared solution of bis(tetraethylammonium)

ethyl phosphate (93 mg, 0.25 mmol) in 5 mL CH₂Cl₂ was then added via syringe. The reaction allowed to stir overnight at room temperature. The reaction mixture was concentrated on a rotary evaporator and resuspended in 2.5 mL of CH₂Cl₂. Filtration of the suspension gave an organic solution that was extracted three times with 2 mL of water. Combined aqueous extracts were washed with 2 mL of CHCl₃ followed by lyophilization to give a yellow foam, 87.9 mg (55%). Analytical sample obtained by reverse phase HPLC. ¹H NMR (300 MHz, CDCl₃) δ 11.41 (s, 1H), 7.67 (s, 1H), 7.62 – 7.42 (m, 3H), 7.12 – 6.88 (m, 3H), 5.58 (d, *J* = 8.2 Hz, 1H), 5.47 (s, 2H), 4.80 – 4.60 (m, 1H), 4.18 – 4.01 (m, 2H), 3.96 (s, 3H), 3.81 (s, 3H), 3.42 (d, *J* = 4.6 Hz, 2H), 2.93 (q, *J* = 7.3 Hz, 8H), 1.28 (t, *J* = 7.0 Hz, 3H), 1.01 (t, *J* = 7.1 Hz, 12H). ¹³C NMR (75 MHz, CDCl₃) δ 168.76, 168.63, 155.30, 153.81, 148.02, 139.33, 136.58, 128.41, 128.36, 125.17, 120.96, 118.74, 117.72, 112.43, 110.09, 108.07, 107.85, 77.45, 77.02, 76.60, 63.40, 62.13, 62.04, 56.60, 56.39, 52.25, 27.15, 16.68, 16.58, 7.25. ³¹P NMR (121 MHz, CDCl₃) δ -7.76. HRMS ES (–) *m/z* for C₂₃H₂₅N₃O₁₁P, found 550.1229, calculated 550.1227.

Tetraethylammonium NVOC-5-fluorotryptophan ethyl phosphate (3d). A round bottom flask was charged with α-NVOC-5-fluorotryptophan (82 mg, 0.18 mmol) and *N,N'*-dicyclohexylcarbodiimide (42 mg, 0.20 mmol) in 5 mL of dry THF. The reaction was allowed to stir for 10 min at room temperature. A separately prepared solution of bis(tetraethylammonium) ethyl phosphate (72 mg, 0.19 mmol) in 5 mL dry CH₂Cl₂ was added via syringe. The reaction was allowed to stir for 24 h at room temperature. The reaction mixture was concentrated and resuspended in 3 mL of CH₂Cl₂. Upon filtration, the organic solution was extracted three times with 4 mL of water. Saturated NaCl

solution was added dropwise to aid in emulsion breaking. The combined aqueous extracts were lyophilized. The resulting solid was extracted with CH_2Cl_2 and filtered. Concentration of the CH_2Cl_2 solution gave a yellow foam 55 mg (44 %). Analytical sample obtained by reverse phase HPLC. ^1H NMR (400 MHz, CDCl_3) δ 11.71 (s, 1H), 7.66 (s, 1H), 7.58 (d, $J = 2.1$ Hz, 1H), 7.53 (dd, $J = 8.7, 4.6$ Hz, 1H), 7.09 (dd, $J = 9.9, 2.3$ Hz, 1H), 6.95 (s, 1H), 6.79 (td, $J = 9.1, 2.4$ Hz, 1H), 5.59 (d, $J = 8.2$ Hz, 1H), 5.45 (d, $J = 4.0$ Hz, 2H), 4.70 – 4.62 (m, 1H), 4.14 – 4.04 (m, 2H), 3.93 (s, 3H), 3.86 (s, 3H), 3.35 (ddd, $J = 20.0, 14.9, 4.6$ Hz, 2H), 2.98 (q, $J = 7.3$ Hz, 8H), 1.28 (t, $J = 7.1$ Hz, 3H), 1.03 (t, $J = 7.2$ Hz, 12H). ^{13}C NMR (126 MHz, CDCl_3) δ 168.75, 168.68, 158.52, 156.67, 155.32, 153.79, 148.02, 139.42, 133.12, 128.51, 128.44, 128.12, 127.17, 113.18, 113.11, 110.08, 109.25, 109.04, 108.02, 107.84, 107.81, 102.35, 102.16, 63.52, 62.19, 62.14, 56.53, 56.37, 52.23, 27.08, 16.62, 16.56, 7.23. ^{31}P NMR (162 MHz, CDCl_3) δ -7.83. HRMS ES (–) m/z for $\text{C}_{23}\text{H}_{24}\text{N}_3\text{O}_{11}\text{FP}$, found 568.1110, calculated 568.1133.

Tetraethylammonium NVOC-phenylalanine ethyl phosphate (3e). A round bottom flask was charged with α -NVOC-phenylalanine (90 mg, 0.22 mmol) and N,N' -dicyclohexylcarbodiimide (47 mg, 0.23 mmol) in 3 mL of dry THF. The reaction was allowed to stir for 10 min at room temperature. A separately prepared solution of bis(tetraethylammonium) ethyl phosphate (76 mg, 0.20 mmol) in 3 mL of dry THF and 6 mL of dry CH_2Cl_2 was added via syringe. The reaction allowed to stir for 2.75 h at room temperature. The reaction mixture was concentrated and resuspended in 4.5 mL of CH_2Cl_2 . Upon filtration, the organic solution was extracted three times with 5 mL of water. The combined aqueous extracts were lyophilized to give 96.5 mg (76 %). ^1H NMR (300 MHz, D_2O) δ 7.48 (s, H) 7.13 (br, 5H), 6.69 (s, 1H), 5.07 (br, 2H), 4.43 (m,

1H), 3.83 (m, 2H), 3.72 (s, 3H), 3.65 (s, 3H), 3.11 (q, $J = 7.3$ Hz, 8H), 2.82 (m, 2H), 1.11 (m, 12H). ^{31}P NMR (121 MHz, D_2O) δ -6.14.

Tetraethylammonium N α -NVOC-N ϵ -BOC-lysine ethyl phosphate (3f). A round bottom flask was charged with *N α -NVOC-N ϵ -BOC-lysine* (105 mg, 0.22 mmol) and *N,N'*-dicyclohexylcarbodiimide (46 mg, 0.22 mmol) in 10 mL of dry CH_2Cl_2 . The reaction was allowed to stir for 10 min at room temperature. A separately prepared solution of bis(tetraethylammonium) ethyl phosphate (66 mg, 0.17 mmol) in 5 mL of dry CH_2Cl_2 was added via syringe. The reaction was allowed to stir for 2 h at room temperature. The reaction mixture was concentrated and resuspended in 3 mL of CH_2Cl_2 . Upon filtration, the organic solution was extracted with 6 mL of water. An emulsion formed which was broken with 10 mL CH_2Cl_2 and 1 mL saturated aqueous NaCl. The organic layer was additionally extracted 2x with 10 mL water. The combined aqueous extracts were lyophilized to give a solid mixed with NaCl. The solid was extracted with chloroform, which upon concentration gave 75.2 mg of yellow foam (60 %). ^1H NMR (300 MHz, CDCl_3) δ 7.59 (s, 1H), 7.04 (s, 1H), 6.27 (d $J = 8.1$ Hz, 1H), 5.38 (m, 2H), 5.02 (br, 1H), 4.83 (br, 2H), 4.18 (br, 1H), 3.94 (s, 3H), 3.85 (s, 3H), 3.29 (q, $J = 7.3$ Hz, 8H), 2.98 (br, 2H), 1.73 (m, 3H), 1.32 (m, 15H), 1.25 (t, $J = 7.3$ Hz, 12H). ^{31}P NMR (121 MHz, CDCl_3) δ -7.89. HRMS TOF-ES (+) m/z for $\text{C}_{23}\text{H}_{37}\text{N}_3\text{O}_{13}\text{P}$, found 594.2063, calculated 594.2064.

4.5 REFERENCES

1. Dougherty DA (2000) Unnatural amino acids as probes of protein structure and function. *Curr. Opin. Chem. Biol.* 4(6):645-652.
2. Young TS & Schultz PG (2010) Beyond the Canonical 20 Amino Acids: Expanding the Genetic Lexicon. *J. Biol. Chem.* 285(15):11039-11044.
3. Link AJ & Tirrell DA (2005) Reassignment of sense codons in vivo. *Methods* 36(3):291-298.

4. Nowak MW, *et al.* (1998) In vivo incorporation of unnatural amino acids into ion channels in xenopus oocyte expression system. *Methods Enzymol.* 293(Ion Channels, Part B):504-529.
5. Ohuchi M, Murakami H, & Suga H (2007) The flexizyme system: a highly flexible tRNA aminoacylation tool for the translation apparatus. *Curr. Opin. Chem. Biol.* 11(5):537-542.
6. Arnez JG & Moras D (1997) Structural and functional considerations of the aminoacylation reaction. *Trends Biochem.Sci.* 22(6):211-216.
7. Liu CC & Schultz PG (2010) Adding New Chemistries to the Genetic Code. *Annual Review of Biochemistry, Vol 79*, Annual Review of Biochemistry, eds Kornberg RD, Raetz CRH, Rothman JE, & Thorner JW (Annual Reviews, Palo Alto), Vol 79, pp 413-444.
8. Robertson SA, Ellman JA, & Schultz PG (1991) A general and efficient route for chemical aminoacylation of transfer RNAs. *J. Am. Chem. Soc.* 113(7):2722-2729.
9. Tzvetkova S & Kluger R (2007) Biomimetic Aminoacylation of Ribonucleotides and RNA with Aminoacyl Phosphate Esters and Lanthanum Salts. *J. Am. Chem. Soc.* 129(51):15848-15854.
10. Kluger R, Li X, & Loo RW (1996) 1996 Bader Award Lecture Aminoacyl ethyl phosphates Biomimetically activated amino acids. *Can. J. Chem.* 74(12):2395-2400.
11. Petersson EJ, Shahgholi M, Lester HA, & Dougherty DA (2002) MALDI-TOF mass spectrometry methods for evaluation of in vitro aminoacyl tRNA production. *RNA* 8(4):542-547.
12. Milligan JF, Groebe DR, Witherell GW, & Uhlenbeck OC (1987) Oligoribonucleotide Synthesis Using T7 RNA-Polymerase and Synthetic DNA Templates. *Nucleic Acids Res.* 15(21):8783-8798.
13. Kao C, Zheng M, & Rudisser S (1999) A simple and efficient method to reduce nontemplated nucleotide addition at the 3' terminus of RNAs transcribed by T7 RNA polymerase. *RNA* 5(9):1268-1272.
14. Caravan P, Ellison JJ, McMurry TJ, & Lauffer RB (1999) Gadolinium(III) chelates as MRI contrast agents: Structure, dynamics, and applications. *Chem. Rev.* 99(9):2293-2352.
15. Parker D, Dickins RS, Puschmann H, Crossland C, & Howard JAK (2002) Being excited by lanthanide coordination complexes: Aqua species, chirality, excited-state chemistry, and exchange dynamics. *Chem. Rev.* 102(6):1977-2010.
16. Dougherty DA (2008) Cys-loop neuroreceptors: Structure to the rescue? *Chem. Rev.* 108(5):1642-1653.
17. Saks ME, *et al.* (1996) An engineered Tetrahymena tRNA(Gln) for in vivo incorporation of unnatural amino acids into proteins by nonsense suppression. *J. Biol. Chem.* 271(38):23169-23175.
18. Rodriguez EA, Lester HA, & Dougherty DA (2007) Improved amber and opal suppressor tRNAs for incorporation of unnatural amino acids in vivo. Part 1: Minimizing misacylation. *RNA* 13(10):1703-1714.
19. Rodriguez EA, Lester HA, & Dougherty DA (2007) Improved amber and opal suppressor tRNAs for incorporation of unnatural amino acids in vivo. Part 2: Evaluating suppression efficiency. *RNA* 13(10):1715-1722.

20. Xiu XA, Puskar NL, Shanata JAP, Lester HA, & Dougherty DA (2009) Nicotine binding to brain receptors requires a strong cation-pi interaction. *Nature* 458(7237):534-U510.
21. Torrice MM, Bower KS, Lester HA, & Dougherty DA (2009) Probing the role of the cation-pi interaction in the binding sites of GPCRs using unnatural amino acids. *Proc. Natl. Acad. Sci. U. S. A.* 106(29):11919-11924.

Appendix A1

Schild Analysis

A1.1 INTRODUCTION

The concept of a “receptor” was established well before any molecular basis of protein-ligand interactions were recognized.¹ The action of a ligand-gated ion channel (LGIC) can be described by a basic model separating binding and activation steps, and this model was also proposed before establishing LGICs as proteins.² We now regularly examine the molecular basis of LGIC function, and agonist-receptor interactions are well established.³ Many of these agonist-receptor interactions were determined through a functional measure known as the EC_{50} , which is the effective concentration to induce half-maximal response. Measurement of an antagonist-receptor interaction, however, requires special consideration. By definition, an antagonist does not elicit receptor activation, and an assay using electrophysiology cannot consist of the antagonist and receptor alone. In Chapter 2, a methodology called Schild analysis was introduced for measuring an equilibrium dissociation constant of an antagonist, K_b .⁴ This appendix gives a more thorough discussion of Schild analysis and attempts at its implementation.

In situations where Schild analysis is applicable (discussed below), the Schild equation is as follows:

$$r = 1 + \frac{[B]}{K_B} \quad (1)$$

where r is the dose-ratio (or concentration-ratio), $[B]$ is the concentration of antagonist, and K_b is the equilibrium binding constant.⁵ The dose-ratio is the ratio of agonist

required to achieve the same signal for a given concentration of antagonist to the agonist required in the absence of antagonist. In this equation, there are no terms for the agonist. A series of concentration-response curves can be constructed, each in the presence of a constant dose of the antagonist, which should result in shifts of the concentration-response curve regardless of the nature of the agonist (Figure A1.1a). From these data, the EC_{50} is usually taken to determine the dose-ratio, r . For example, suppose a hypothetical receptor has an EC_{50} value of 2 μM for an agonist. In the presence of 1 μM of an antagonist, the EC_{50} for the agonist for the hypothetical receptor might shift to 10 μM . The dose-ratio for 1 μM antagonist is then $10 \mu\text{M} / 2 \mu\text{M} = 5$.

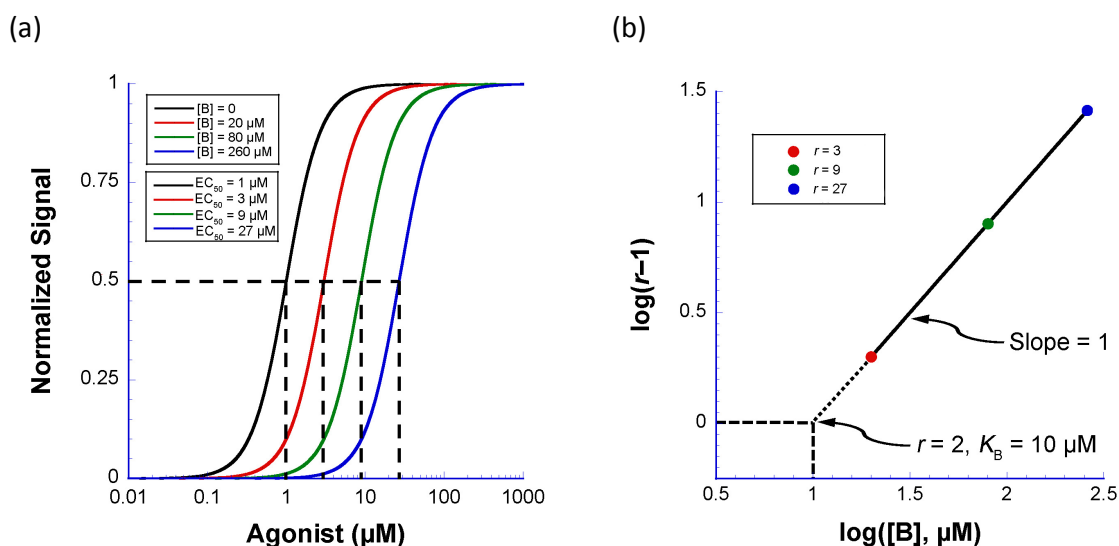


Figure A1.1. Idealized data for Schild analysis. (a) Parallel shifts of concentration-response curves of an ideal receptor in the presence of different concentrations of an antagonist, B. (b) Plot of $\log(r-1)$ derived from EC_{50} data against $\log([B], \mu\text{M})$. Extrapolation of a linear fit with slope = 1 to the ordinate intercept gives the K_B . For these idealized data, the antagonist K_B is 10 μM .

Rearranging the Schild equation and taking the logarithm gives:

$$\log(r-1) = \log([B]) - \log(K_B) \quad (2)$$

A plot of $\log(r-1)$ versus $\log([B])$ gives the so-called Schild plot, which is a straight line with a slope of 1, and an extrapolation to the intercept gives K_B (Figure A1.1b).⁵

The K_B for granisetron, the antagonist examined in Chapter 2, has been determined for the serotonin type 3A receptor (5-HT₃AR) by radioligand binding.⁶ Schild analysis, though, provides a method for determining the K_B of an antagonist by direct functional measurements of the receptor. In addition, the nonsense suppression method of introducing an unnatural amino acid reduces the efficiency of transcription.^{7,8} Electrophysiological measurements are sensitive enough to easily detect small amounts of protein, and coupled with Schild analysis, the K_B values of a receptors bearing unnatural amino acids appear to be easily obtained.

In order for Schild analysis to be used, there are requirements that must be met. Described by Colquhoun,⁹ they are as follows:

- (1) The antagonist, B, is a true antagonist that, alone, does not change the conformation of the receptor.
- (2) Binding of agonist, A, and antagonist, B, is mutually exclusive at every binding site.
- (3) B has the same affinity for every binding site.
- (4) The observed response is the same if the occupancy of each site by A is the same, regardless of how many sites are occupied by B.
- (5) Measurements are made at equilibrium.

Systems that do not meet all the requirements can be identified either by the behavior of the shifts in the concentration-response curves, or the Schild plot itself. First, increasing concentration of antagonist should shift the concentration-response curve in a parallel manner; there should be no large change in Hill slope. Second, inhibition should be surmountable; a sufficiently large dose of agonist should be able to overcome inhibition and give the same maximal signal as measured in the absence of antagonist. An antagonist displaying insurmountable inhibition by covalent attachment, allosteric inhibition, or for non-equilibrium measurements will display concentration-response curves, as shown in Figure A1.2. Finally, when the Schild plot is constructed, a large

deviation of the slope from unity is indicative of the system not meeting all the requirements for Schild analysis.

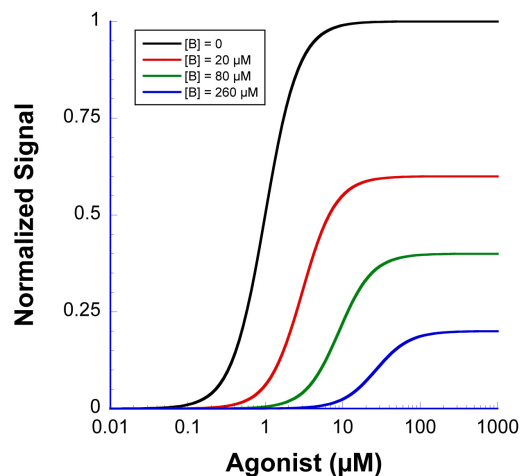


Figure A1.2. Idealized data showing insurmountable inhibition by an antagonist.

In order to implement Schild analysis for the determination of K_B values in receptors subjected to unnatural amino acid mutagenesis, data were collected by parallel multichannel electrophysiology for various combinations of antagonists of the 5-HT₃AR.

A1.2 RESULTS AND DISCUSSION

In Chapter 2, a Schild analysis of the 5HT₃ receptor was attempted with the antagonists granisetron and ondansetron. As shown in Figure A1.3, granisetron and ondansetron display insurmountable inhibition of 5-HT₃A. This was attributed to a non-equilibrium condition related to the slow off rates of the antagonists. Following this conclusion, Schild analysis was attempted for antagonists of lower affinity.

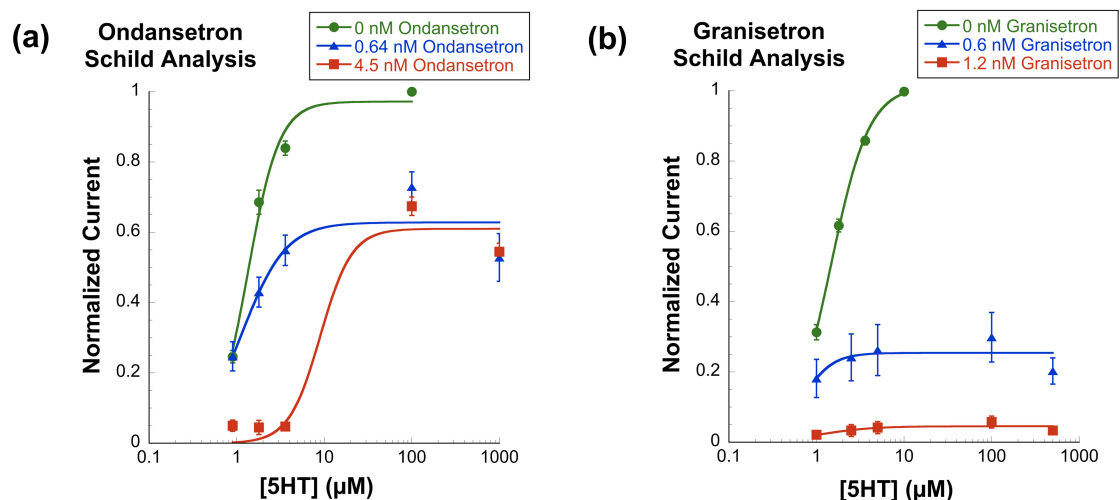


Figure A1.3. Dose-response curves of wild-type 5-HT_{3A} receptor. Responses to 5-HT with increasing concentrations of (a) ondansetron, and (b) granisetron. Data fit to the Hill equation.

The K_B at 5-HT_{3A} is 1 nM and 6 nM for granisetron and ondansetron, respectively.¹⁰ Serotonin (5-HT) binds to 5-HT_{3A} with a K_D of 110 nM, while the agonist 5-fluorotryptamine (5-HT) is 830 nM.¹¹ For the mutant 5-HT_{3A} receptor E129Q, 5-HT was shown to become an antagonist.¹² If the inability to reach full equilibrium simultaneously with 5-HT and granisetron/ondansetron was the cause of the apparent insurmountable inhibition, a Schild analysis of 5-HT might be possible. Extended incubation of granisetron or ondansetron with 5-HT to reach full equilibrium is not possible, as the receptor enters a quiet state in the presence of agonist in a process called desensitization. As shown in Figure A1.4a, inhibition of 5-HT was insurmountable by 5-HT. The signal for the four doses of 5-HT at 8.6 μM and 14.3 μM 5-HT indicates a plateau without increasing to the level seen for 5-HT in the absence 5-HT.

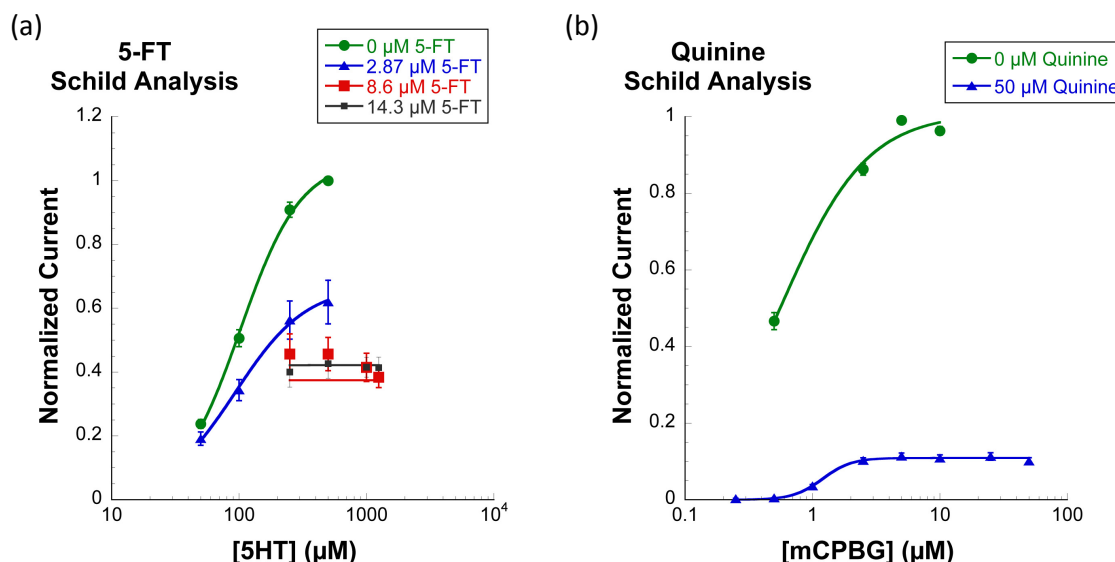


Figure A1.4. Dose-response curves of (a) E129Q mutant and (b) wild-type 5-HT₃A receptors. Responses to (a) 5-HT or (b) mCPBG with increasing concentrations of (a) 5-FT and (b) quinine. Data fit to the Hill equation.

While the affinity of 5-FT for 5-HT₃A is considerably less than those for granisetron or ondansetron, it is possible that a very low affinity antagonist might still be suitable for Schild analysis. The antimalarial drug quinine was reported to inhibit 5-HT₃A with an affinity of 15 μM, and Schild analysis was applied to 5-HT₃A for quinine in *Xenopus* oocytes.¹³ Attempting to replicate these results, however, was not successful. As shown in Figure A1.4b, inhibition by quinine was insurmountable. This is in direct contrast to the results of Thompson *et al.*¹³ The discrepancy of the data in Figure A1.4b and the data from Thompson *et al.*¹³ is not easily explained. The agonist used in the appendix was *meta*-chlorophenylbiguanide (mCPBG), but in Schild analysis the identity of the agonist should not matter.

Looking at just the data in this appendix, there are multiple possible explanations as to the inapplicability of Schild analysis. The 5-HT₃AR is a pentameric LGIC that has five identical orthosteric binding sites (where the agonist binds). It is known that for the

antagonists examined, the site of action is the orthosteric binding site. What is unknown, however, is what level of occupancy by antagonist versus agonist leads to channel inhibition. In other words, it is unknown if binding of the antagonist at a *remote* orthosteric site is sufficient for inhibition of channel opening, even upon binding of an agonist at an unoccupied orthosteric site. This can also be related to point (1) above. The occupation of an orthosteric site by an antagonist could result in a conformational change that stabilizes the closed state, in which case the antagonist is not a *true* antagonist, but rather an “inverse agonist.” While this discussion is speculative, it is clear that whatever the true mechanism of inhibition is, it cannot be determined through Schild analysis.

A1.3 SUMMARY

While Schild analysis held the possibility of a straightforward method for determining the K_B of an antagonist for a receptor bearing an unnatural amino acid, its inapplicability to the antagonists measured at conventional 5-HT₃ARs suggests this is not the case. Measurement of K_B values using radioligand binding assays is a viable alternative, noting that the decreased expression of receptor under nonsense suppression conditions will have to be overcome.

A1.4 METHODS

Molecular biology, *Xenopus* oocyte injection, and electrophysiology were described in Chapter 2. In order to measure shifts in the concentration-response curves, a constant concentration of the antagonist of interest was applied in all solutions exposed to the oocyte including the wash buffer and all agonist solutions. Concentrations of antagonist were measured from lowest to highest.

A1.5 REFERENCES

1. Rang HP (2006) The receptor concept: pharmacology's big idea. *Br. J. Pharmacol.* 147:S9-S16.
2. del Castillo J & Katz B (1957) Interaction at End-Plate Receptors Between Different Choline Derivatives. *Proc. Roy. Soc. B.* 146(924):369-380.
3. Van Arnem EB & Dougherty DA (2014) Functional Probes of Drug–Receptor Interactions Implicated by Structural Studies: Cys-Loop Receptors Provide a Fertile Testing Ground. *J. Med. Chem.* In press. DOI: 10.1021/jm500023m.
4. Schild HO (1949) pAx and Competitive Drug Antagonism. *Br. J. Pharmacol. Chemother.* 4(3):277-280.
5. Wyllie DJA & Chen PE (2007) Taking the time to study competitive antagonism. *Br. J. Pharmacol.* 150(5):541-551.
6. Thompson AJ, *et al.* (2005) Locating an antagonist in the 5-HT₃ receptor binding site using modeling and radioligand binding. *J. Biol. Chem.* 280(21):20476-20482.
7. Dougherty DA (2000) Unnatural amino acids as probes of protein structure and function. *Curr. Opin. Chem. Biol.* 4(6):645-652.
8. Dougherty DA (2008) Physical organic chemistry on the brain. *J. Org. Chem.* 73(10):3667-3673.
9. Colquhoun D (2007) Why the Schild method is better than Schild realised. *Trends Pharmacol. Sci.* 28(12):608-614.
10. Rojas C, *et al.* (2008) Palonosetron exhibits unique molecular interactions with the 5-HT₃ receptor. *Anesth. Analg.* 107(2):469-478.
11. Bower KS, *et al.* (2008) 5-fluorotryptamine is a partial agonist at 5-HT₃ receptors, and reveals that size and electronegativity at the 5 position of tryptamine are critical for efficient receptor function. *Eur. J. Pharmacol.* 580(3):291-297.
12. Miles TF, Bower KS, Lester HA, & Dougherty DA (2012) A Coupled Array of Noncovalent Interactions Impacts the Function of the 5-HT(3)A Serotonin Receptor in an Agonist-Specific Way. *ACS Chem. Neurosci.* 3(10):753-760.
13. Thompson AJ, Lochner M, & Lummis SCR (2007) The antimalarial drugs quinine, chloroquine and mefloquine are antagonists at 5-HT₃ receptors. *Br. J. Pharmacol.* 151(5):666-677.

Appendix A2

The Screening of Ondansetron Analogs

A2.1 INTRODUCTION

As a validated therapeutic target,^{1,2} the serotonin type 3A receptor (5-HT₃AR) continues to be an attractive target for further drug development. Ondansetron is a prototypical 5-HT₃A antagonist,³ which is currently used as an antiemetic drug. Ondansetron is currently sold as the racemate, and both enantiomers are reported as equipotent on rat vagus nerve.³ The adverse effects of racemic ondansetron treatment, however, may be a result of the S(–) enantiomer.⁴ Enantiopure analogs of ondansetron may therefore have the potential for improved 5-HT₃AR antagonism and possible therapeutic applications.

The Stoltz research group developed an asymmetric allylic alkylation reaction,⁵ which was later applied to lactam substrates.⁶ Following this line of inquiry, Douglas Duquette adapted this reaction for enaminone substrates (Figure A2.1), which upon conversion to an indole gave compounds with structural similarities to ondansetron (Figure A2.2). This chemistry allows for exploration of functionality at the stereocenter of ondansetron in a stereoselective fashion. An initial series of compounds synthesized by Douglas Duquette was tested for 5-HT₃AR antagonism, starting with an exploration of the moiety that makes a cation- π interaction with TrpB (Chapter 2). At this point in testing, enantiopure compounds had not been prepared.

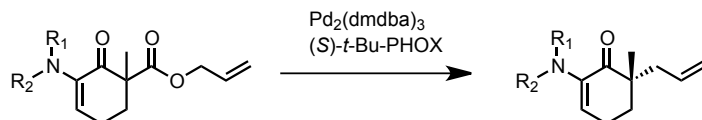


Figure A2.1. Example of enaminone allylic alkylation performed by Douglas Duquette.

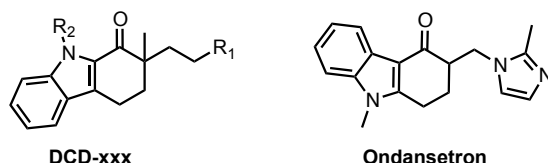


Figure A2.2. Structures of ondansetron and analogs prepared for this study. R_1 and R_2 defined in Table A2.1.

A2.2 RESULTS AND DISCUSSION

To quickly assess the inhibitory ability of the compounds, a single-point inhibition assay was developed. The assay also measured the whether the compounds cause activation of 5-HT_{3A}. Channel function was determined through three initial EC₂₅ (1 μ M) doses of serotonin (5-HT), where the first, priming dose was excluded from the analysis. The compound of interest as a 10 μ M solution was then applied to the channels, and allowed to incubate for 1 minute. During this period, any possible channel activation was noted. Immediately following compound incubation, a mixture of 10 μ M of the compound and an EC₂₅ dose of 5-HT was applied. The signal from this co-application was compared to the average of the initial EC₂₅ doses of 5-HT to determine the inhibitory ability of each compound (Figure A2.3). The structures of the tested compounds and the percentage of signal inhibition of an EC₂₅ dose of 5-HT are shown in Table A2.1. Receptor recovery from inhibition was then assessed by two additional doses of 5-HT, which were averaged. A 1 μ M dose of ondansetron and a representative solution without compound were used as controls.

With a 10 μM dose, the compounds tested inhibited an EC_{25} dose of 5-HT to varying degrees. None of the compounds activated 5-HT_{3A}. As expected, the methoxyamine DCD006 did not inhibit 5-HT signal, as it is likely not protonated at pH 7.4 and cannot make a cation- π interaction with TrpB. It is interesting that the morpholine DCD003 also did not inhibit 5-HT signal, especially when compared to the piperidine DCD001. The best inhibition was seen with the smallest of the measured amines (DCD005 and DCD007). When channel recovery was assessed, an increase in signal was noted for all

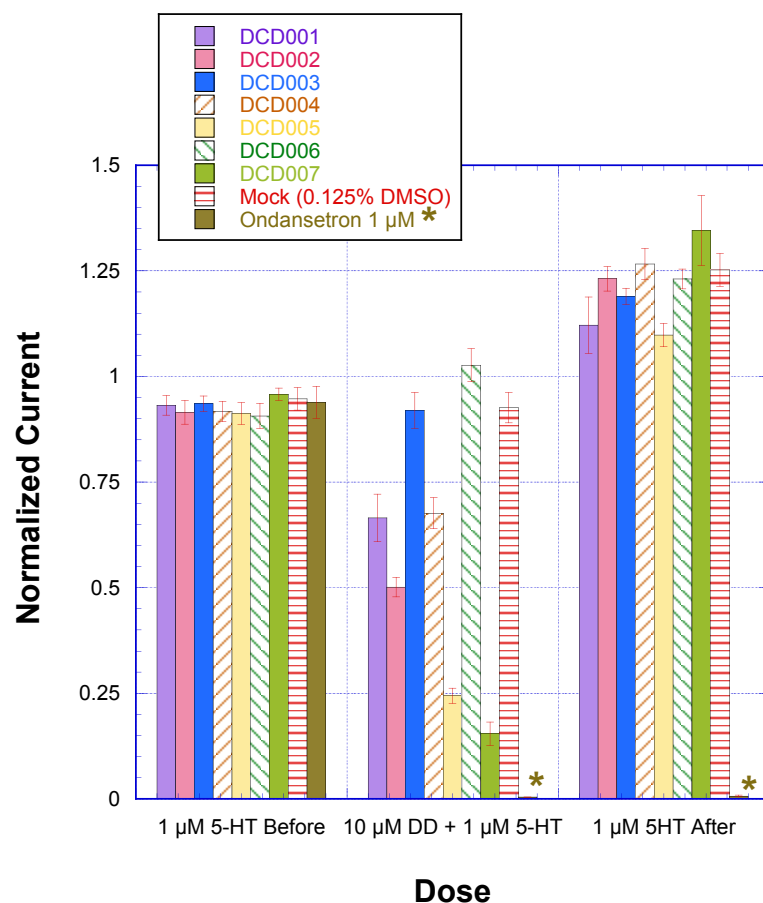
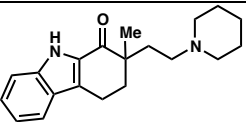
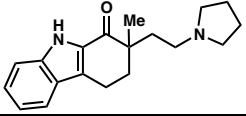
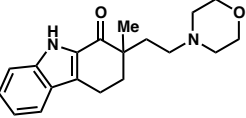
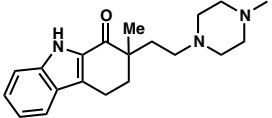
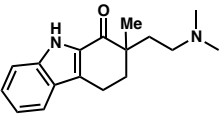
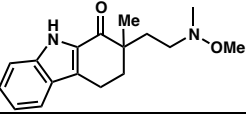
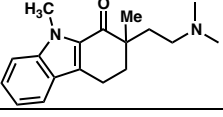
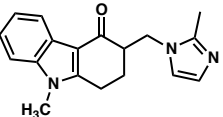


Figure A2.3. Average signal of 5-HT_{3A} to 1 μM 5-HT (EC_{25}). The first column shows the 1 μM 5-HT doses applied before compound testing. The second column shows the co-application of 1 μM 5-HT and 10 μM compounds, compound-free, or 1 μM ondansetron. The third column shows the 1 μM 5-HT doses applied after compound testing. Number of oocytes for each measurement and the structure of the tested compounds are shown in Table A2.1.

compounds tested (Figure A2.3). This increase in EC₂₅ signal was also noted in the compound-free control, and therefore is not potentiation by the tested compounds. Inhibition from 1 μ M ondansetron was complete and did not wash out over the standard 2 minute superfusion time.

Table A2.1. The percent inhibition of the EC₂₅ (1 μ M) 5-HT signal from co-application with 10 μ M solutions of DCDxxx compounds of the 5-HT₃AR.

Compound	Structure	Mouse 5-HT ₃ AR 10 μ M DCDxxx Dose % inhibition of 5-HT signal at EC ₂₅ (1 μ M)
DCD-001		33 \pm 6 <i>N</i> = 8
DCD-002		50 \pm 2 <i>N</i> = 8
DCD-003		8 \pm 4 <i>N</i> = 7
DCD-004		32 \pm 4 <i>N</i> = 7
DCD-005		76 \pm 2 <i>N</i> = 8
DCD-006		-3 \pm 4 <i>N</i> = 8
DCD-007		84 \pm 3 <i>N</i> = 6
Mock (0.125% DMSO)	—	7 \pm 4 <i>N</i> = 4
Ondansetron		99.57 \pm 0.01 <i>N</i> = 2

Compound codes and structures shown. The number of oocytes for each measurement shown in italics as *N* = *x*.

An IC₅₀ value for the compounds with the best inhibition, DCD005 and DCD007, was measured in order to more directly compare with ondansetron. As described in Chapter 2, the IC₅₀ values were determined at 2-fold EC₅₀ 5-HT (3.14 μ M). Both compounds had IC₅₀ values in the tens of μ M, which contrasts with the IC₅₀ value of 0.87 nM measured for ondansetron (Table A2.2).

Table A2.2. IC₅₀ data for 5-HT₃AR for ondansetron and DCDxxx compounds in response to 5-HT.

Antagonist	Agonist	N ^a	IC ₅₀ (nM) ^b	Hill ^c
Ondansetron		21	0.87 \pm 0.04	-1.6 \pm 0.09
DCD005	5HT	7	22 \times 10 ³ \pm 1 \times 10 ³	-2.4 \pm 0.2
DCD007		7	18.3 \times 10 ³ \pm 0.6 \times 10 ³	-2.7 \pm 0.1

^aNumber of oocytes averaged in IC₅₀ determination. ^bThe effective concentration for half-maximal receptor inhibition. ^cThe Hill coefficient, n_H , as determined from fitting the Hill equation.

A2.3 SUMMARY

Data has been collected for new inhibitors of 5-HT₃A that have structural similarity to ondansetron. Additional analogs, including enantiopure compounds, will be necessary to further develop a structure-activity relationship for development of an inhibitor that can rival ondansetron.

A2.4 METHODS

Detailed descriptions of oocyte protein expression and electrophysiology methods are found in Chapter 2. DCDxxx compounds were dissolved as stock solutions in aqueous DMSO (10-20%) such that diluted oocytes would not be superfused with a solution containing more than 0.125% DMSO. Solubility was aided by conversion to the HCl salt by addition of 1 eq. of 1 N aq. HCl.

For the single point inhibition assay, oocytes were superfused with running buffer at 1 mL/min for 30 s before application of EC₂₅ 5-HT (1 μ M) for 15 s followed by a 116 s

wash with the running buffer. This dose was applied three times. DCDxxx compounds or ondansetron was then pre-applied and the oocyte allowed to incubate for 60 s, followed by application of a mixture of the antagonist dose with EC₂₅ 5-HT (1 μ M) for 15 s. The oocytes were then washed with the running buffer for 116 s. Channel recovery was determined by application of two doses of EC₂₅ 5-HT (1 μ M) for 15 s followed by a 116 s wash with the running buffer.

IC₅₀ values for DCDxxx compounds were determined as described in Chapter 2.

A2.5 REFERENCES

1. Machu TK (2011) Therapeutics of 5-HT₃ receptor antagonists: Current uses and future directions. *Pharmacol. Ther.* 130(3):338-347.
2. Thompson AJ & Lummis SC (2007) The 5-HT₃ receptor as a therapeutic target. *Expert Opin. Ther. Targets* 11(4):527-540.
3. Butler A, Hill JM, Ireland SJ, Jordan CC, & Tyers MB (1988) Pharmacological Properties of GR38032F, a Novel Antagonist at 5-HT₃ Receptors. *Br. J. Pharmacol.* 94(2):397-412.
4. Young JW (1995) Treating emesis, nausea and other disorders using optically pure (R)-(+)-ondansetron. US Patent 5,470,868.
5. Behenna DC & Stoltz BM (2004) The enantioselective Tsuji allylation. *J. Am. Chem. Soc.* 126(46):15044-15045.
6. Behenna DC, *et al.* (2012) Enantioselective construction of quaternary N-heterocycles by palladium-catalysed decarboxylative allylic alkylation of lactams. *Nat. Chem.* 4(2):130-133.

Appendix A3

Synthesis of 4,7-Difluoroindole

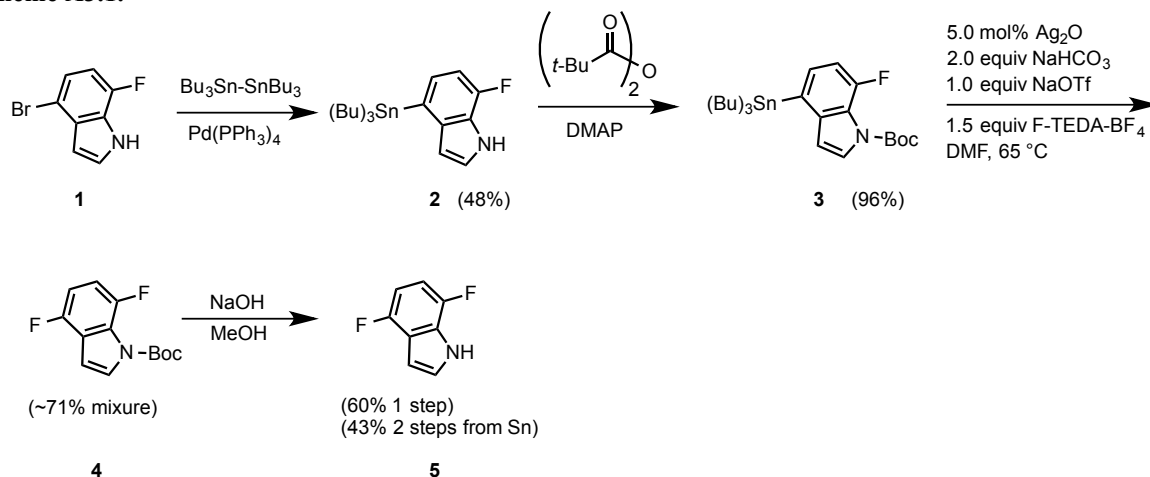
A3.1 INTRODUCTION

In Chapter 2, the synthesis of 4,7-F₂Trp was described using 4,7-difluoroindole. The direct formation of 4,7-difluoroindole from a nitrodifluorobenzene and vinyl magnesium bromide was not the initial route examined. The need for 4,7-difluoroindole provided an opportunity to test the utility of the late stage fluorination chemistry reported by Ritter.¹ This appendix reports an alternate synthesis of 4,7-difluoroindole.

A3.2 RESULTS AND DISCUSSION

The fluorination conditions reported by Ritter use a tributylarylstannane species to participate in a Ag(I) catalytic cycle.¹ Starting with commercially available 4-bromo-7-fluoroindole, a stannylation using Pd(PPh₃)₄ was performed to generate the arylstannane **2** (Scheme A3.1). Purification of **2** was performed using alumina chromatography, as decomposition on silica was observed. Submitting **2** to fluorination conditions did not result in the desired difluoroindole **5**. It was reported that basic amines, sulfides, and protic functional groups are incompatible with the reaction conditions,¹ so it was theorized that the failure to fluorinate was a result of the indole nitrogen.

Scheme A3.1.



Arylstannane **2** was protected using di-*t*-butyl dicarbonate, and then subjected to fluorination conditions. Boc protected difluoroindole **4** was formed; however, destannylation to form the monofluoro also occurred. Separation of the monofluoroindole and the difluoroindole was difficult. The mixture was subjected to deprotection using sodium hydroxide in methanol, followed by silica gel purification to yield 4,7-difluoroindole **5** as a slightly volatile dark oil.

A3.3 SUMMARY

Starting from 4-bromo-7-fluoroindole, the desired 4,7-difluoroindole **5** was prepared in 20% overall yield. The yield could be improved with optimization of the stannylation and the Boc deprotection. Direct formation as described in Chapter 2 was performed in 18% yield; however, the desired 4,7-difluoroindole required purification from a mixture of many side products. The preparation in this appendix provided authentic material as a reference to aid in the isolation from the mixture obtained in Chapter 2.

A3.4 METHODS

A3.4.1 Synthesis. *7-fluoro-4-(tributylstannyl)indole (2)*. In a dry round bottom flask 518 mg (2.42 mmol) of 4-bromo-7-fluoroindole was added. A solution of 140 mg (0.121

mmol, 5 mol%) of $\text{Pd}(\text{PPh}_3)_4$ in 10 mL of dry toluene was added to the round bottom flask. Hexa-*n*-butylditin (1.8 mL, 3.57 mmol) was added via syringe. The reaction was stirred at 100 °C for 19 h under argon. The reaction was filtered and purified using an alumina column running 5% CH_2Cl_2 in hexanes to 10% CH_2Cl_2 in hexanes to yield 488 mg (48%) of a clear to slightly yellow oil. ^1H NMR (300 MHz, CD_3OD) δ 7.27 (d, J = 3.1 Hz, 1H), 7.00 (dd, J = 7.6, 5.4 Hz, 1H), 6.80 (dd, J = 12.0, 7.6 Hz, 1H), 6.44 (dd, J = 3.6, 3.1 Hz, 1H), 1.66 – 1.45 (m, 6H), 1.42 – 1.23 (m, 6H), 1.21 – 1.08 (m, 6H), 0.86 (t, J = 7.3 Hz, 9H). ^{19}F NMR (282 MHz, Methanol- d_4) δ -131.63 – -144.53 (m).

7-fluoro-4-(tributylstannyl)-N-(Boc)indole (3). In a round bottom flask 364 mg (0.858 mmol) of indole **2** was dissolved in 5 mL of CH_2Cl_2 . A solution of 289 mg (1.32 mmol) of di-*t*-butyl carbonate and 5.3 mg (0.043 mmol) of DMAP in 5 mL of CH_2Cl_2 was added to the reaction. The reaction was stirred at room temperature for 2.5 h. After concentration under reduced pressure, the material was dissolved in 10% CH_2Cl_2 in hexanes and passed through an alumina plug to recover 431 mg (96%) of the desired product. ^1H NMR (300 MHz, CD_2Cl_2) δ 7.70 (dd, J = 3.7, 0.5 Hz, 1H), 7.29 (dd, J = 7.7, 4.7 Hz, 1H), 7.02 (dd, J = 13.2, 7.7 Hz, 1H), 6.58 (dd, J = 3.7, 2.1 Hz, 1H), 1.67 (s, 9H), 1.64 – 1.51 (m, 6H), 1.45 – 1.28 (m, 6H), 1.24 – 1.14 (m, 6H), 0.91 (t, J = 7.3 Hz, 9H). ^{19}F NMR (282 MHz, CD_2Cl_2) δ -117.08 – -117.27 (m).

4,7-difluoro-N-(Boc)indole (4). Into a round bottom flask, solid silver(I) oxide (10.5 mg, 0.045 mmol, 5 mol%), sodium triflate (143 mg, 0.829 mmol), sodium bicarbonate (142 mg, 1.69 mmol), and Selectfluor (1-chloromethyl-4-fluoro-1,4-diazonia-bicyclo[2.2.2]octane bis(tetrafluoroborate)) (439 mg, 1.24 mmol) were added. A solution of 431 mg (0.821 mmol) of indole **3** in 20 mL of DMF was added to the reaction.

Methanol (167 μ L, 4.13 mmol) was added to the reaction, and the flask was immediately sealed. The sealed reaction flask was heated to 65 $^{\circ}$ C and stirred for 4 h. The reaction was cooled to room temperature and then filtered. Silica gel chromatography eluting with 2% EtOAc in hexanes to 4% EtOAc in hexanes yielded 148 mg of a mixture of the desired difluoroindole and monofluoroindole as detected by ^{19}F NMR. The mixture was carried on to the next reaction. ^{19}F NMR (282 MHz, CD_2Cl_2) δ -121.32 – -122.90 (m), -128.48 – -129.81 (m).

4,7-difluoroindole (**5**). The mixture **4** was dissolved in 8 mL methanol and 0.1 mL of concentrated NaOH was added. The reaction was stirred at 60 $^{\circ}$ C for 1 h and then concentrated under reduced pressure. To the concentrated oil was added 10 mL of water and 10 mL of CH_2Cl_2 . The aqueous layer was separated and washed with 1 x 10 mL of CH_2Cl_2 . The combined organics were washed with 1 x 10 mL of brine, dried over Na_2SO_4 and concentrated under reduced pressure. The crude oil was run down a silica column eluting with a gradient starting at 1% EtOAc in hexanes to 10% EtOAc in hexanes to give 54 mg (60%) of a volatile dark oil. ^1H NMR (300 MHz, CDCl_3): δ 8.47 (br, 1H), 7.18 (t, J = 2.8 Hz, 1H), 6.78 (ddd, J = 10.3, 8.6, 3.5 Hz, 1H), 6.71 – 6.60 (m, 2H). ^{19}F NMR (282 MHz, CDCl_3): δ -124.1 – -129.8 (m), -139.4 – -142.3 (m). ^{13}C NMR (126 MHz, CDCl_3): δ 152.2 (dd, J = 239, 2.4 Hz), 145.8 (dd, J = 238.6, 3.0 Hz), 126.0 (dd, J = 15.9, 11.5 Hz), 124.7, 119.9 (dd, J = 24.9, 5.7 Hz), 106.4 (dd, J = 18.9, 8.2 Hz), 103.9 (dd, J = 18.9 8.2 Hz), 99.8. HRMS EI(+) m/z for $\text{C}_8\text{H}_5\text{NF}_2$ found 153.0395, calculated 153.0390 ($\text{M}+\bullet$).

A3.5 REFERENCES

1. Tang PP, Furuya T, & Ritter T (2010) Silver-Catalyzed Late-Stage Fluorination. *J. Am. Chem. Soc.* 132(34):12150-12154.

Appendix A4

Preparation of Acylated tRNA Through Adenosine Phosphoroanhydrides

A4.1 INTRODUCTION

In Chapter 4, a chemical method for acylation of tRNA was discussed as an alternative to acylation of the dinucleotide deoxycytidine-adenosine (dCA, Figure A4.1). As the chemical acylation of tRNA remains a challenging problem, many research labs continue to seek new methods. A publication by the Hecht lab describing the preparation of diacylated tRNA implemented a method using adenosine phosphoroanhydrides (AppA) shown in Figure A4.1.¹ Attachment of both acylated dCA and acylated AppA is accomplished using T4 RNA ligase. The tRNA substrates, however, are of differing length: a 74mer is used with dCA and a 75mer is used with AppA. Use of AppA to generate acylated tRNA was explored as an alternative to the use of dCA.

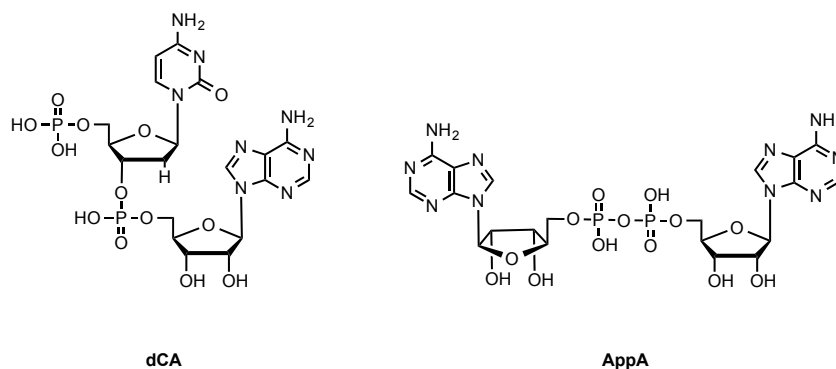


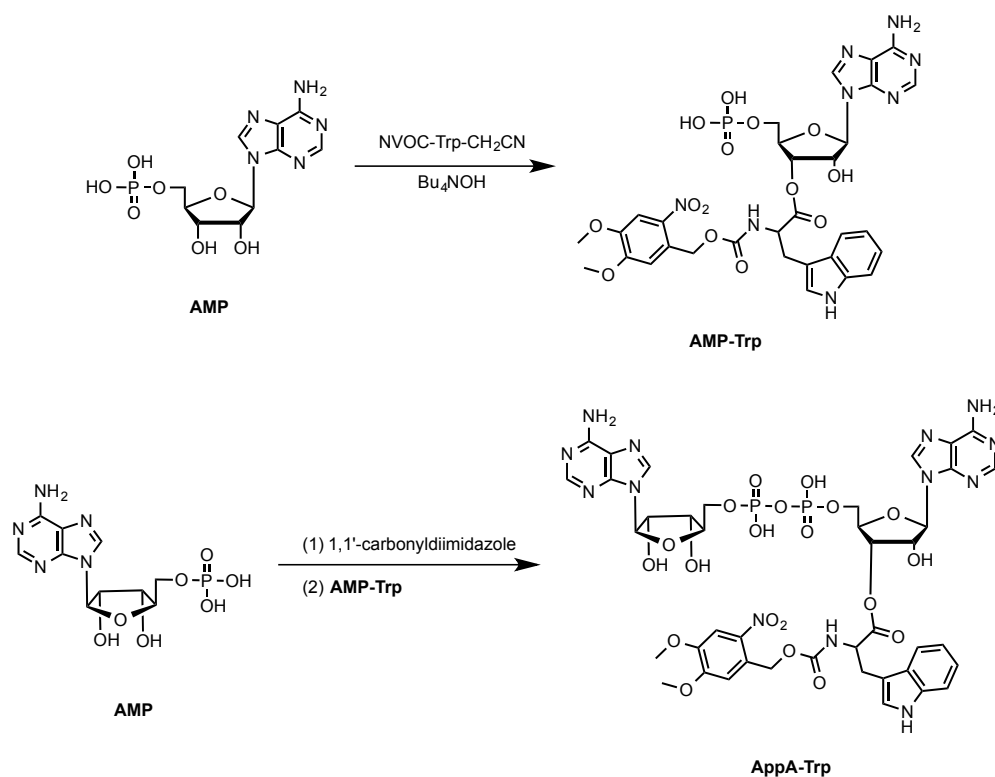
Figure A4.1. Structures of nucleotide species for preparation of acylated tRNA.

A4.2 RESULTS AND DISCUSSION

The preparation of acylated AppA and its ligation to tRNA was described before the use of dCA was described.² Adenosine mono-phosphate (**AMP**) was acylated using the cyanomethyl ester of nitroveratryl protected tryptophan similarly to previously published

procedures (Scheme A4.1).^{1,3} The tryptophan phosphoroanhydride (**AppA-Trp**) was prepared by coupling to **AMP** using 1,1'-carbonyldiimidazole following a procedure described by Hecht.² The reaction generated **AppA-Trp** as a minor component, but enough material was synthesized for the examination of the T4 RNA ligase reaction. Additional synthesis of **AppA-Trp** would likely benefit from more modern coupling methods.^{4,5}

Scheme A4.1.



To obtain 75 mer tRNA, a synthetic DNA oligonucleotide for the THG73 tRNA⁶ was purchased from Eurofins Operon Genomics and mixed with a short complementary strand for T7 polymerase promoter region (Figure A4.3).⁷ This oligo contains 2'-OMe modifications on the last two bases, and this modification reduces non-templated N+1 addition at the 3' end of the tRNA.^{8,9}

5' -TAATACGACTCACTATAG-3'
 3' -ATTATGCTGAGTGATATCCAAGATATCATATCGCCAATCATGACCCCTGAGATTTAGGGAAGCTGGACCCAAGCTTAGGGTCATCCTGGCG*G*-5'

Figure A4.3. Sequence of the synthetic oligonucleotides used to transcribe THG75-75mer tRNA. Bases marked (*) contain a 2'-OMe modification.

Ligation of **AppA-Trp** to THG73-75mer was attempted using T4 RNA ligase as previously described without ATP in the reaction mix.¹ Ligation efficiency was determined using MALDI-TOF-MS.¹¹ As shown in Figure A4.4, ligation efficiency is very low. The identity of the MALDI peak was confirmed by using this sample in a *Xenopus* oocyte nonsense suppression experiment of the 5-HT₃A receptor at W183TAG, as described in Chapter 4 (Figure A4.5a). As a positive suppression control, an acylated THG73 derived from dCA was also examined (Figure A4.5b). No signal was detected in response to serotonin (5-HT) when untreated THG73-75mer was used in the suppression experiment. These data indicate tryptophan was selectively incorporated at W183 in 5-HT₃A, and the identity of the small peak in Figure A4.4 is confirmed to be THG73-76mer-Trp. The difference in maximal currents measured for the dCA and AppA-Trp derived tRNAs are similar to those obtained in Chapter 4, again reiterating the low ligation efficiency.

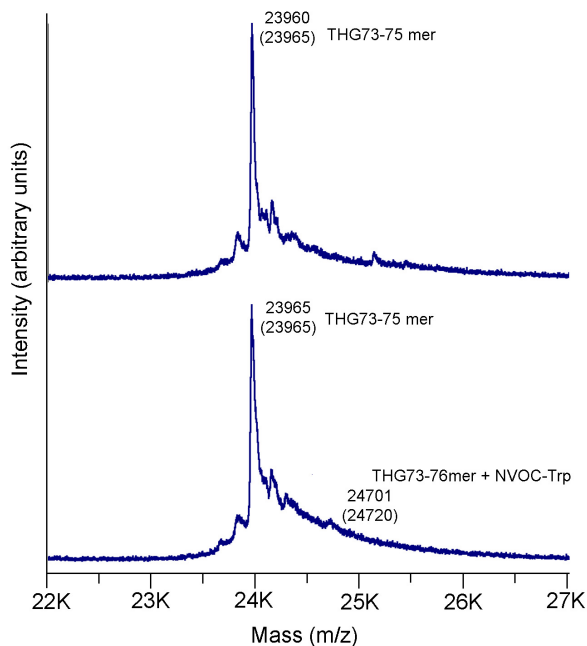


Figure A4.4. MALDI mass spectra of THG73 75mer (top) or 75mer tRNA after treatment with AppA-Trp and T4 RNA ligase (bottom). Observed masses shown, theoretical masses in parentheses.

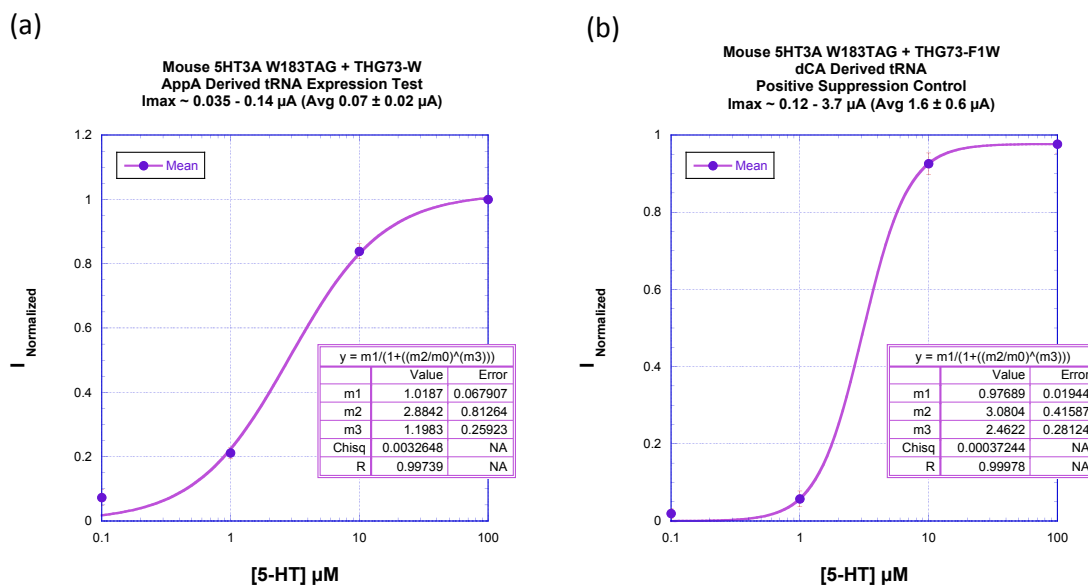


Figure A4.5. Dose-response curves of mouse 5-HT₃A, W183TAG when injected with THG73 tRNA bearing marked amino acid derived from ligation with T4 RNA ligase and (a) AppA-Trp, or (b) dCA-5-F₁Trp.

A4.3 SUMMARY

The exact conditions reported by Hecht¹ were successful in preparing acylated tRNA that can participate in nonsense suppression in *Xenopus* oocytes. These results show that AppA can be a substrate for T4 RNA ligase; however, ligation efficiency is extremely low, especially as compared to the nearly quantitative ligation of dCA by T4 RNA ligase.

A4.4 METHODS

Molecular biology, *Xenopus* oocyte injection, and electrophysiology were described in Chapter 2.

A4.4.1 Synthesis. AMP-Trp. In a round bottom flask, 70.7 mg of NVOC-Trp-CH₂CN (0.146 mmol) and 41.3 mg of AMP•H₂O (0.113 mmol) were dissolved in 4 mL of dry DMF. Using a micropipette, 93 μ L of 1.54 M tetrabutylammonium hydroxide (0.143 mmol) was added. The reaction was stirred at room temperature for 48 h. AMP-Trp isolated by multiple rounds of reverse phase HPLC. Recovered 24.5 mg (28%). ESI-MS(+) *m/z* for C₃₁H₃₄N₈O₁₄P found 773.0, calculated 773.6 (M+H⁺).

AppA-Trp. In a round bottom flask, 54 mg of AMP•H₂O (0.148 mmol) and 73.5 mg of CDI (0.453) were dissolved in 2.5 mL of dry DMF. The reaction was allowed to stir at room temperature for 15 h. AMP-Trp (10 mg, 0.013 mmol) was added and the reaction allowed to stir an additional 72 h. AppA-Trp was isolated by multiple rounds of reverse phase HPLC to recover 2 mg (14%). HRMS ES (+) *m/z* for C₁₀₈H₁₄₅N₃₂O₄₉P₅, found 1102.2457, calculated 1102.2452 (M+H).

A4.4.2 Ligation of tRNA. Ligation reaction conditions as follows: 35 μ g tRNA (~15 μ M), 100 mM HEPES pH 7.5, 41 μ M AppA-Trp, 15 mM MgCl₂, and 200 units T4 RNA ligase in a final volume of 100 μ L with 15% DMSO. The reaction was kept at 37 °C for

30 min. The reaction was quenched by addition of 12.5 μ L of 3.0 M NaOAc pH 5.0. Protein was extracted away with 1 volume of 25:24:1 phenol:chloroform:isoamyl alcohol, pH 5.2. The organic layer was then extracted with 0.5 volume of NaOAc quench solution. The combined aqueous solutions were then washed with 1 volume of 24:1 chloroform:isoamyl alcohol. tRNA was then precipitated by addition of 3 volumes of ethanol and stored at -20 °C overnight. tRNA was pelleted by centrifugation and dissolved in 1 mM NaOAc pH 4.5. The resulting tRNA solution was used directly for MALDI-MS analysis or protein expression.

A4.5 REFERENCES

1. Nangreave RC, Dedkova LM, Chen SX, & Hecht SM (2011) A New Strategy for the Synthesis of Bisaminoacylated tRNAs. *Org. Lett.* 13(18):4906-4909.
2. Hecht SM, Alford BL, Kuroda Y, & Kitano S (1978) Chemical Aminoacylation of tRNAs. *J. Biol. Chem.* 253(13):4517-4520.
3. Robertson SA, Ellman JA, & Schultz PG (1991) A General and Efficient Route for Chemical Aminoacylation of Transfer-RNAs. *J. Am. Chem. Soc.* 113(7):2722-2729.
4. Mohamady S & Taylor SD (2011) General Procedure for the Synthesis of Dinucleoside Polyphosphates. *J. Org. Chem.* 76(15):6344-6349.
5. Mohamady S, Desoky A, & Taylor SD (2012) Sulfonyl Imidazolium Salts as Reagents for the Rapid and Efficient Synthesis of Nucleoside Polyphosphates and Their Conjugates. *Org. Lett.* 14(1):402-405.
6. Saks ME, *et al.* (1996) An engineered Tetrahymena tRNA(Gln) for in vivo incorporation of unnatural amino acids into proteins by nonsense suppression. *J. Biol. Chem.* 271(38):23169-23175.
7. Milligan JF, Groebe DR, Witherell GW, & Uhlenbeck OC (1987) Oligoribonucleotide Synthesis Using T7 RNA-Polymerase and Synthetic DNA Templates. *Nucleic Acids Res.* 15(21):8783-8798.
8. Van Arnen EB. Personal Communication, 2010.
9. Kao C, Zheng M, & Rudisser S (1999) A simple and efficient method to reduce nontemplated nucleotide addition at the 3' terminus of RNAs transcribed by T7 RNA polymerase. *RNA* 5(9):1268-1272.
10. Nowak MW, *et al.* (1998) In vivo incorporation of unnatural amino acids into ion channels in Xenopus oocyte expression system. *Methods Enzymol.* 293:504-529.
11. Petersson EJ, Shahgholi M, Lester HA, & Dougherty DA (2002) MALDI-TOF mass spectrometry methods for evaluation of in vitro aminoacyl tRNA production. *RNA* 8(4):542-547.